Wear mechanism of coated carbide tools in the machining of ductile cast iron

(ダクタイル鋳鉄の機械加工における被覆工具の摩耗メカニズム)

学位取得年月 2017年3月

Israel Martínez Ramírez

Contents

List of figures

List of tables

List of figures

List of tables

1. Introduction

1.1 Background

1.1.1 Machining process

Machining process is the manufacturing process that deals with controlled material-removal. The principal machining operations by cutting are turning, drilling and milling; these operations are often referred in literature as the most widespread metal shaping process in the manufacturing industry [1]. Machining science or metal cutting science has as primordial objective the study of all factors and interaction between factors involved in the cutting operation such as cutting conditions, workpiece materials and tools. An overview of factors involved in material cutting are shown in Fig. 1.

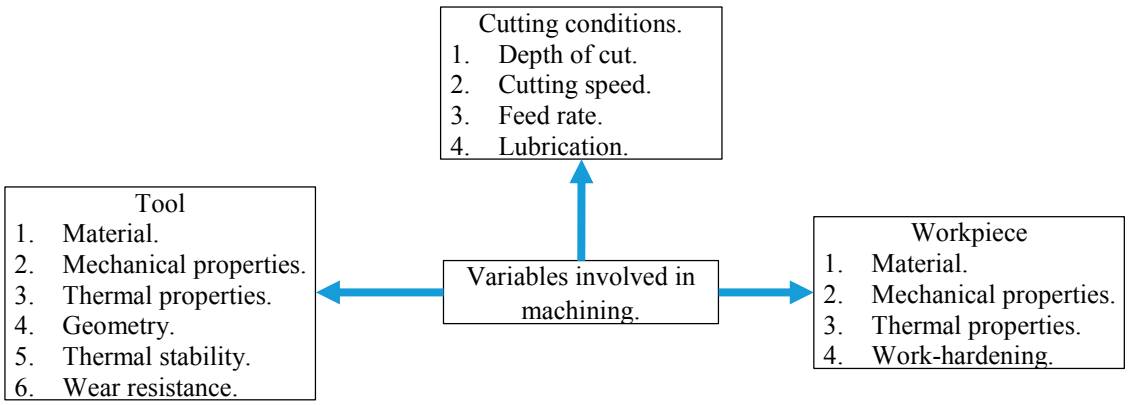

Fig. 1. Overview of factors involved in material cutting

Cutting conditions depends mainly on a machining method, tool, workpiece and final application of machined part.

Machinability is a term commonly used to describe how easy a workpiece can be cut under a given cutting conditions. Workpiece materials that can be processed by machining are practically all materials used in the industry such as metals, composites, plastics and ceramics. Tool shape and tool material depend strongly on a machining method, workpiece material and cutting conditions. The choice of cutting conditions, tool shape and tool material are of primary importance for an efficient machining operation. For instance, if tool wear become high, workpiece accuracy and surface finish are negatively affected; for this reason result important and interesting to study the effect of cutting condition and workpiece material on tool wear.

1.1.2 Tool wear

1.1.2.1 Types of wear

Tool wear is classified according to the affected zone on tool. Fig. 2 shows the types of wear.

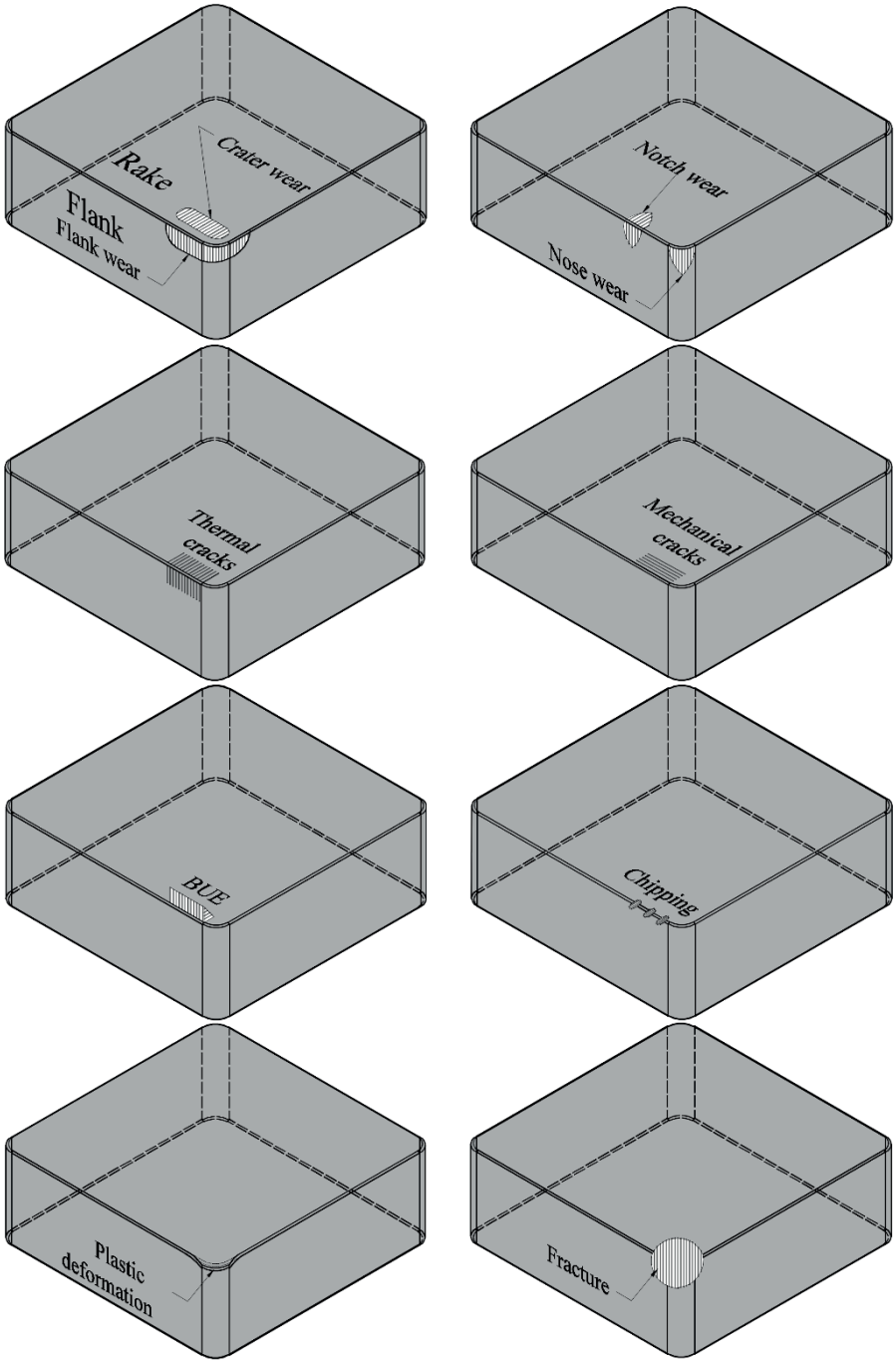

Fig. 2. Types of wear.

Flank wear is one of the most common types of wear. Flank wear is result of abrasive wear mechanism caused by the rubbing action of work material against relief (flank) face. Flank wear is one of the most common types of wear; for this reason the wear width of this type of wear is usually used as tool life criteria.

The behavior of flank wear against cutting time (or cutting length) is commonly characterized by three stages as shown in Fig. 3. In initial wear is commonly small. The initial wear is followed by a steady increase in wear then flank wear rate increase and flank wear finally becomes severe.

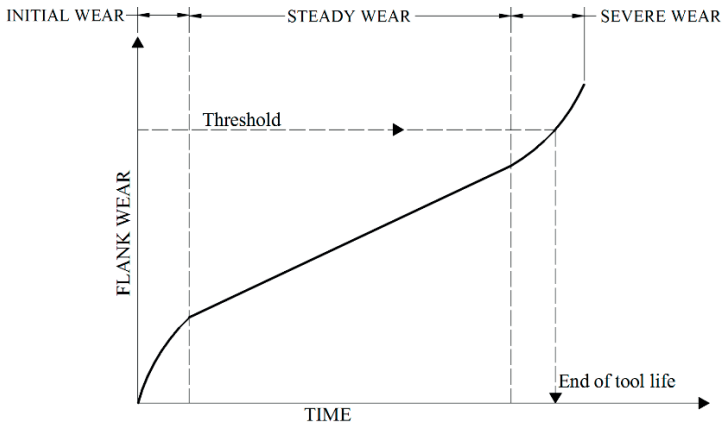

Fig. 3. Typical plot of cutting time vs flank wear

Flank wear affects negatively surface roughness and workpiece accuracy. When flank wear is the dominant factor in tool life, flank wear is usually used as tool life criteria. In this case, a threshold values is set, then, the cutting time in which flank wear reaches the threshold, correspond to the tool life. The ISO standard test stipulates the limit of tool life when flank wear reaches 0.5 mm [2]. Other common values used as threshold are 0.2 mm and 0.3 mm. In some instances, not only flank wear is used as tool life criteria, but also crater depth, notch wear, surface roughness or workpiece accuracy are used as tool life criteria.

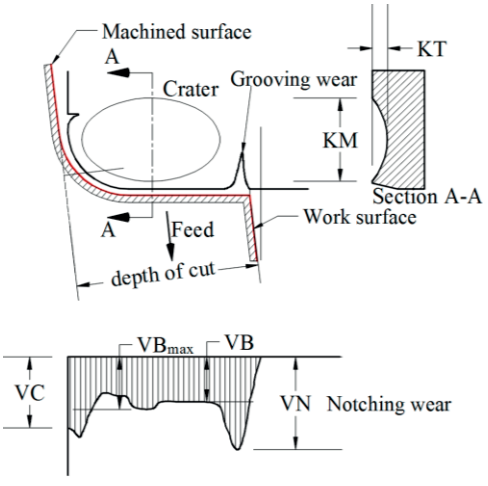

Fig. 4. Typical wear patterns of carbide tools

Fig. 4 shows a typical wear pattern of carbide tool [3]. In Fig. 4, wear parameters that can be measured on flank face and rake face are shown. Typically, average flank wear (VB) and maximum crater depth (KT) are often used as tool life criterion.

Crater wear as the name suggests, is a crater localized on a rake face. When the crater depth becomes large, the tool weakens and can lead into fracture or plastic deformation. Crater wear is cause by thermal activated wear mechanisms, such as chemical wear and diffusion wear.

Notch wear occurs in the depth of cut line on the flank face. Notch wear can be formed as result of a workpiece with work-hardening ability or hard surface layer, material that produce abrasive chips and oxidation wear when the tool is exposed to the atmosphere or coolant is used.

Nose wear takes place in tool nose. This type of wear is commonly found by abrasive wear mechanism.

Built-up edge BUE is accumulated workpiece material on the cutting edge. It is frequently found when cutting very ductile material such as ferritic ductile cast iron (as will be shown in chapter 3) under specific cutting conditions (especially at low cutting speed). Increasing of the cutting speed, reduces the BUE because of the rise in temperature of chip-work interface. As the temperature rises the strength of workpiece reduces as result the accumulated workpiece easily goes away from the cutting edge [4].

Thermal and mechanical cracks usually result from cyclic loading of the tool in interrupted cutting or when machining material which generate high tool-chip temperatures. Two types of cracks may occur: cracks perpendicular to the cutting edge, which usually result from cyclic thermal loads, and crack parallel to the cutting edge, which usually result from cyclic loads [4].

Plastic deformation occurs in the presence of excessive cutting force.

Chipping occurs when cutting materials that produce very abrasive chips. Chipping also increases flank wear.

Tool fracture occurs when stresses induced on the tool over pass its strength.

1.1.2.2 Wear mechanism

Tool wear mechanisms describe the process of how each types of wear are generated. Tool wear mechanisms are influenced by the type of workpiece and cutting conditions. About cutting condition, cutting speed has the highest impact on wear mechanism because high cutting speed is associated with high temperature. Fig. 5 shows an illustrative plot related with wear mechanisms and cutting temperature. Fig. 5 suggests that the main cause of wear changes with the cutting temperature.

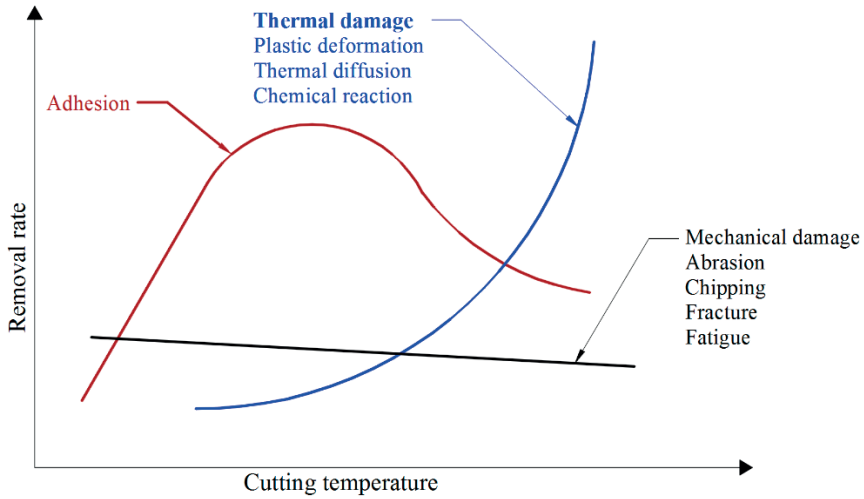

Fig. 5. Tool wear mechanisms and cutting temperature [1].

Abrasive wear occurs when hard particles from workpiece or tool rubs over tool surface removing part of tool. Abrasive wear reduces as long as tool hardness increases. Usually, tool hardness reduces as cutting temperature increases, thus abrasive wear can't be completely independent of temperature but abrasive wear does not increase unlike the chemical wear or diffusion wear does.

Adhesive wear takes place when workpiece particles weld with the tool removing small parts of the tool. This wear mechanism usually occurs at low cutting speeds.

Diffusion wear occurs at high cutting temperatures if elements in cutting tool and work material diffuses into each other's microstructure [1]. Diffusion wear depends on the solubility between tool and work, and the contact time between the tool and work.

Oxidation wear appear when the constituents of the tool react with the atmospheric oxygen. Oxidation often results in sever depth-of-cut notch and can be recognized by the fact that the tool material is typically discolored in the region near the notch [4].

Chemical wear caused by chemical reaction between the constituents of workpiece and tool or cutting fluid, produces both flank wear and crater wear. This type of wear is commonly observed when machining highly reactive materials such as titanium alloys [4].

1.1.3 Ductile cast iron

In casting process molten metal is poured inside a mold. This process is widely applied in industry because complex shapes can be manufactured. Cast iron is a Fe-C family of materials with carbon content of 2-4 % and 0.5-3% of Si [5]. Cast iron is widely used because of its good casting ability and its low price. The four basic types of cast iron, shown in Fig. 6, which are: white, gray, ductile and malleable. The terminology

gray and white is due to the fracture appearance. White cast iron has a reflecting surface and is characterized by precipitation of cementite. Grey cast iron has greyish appearance and its matrix contains precipitated graphite [6].

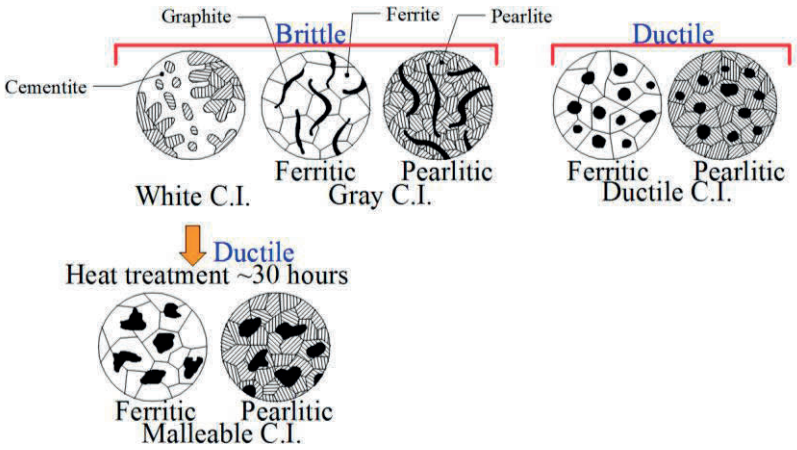

Fig. 6. Basic types of cast iron and its microstructure.

The microstructure of white cast iron contain massive amount of carbides, thus it is brittle and their use is limited to applications where high wear resistance is required [5]. The carbon content and silicon content in gray cast iron is typically 3.2% and 2.5% respectively; thus graphite forms in flake shape. The flake shape of the graphite in gray cast iron acts like stress riser causing low resistance and ductility [7]. However, it has very good damping vibrations capacity. For this reason gray cast iron is applied to make bases for lathes and milling machines. Gray cast iron is also cheap, thus commonly used for the manufacturing of drainage cover, lamp posts, benches, and other no high-stress demanding application.

Malleable cast iron has similar properties to ductile cast iron, however the required heat treatment for making it is long, and therefore it is expensive.

Ductile cast iron was made for first time in 1943 by Keith Millis and L. Gagnebine. They were trying to find a substitute for chromium as carbide stabilizer in white cast iron. They tried with most element in the periodic table. When they added magnesium, they found that the carbon had spheroid shape [5]. Ductile cast iron is also known as spheroidal or nodular cast iron because of graphite spheroid shape or nodular shape. Ductile cast iron has excellent mechanical properties, especially as its name suggest, ductility; therefore, in applications where economy, ductility and strength are required, ductile cast iron is preferred over gray and malleable cast iron.

The matrix of cast iron is essentially steel. The type of matrix (ferrite, pearlite, martensite, bainite or austenite) depends on the chemical composition and heat treatment [5]. The type of matrix define mechanical properties and also influence in wear behavior, as is discussed in detail in Chapter 3. Specific data about the grades ductile cast iron used in the experiments are provided in the section of materials in Chapter 3.

1.1.4 Coated tools

After the developing of the early coatings made by Chemical Vapor Deposition (CVD) in the early 1970's, coated tools became widely used due to its improved properties in comparison with the substrate material. Estimates points out that, currently, around 70% of cemented carbide sold for turning and 25% for milling, to up to 80% of all carbides, are coated [1]. The coated layer protects the substrate against mechanical wear mechanisms and thermal wear mechanisms; as a consequence higher cutting speed can be used without sacrifice tool life. The most common process for manufacturing coated tools are Chemical Vapor Deposition (CVD) and physical vapor deposition (PVD).

CVD is applied in higher temperatures (~1000ºC) than PVD process (~500ºC). Typical coating thickness achievable by CVD process is 5-15 μm. The bond between a CVD coating and substrate is metallurgical while the bond in a PVD is mechanical; as result CVD coatings are stronger than PVD coatings. However CVD coating has tendency to induce residual tensile stress because of its higher expansion coefficient than the substrate; this may lead in transverse cracks in interrupted cutting. In medium-temperature CVD (MT-CDV) the process temperature is from 700 to 900ºC. This increases the toughness and minimizes chipping and improves surface finishing of the coated layer [4].

Typical PVD coatings thickness are 2-5 μm. PVD coatings are free of thermal cracks that are common for CVD. PVD coating are fined grained and are generally smoother and more lubricious than CVD coatings, which is convenient to make tools with sharp corners.

Common coating materials used for single layer tools include titanium nitride (TiN), titanium carbo-nitride (TiCN), titanium aluminum nitride (TiAlN), titanium carbide (TiC), aluminum oxide (Al_2O_3), chromium nitride (CrN), hafnium nitride (HfN), titanium niboride (TiB_2), boron carbide and WC/C. PVD TiN, TiCN and TiAlN. TiAlN has higher ductility and higher stability at high temperatures than TiN and TiCN. TiAlN

provides high resistance to oxidation, high thermal conductivity, high hot hardness and enhanced chemical resistance [8].

1.2 Objective and justification

Ductile cast irons present a wide range of tensile strength and they are more ductile than other cast irons. Furthermore, casting process allows the manufacturing of complex shape components. However further process is often required in order to improve the quality of parts made by casting. In other words, casting process can hardly achieve accuracy and surface finishing that machining process can do. One popular application of ductile cast iron is in the automotive industry for manufacturing crank shaft, brake drums, engine parts and bushings, other applications include the manufacturing of pipes, piping fittings and valves. Therefore, it is interesting for the industry to know the machinability of the different grades of ductile cast iron. In old days, the machinability of ductile cast iron was investigated by using uncoated tool. However, nowadays most of the tools used in practice are coated. The efficient cutting operation depends on the correct choice of a coated tool. It is essential for the correct coating choice to understand the wear behavior. For this reason is important to investigate the wear characteristics when machining ductile cast irons.

The aim of this work is to investigate the wear characteristics of coated carbide tools in the machining of ductile cast irons experimentally. The conclusions regarding the machinability of ductile cast iron confirmed the results of already published data. However the wear mechanism proposed when machining ductile cast iron will provide valuable information for tool makers in order to improve the coating characteristics and, thus improve efficiency when machining ductile cast iron.

2. State of the art

This chapter gives a summary of previous research works reporting on the machining of ductile cast iron and on the occurrence of loss coating in machining of different types of workpiece materials. With help of a conscientious knowledge of the available research works, it becomes easy to realize the position of present work with respect to previously published research. Finally, the contribution of the present works are stated as “new purposed ideas”.

2.1 Machining of ductile cast iron

Mechanical properties and machinability of ductile cast iron are mainly affected by the microstructure of the matrix where the spheroidal graphite is disperse. Ductile cast iron with ferritic matrix has high ductility but low strength. In contrast, ductile cast iron with pearlitic matrix has high strength but low ductility. Hence the mechanical properties of ductile cast iron with ferritic-pearlitic matrix are determined by the amount of ferrite and perlite. Therefore the tool performance is also affected by the matrix constituents. For this reason the machinability of ductile cast iron should not be judge as good or bad unconditionally but depends on the type of ductile cast iron tested. The next paragraphs summarizes the most relevant published research related with machining of ductile cast iron.

The early research works of Hitomi and Thuering in 1960's ([9], [10] and [11]) deal with the machinability of ductile cast iron having ferritic, pearlitic and ferritic-pearlitic matrix machined with carbide tools and ceramic tools. These research work was divided into three publications. In the first publication, Hitomi and Thuering documented cutting forces and horse power needed to cut ductile cast iron. They realized that adhesion (BUE) was formed on carbide tools when turning grade 60 nodular cast iron. They argued that flank build-up formed on carbides, and its decrease at high cutting speed when machining grade 60 nodular iron can be explained by the oxide film theory [9]. In the second publication, Hitomi and Thuering investigated the effect of cutting conditions on flank adhesion. In that investigation some recommendation were suggested in order to avoid flank adhesion; such recommendations are: large clearance angles, cutting fluid, ceramic tools and very low or very high cutting speed [10]. Finally in the third publication, the tool life of carbide and ceramic tools when turning ductile cast iron was reported. The tool life for grade 60 was longer than for 80 and 100 [11]

After the developing of the first coatings made by Chemical Vapor Deposition (CVD) in the early 1970's, most of research work focus on the performance of coated tools.

Grzesik et al. reported cutting forces, cutting temperature and Peclet number in the machining of pearlitic-ferritic cast iron (EN-GJS-500-7) with coated carbide and silicon nitride ceramic tools. It was concluded that coated tools performed better than the uncoated regarding cutting temperature and cutting forces [12]. Grzesik et al. calculated the Peclet number using the formulae

$$Pe_c = \frac{v_{ch} l_{nc}}{\alpha_w} \quad (1)$$

Where v_{ch} is the chip velocity, l_{nc} is the natural chip-tool contact length and α_w is the thermal diffusivity of the workpiece materials. For larger values of Peclet number, heat transfer to the stationary element is less intensive.

In addition, Grzesik and Malecka used the same tools as in the previous published work [12] in order to find the wear mechanism when cutting ductile cast iron grade EN-GJS-500-7. They reported notch wear on the uncoated Si_3N_4 due to oxidation wear. CVD-Al2O3/TiN coated nitride ceramic tools indicated higher resistance to abrasive wear and they recommended these coated tool for medium and finish machining of ductile cast iron with cutting speeds from 160 to 240 m/min. Finally, the dominant wear mechanisms founded were adhesion and abrasion [13].

Yigit et al. used TiCN+TiC+TiCN+Al_2O_3+TiN and TiCN+TiC+TiCN+Al_2O_3+TiN multilayer coated inserts in turning of GGG50 (equivalent to EN-GJS-500-7). The important conclusion was that multicoated tools exhibited better performance compared with uncoated inserts concerning to cutting forces, flank wear and surface roughness [14].

Camuşcu investigated the effect of cutting speed on the wear of cutting characteristics of TiN coated Al_2O_3 + TiCN mixed ceramic, SiC whisker reinforced Al_2O_3 and uncoated Al_2O_3 + TiCN mixed ceramic tool when machining a pearlitic ductile cast iron. After a comparison of flank wear, surface finish and cutting forces, they concluded that in the machining pearlitic cast iron at high cutting speed (>600 m/min), TiN coated Al_2O_3+TiCN mixed ceramic tool was more suitable than the uncoated ceramic tool in reference to tool wear, surface finish and cutting force [15].

The effect of ductile cast iron microstructure on its machinability was considered previously in the research work of Cemal Cakir et al. The machinability of ferritic-pearlitic, tempered martensitic, lower ausferritic and austempered ductile iron was evaluated in base to cutting forces, wear width and surface roughness [16]. Cemal Cakir concluded that ferritic-pearlitic had the best machinability because of the low hardness of ferritic-pearlitic cast iron. This conclusion implies that only abrasive wear is the cause of tool wear in the turning of ferritic-pearlitic ductile cast iron; however, the effect of cutting temperature was not considered. Furthermore the type of tool material used in this investigation was not specified and the wear mechanism was not investigated.

The number of published work in interrupted cutting is more limited than that in continuous cutting. Prengel et al. used ductile cast iron grade 80-55-06 (pearlitic ductile cast iron) for comparing the tools life of TiAlN

multilayer coating, TiAlN monolayer coating and TiN/TiCN/TiAlN-multilayer in face milling [17]. They concluded that in dry conditions TiAlN multilayer had the best performance; however in wet condition TiAlN monolayer was the best.

Jaharah et al. [18], used statistical techniques (ANOVA) in order to find the influence of cutting conditions on cutting force and tool life of a coated carbide tool in the face milling of FCD 500. The authors used FC 500 and FCD 500 to name the materials; this nomenclature corresponds to the JIS standard. However, FC is used to refer gray cast iron and FCD is used to refer ductile cast iron. The tensile strength reported was 250-350 which is more likely to be the tensile strength of FC 350. Therefore, the type of cast iron tested is uncertain. They concluded that cutting speed is almost negligible compared to feed rate and depth of cut on tool life of carbide cutting tool.

2.2 Loss of coating layer

The interest on coated tools by the scientific community increases as well, mainly due to the better features exhibited by the coated tools in machining operations, and the necessity of finding the correct coating for the machining of a specific combination of materials and applications. In general, the coating acts as barrier against the mechanical and thermal wear [4], as a consequence a longer tool life is achieved. As discussed by Prengel et al. chemical stability, hot hardness, and good adhesion to the substrate are essential characteristics of the coating for tools [19]. However, in machining operation, high pressures, high temperatures and different wear mechanisms cause the loss of coating layer. This phenomenon was documented specially in the machining of difficult-to-cut materials like the Ni-Cr alloy Inconel 718.

Itakura et al. [20] reported abrasive and adhesive wear as a responsible of the coating film peeling, when the tool undergoes high temperatures (990ºK at 30 m/min and 1320ºK at 100 m/min) in the turning of Inconel 718. Additionally diffusion wear and coating peeling were pointed as the cause of increase in wear rate.

Prengel et al. [17] reported coating flaking in early stage in turning of Inconel 718 in all the coated tool tested (TiAlN multilayer, TiAlN monolayer, and TiN/TiCN/TiAlN- multilayer coated inserts).

Bhatt et al. [21] reported loss of bonding strength at the CVD coating-substrate interface which resulted in a reduction of tool life of the multicoated TiCN/Al_2O_3/TiN. At relatively low cutting speed (50 m/min), unexpectedly WC/Co had longer tool life than multicoated CVD TiCN/Al_2O_3/TiN and PVD TiAlN coated

tool. The reason for this were: the low adhesion, residual stresses on sharp edges that can induce coating delamination in the PVD coating and the formation of η-phase, embrittlement, and the development of residual tensile stresses.

In scratch tests, Ducros et al. [22] reported cohesive flaking between nanolayer TiN/AlTiN and AlTiN top-layer, although according with their results, this was not a problem in the machining of Inconel 718, moreover TiAlN-base coating outperformed the CrN/TiN coatings, especially at high cutting speed.

Not only in the machining of Inconel 718, but also in the machining of other materials, loss of coating layer was reported.

In the case of tempered martensitic stainless steel, Noordin et al. [23] reported that catastrophic failure of the tool was preceded by loss of coating, which also caused abrupt increase in wear of TiN/TiCN/TiN coated tool and TiCN/α-Al_2O_3/TiCN/TiN.

Khrais and Lin [24] used a TiAlN coated tool in the machining of AISI 4140 at high cutting speed (210 to 410 m/min). They reported spall of coating, at all cutting speed tested.

Qin et. al [25], assumed that the coating delamination is the cause of rapid wear of the exposed substrate material in the turning of A359/SiC-20p composite with nano-diamond coated tools. The SEM photographs showed evidence of coating delamination in the rake face and in the zone around the cutting edge, however the delamination was not confirmed on the flank face where the wear width was measured, moreover the cutting length in which the photographs were taken was not specified.

2.3 New proposed ideas

The last investigation on the machining of several grades of ductile cast iron was on 1970's. By that time, coated tools were not developed yet. Most of the recent available research on the wear characteristics of coated tools in the machining of ductile cast iron focuses on a single grade. Others describe some of the necessary results (cutting forces, cutting temperature, surface roughness and flank wear) in order to give a judgment about the merits of different coated tools when cutting ductile cast iron, few of them discusses the wear mechanism. Up to now there is not documentation available on the machining of several grades of ductile cast iron with coated carbide tool that states a common wear mechanism for all family of ductile cast iron based on the composite nature of ductile cast iron. If we consider the scale in which metal cutting

is performed, we can realize that the effect of nodules on tool wear characteristics should not be ignored. Furthermore, it is important for the metal manufacturer to elucidate what grade of ductile cast iron is economically feasible regarding machining, in other words, which one can be machined with minimum energy, minimum disposable insert tools and the maximum cutting speed. Additionally, the tool maker would like to know what type of characteristics the coating should possess in order to be effective when cutting ductile cast iron.

Finally a new method for analyzing flank wear of coated tool is proposed. This method uses log-log cutting distance (or cutting time) versus flank wear plots in order to detect the change in wear rate easily. This method is very simple but effective for detecting when coating layer on the cutting edge is worn out. The difficulty of demonstrating the validity of the above mentioned argument lay in the fact that careful inspection of the cutting edge is needed by means of SEM and EDS images.

3. Wear mechanism of coated tools in the turning of ductile cast iron having wide range of tensile strength

3.1 Introduction

Ductile cast iron is widely used in the manufacturing of automotive parts, machine components and piping accessories. The success of this material for industrial applications lies in its higher ductility in comparison with white cast iron and its inexpensive production process in comparison with malleable cast iron. Nowadays, ductile cast iron accounts for about 40% of the cast iron market [5]. However, most of the manufactured parts made of ductile cast iron cannot be used as cast but require to be machined after casting in order to improve its accuracy and surface finishing. For this reason, it is important to evaluate the cutting performance of cutting tools in machining of ductile cast iron.

In the present chapter, the wear characteristics of carbide K15, TiAlN coated tool and TiN coated tool are analyzed in turning of ductile cast iron having ferritic matrix (named in this study F400 and F440), pearlitic matrix (named in this study P520 and P675). The wear mechanism proposed is based on the wear out of coating layer and adhesion of workpiece material on the tool. The tool performance is judged in base of the results obtained from the measurements of cutting force, cutting temperature and wear width.

3.2 Materials and methods

The bars used in the experiments were pre-machined in order to remove the hard as-cast surface. The microstructure depends strongly on the chemical composition; copper is used as pearlite former, manganese acts as pearlite stabilizer and increase tensile strength, on the contrary, silicon promotes structures with greater ferrite, and reduces the tensile strength [26]. This is consistent with the chemical composition shown in Table 1, the mechanical properties shown Table 2 and the microstructure shown in Fig. 8. The ultimate tensile strength shown in the Table 2 as UTS1, means the average value of three specimens taken from the actual bars used in the machining experiments; the first at the center of the bar, the second at 25 mm away from the center and the last at 30 mm away from the center. The values shown in UTS2, means the tensile strength of a specimen separately casted as commonly is made and reported for commercial use according with the ISO 6892 standard. All the specimens used for measuring UTS1 and UTS2 were manufactured

from the same molten iron but different mold. Because the UTS1 was measured from the actual specimen used for the machining experiments, this value was used to refer the workpieces. In order to differentiate the workpieces, they are referred as F for indicating ferritic matrix and as P for indicating pearlite matrix, the next numbers indicates the approximated average of tensile strength (UTS1). For example F400 indicates ferritic matrix with 400 MPa of tensile strength. The microstructure of the materials tested are shown in Fig. 8. It was reported that the type of matrix determines the tool life [27]. For this reason, some grades of ductile cast iron having different matrix were chosen to be tested.

The lathe used for this investigation was the Okuma® LS450 equipped with a variable speed driver and a tachometer for measuring the spindle speed. After removing the irregular as-cast surface of the workpieces, the final dimensions of the bars were approximately 97 mm in diameter and 300 mm in length.

Table 1 Chemical composition in mass % of the material tested.

	C	Si	Mn	P	S	Cu	Sn
F400	3.75	2.17	0.22	0.026	0.008	0.063	0.012
F440	3.65	2.59	0.25	0.03	0.005	0.072	-
P520	3.75	2.53	0.3	0.031	0.01	0.392	0.055
P675	3.75	2.46	0.36	0.019	0.006	0.894	0.05

Table 2. Mechanical properties of workpieces tested

	UTS1 (MPa)	UTS2 (MPa)	Brinell (HB)	Elongation (%)	Vickers (Ferrite)	Vickers (Pearlite)
F400	402	445	147	23.7	233.1	301.3
F440	436	471	149	25.3	246.1	305.4
P520	518	718	235	2.7	301.3	372.4
P675	674	854	248	4	305.4	353.8

As can be observed in the Fig. 8, F400 and F440 materials have mainly ferritic matrix with a low amount of lamellar pearlite. On the other hand P520 and P675 have pearlitic matrix. The spheroidizing rate calculated for F400, F440, P520 and P675 was 80%, 90%, 84% and 72% respectively. This results are the average of six measurements in different position of the workpieces.

The abrasive and adhesive type of wear are directly affected by the hardness of the micro-particles that abrade or adhere in the tool. The matrix possesses much higher hardness than graphite, therefore it worth to evaluate the Vickers hardness of the matrix constituents. The micro Vickers hardness shown in Table 2 represent the mean value of ten measurements for each material. The t-test is used for testing the null hypothesis of equal mean values and detect statistically if there is a significant difference between hardness of the micro-constituents.

For ferritic ductile cast iron t_0 was 2.9054 and $t_{0.025,18,}$ was 2.1, thus was concluded that ferrite hardness of F440 is higher than ferrite hardness of F400. In the case of pearlite hardness of ferritic ductile cast iron, the result is obvious since the mean value for F400 and F440 is practically the same, the value of t_0 equal to 0.54 confirms that the null hypothesis must be accepted and conclude that the mean values are the same.

For pearlite hardness of the pearlitic grades P520 and P675 t_0 was 1.81 and the null hypotheses should be accepted.

The final conclusions about the t-test on the difference in the mean values by assuming equal variances indicated that ferrite's hardness of F440 is higher than that of F440 but there is not difference in the mean values in the case of the pearlite hardness between P675 and P520, furthermore the pearlite hardness of the pearlitic grades is significantly higher than the pearlite in ferritic grades. The assumption of equal variances was confirmed to be reasonably good according to the Levene test [28].

The medium carbon steel AISI 1045 is often used in discussing machinability, therefore additional results on the machining of this carbon steel are presented.

Fig. 7 shows the radar chart with the workpiece properties that has major effect on the cutting forces, cutting temperature, adhesion and chip control. This radar chart shows the ratio of ductile cast iron properties with respect to AISI 1045 properties.

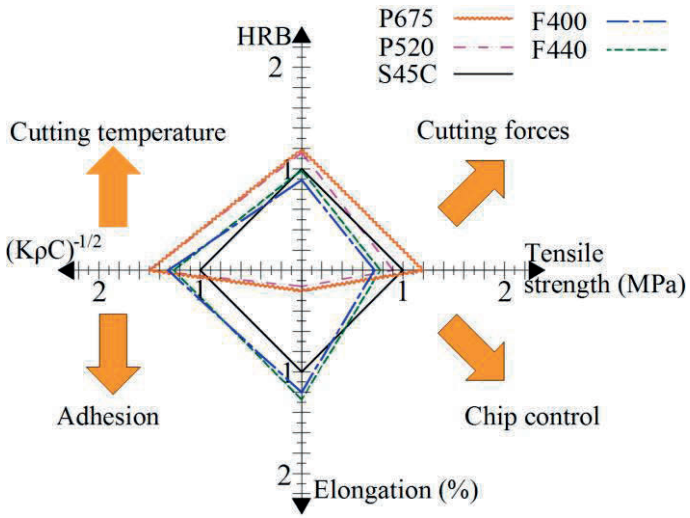

Fig. 7. Machinability radar chart for ferritic ductile cast iron, pearlitic ductile cast iron and AISI 1045

The representation of workpiece properties in form of radar chart was proposed originally by Yamane and Sekiya [29]. The radar chart is an easy and convenient way to evaluate the machinability of workpieces in a fast fashion. For instance, it was expected to find lowest cutting forces when machining ferritic cast iron and highest when machining pearlitic cast iron. The largest adhesiveness was expected when cutting ferritic

ductile cast iron and the lowest when cutting pearlitic ductile cat iron. It is difficult to drawn a clear conclusion on the chip control from the radar chart, because the lines gets crossed in the fourth quadrant.

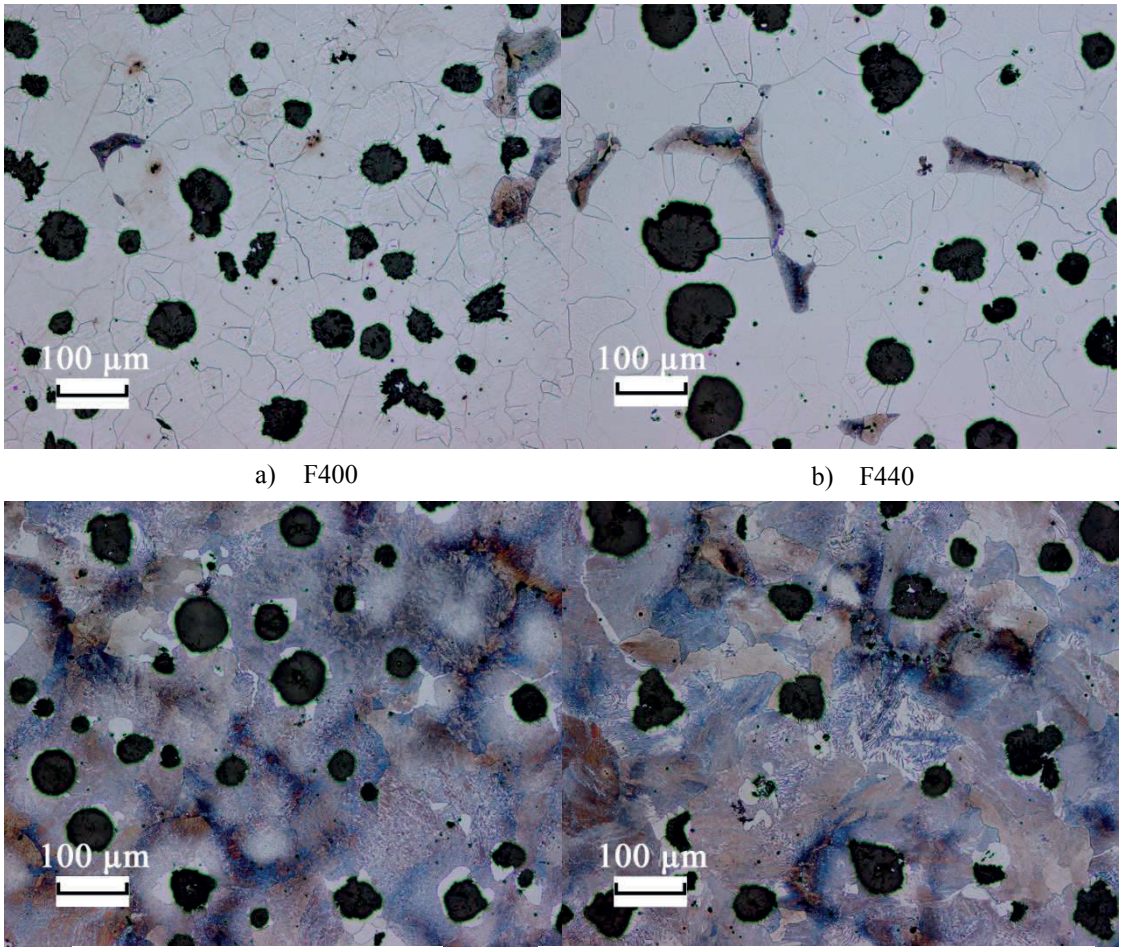

a) F400 b) F440

c) P520 d) P675

Fig. 8. Microphotographs of different grades of ductile cast iron.

3.2.1 Cutting conditions

The cutting condition used in the experiment are shown in Table 3.

Table 3. Cutting conditions.

Tool material:	Tungsten Carbide K15, TiN coated and TiAlN coated
Cutting speed:	50, 100, 150, 200 and 250 m/min.
Depth of cut:	1 mm
Feed:	0.2 mm/rev
Coolant:	Dry

The tool materials used in the experiments were tungsten carbide grade K15, TiAlN coated carbide and TiN coated carbide. The 4 µm coating layer was deposited on a tungsten carbide substrate by using physical

vapor deposition method. All the tools tested had the same geometry. The tool geometry is defined with the code given by the ISO standard for indexable inserts identification system. The corresponding code for the tools used was SNMN120408. The tool holder used was a Mitsubishi N11R-44. The geometrical combination of holder and tool resulted in a side cutting edge angle of 15°, a back rake angle of -5 and a side rake angle of -6° (Fig. 9).

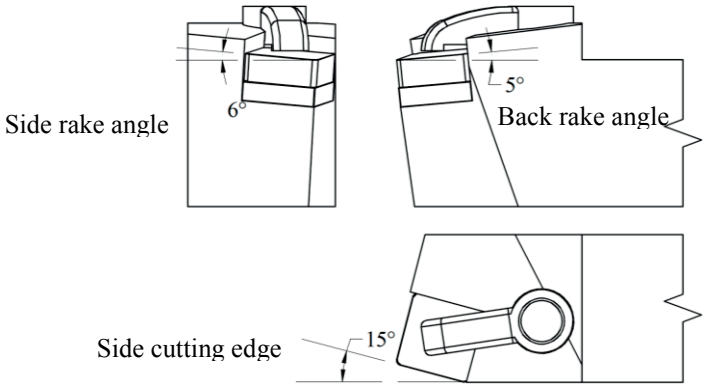

Fig. 9. Tool holder geometry for turning.

3.2.2 Experimental setup

The turning was interrupted in order to measure the flank wear with a toolmaker's microscope Mitutoyo®, additionally, after machining microphotographs were taken with a stereoscopic microscope Nikon® SMZ-U. The photographs revealed adhesion of work material on the tools. Adhesion became severe at low cutting speed and this made difficult to measure the wear width. For this reason the results were presented at cutting speed which the flank wear was clear. The cutting forces were measured with a piezoelectric dynamometer type 9129AA connected to a three channel amplifier Kistler® 5019B and the output was recorded by a digital sampling oscilloscope as shown in Fig. 10. The DC coupling was used when it was wished to observe the entire input signal (DC and AC components). A 500 Hz bandwidth was used for eliminating the noise components from the input signal. The sample rate used was 5 kS/s.

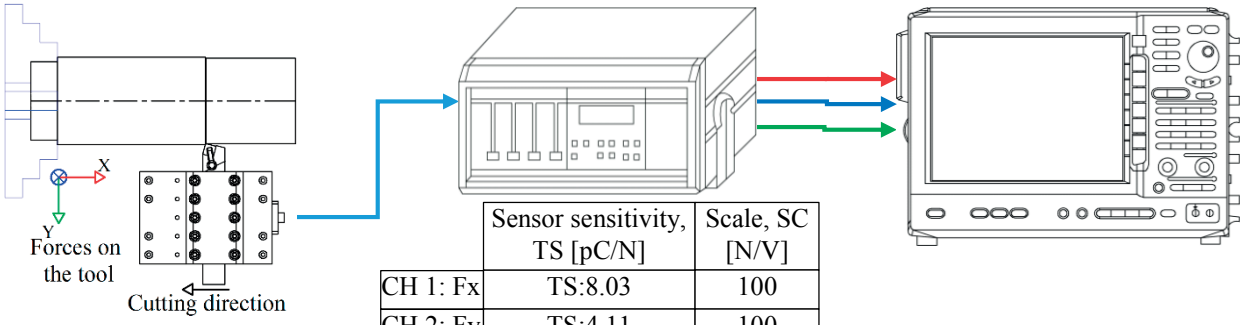

	Sensor sensitivity, TS [pC/N]	Scale, SC [N/V]
CH 1: Fx	TS:8.03	100
CH 2: Fy	TS:4.11	100
CH 3: Fz	TS:4.11	100

Fig. 10. Force measurement setup.

The cutting temperature was measured by means of the tool-work thermocouple method. The calibration curves used in the thermocouple method for the workpieces and tools, were generated by using the set-up shown in the Fig. 11 (a).

The furnace used for heating the contact point between a K thermocouple and a work material or tool material, consisted in an ellipsoidal shape furnace which was internally coated with gold and then polished in order to improve the surface reflectance. Both of the lamp and the contact point are located on the focus of the ellipsoid; therefore all rays are directed to the contact point and a hot junction occurs due to radiation. The temperature of the hot junction can reach 1200°C in a short time (~10 seconds). The difference of temperature between the hot junction and the cold junction causes an electromotive force which was measured according with the circuit shown in the bottom of Fig. 11 (a). The electromotive force was recorded by an analogic X-Y recorder. The final calibration curve used in the tool-work thermocouple method was calculated from the difference between the curves obtained for the tool and for the work [30]. The calibration curve for F400 is shown in the Fig. 11 (b). In Fig. 11 (b), can be observed curves for chromel-tool, and one curve for chromel-workpiece, the final calibration curve result from the difference between curves of chromel-tool and chromel-workpiece. Similar curves were found for the rest of work materials.

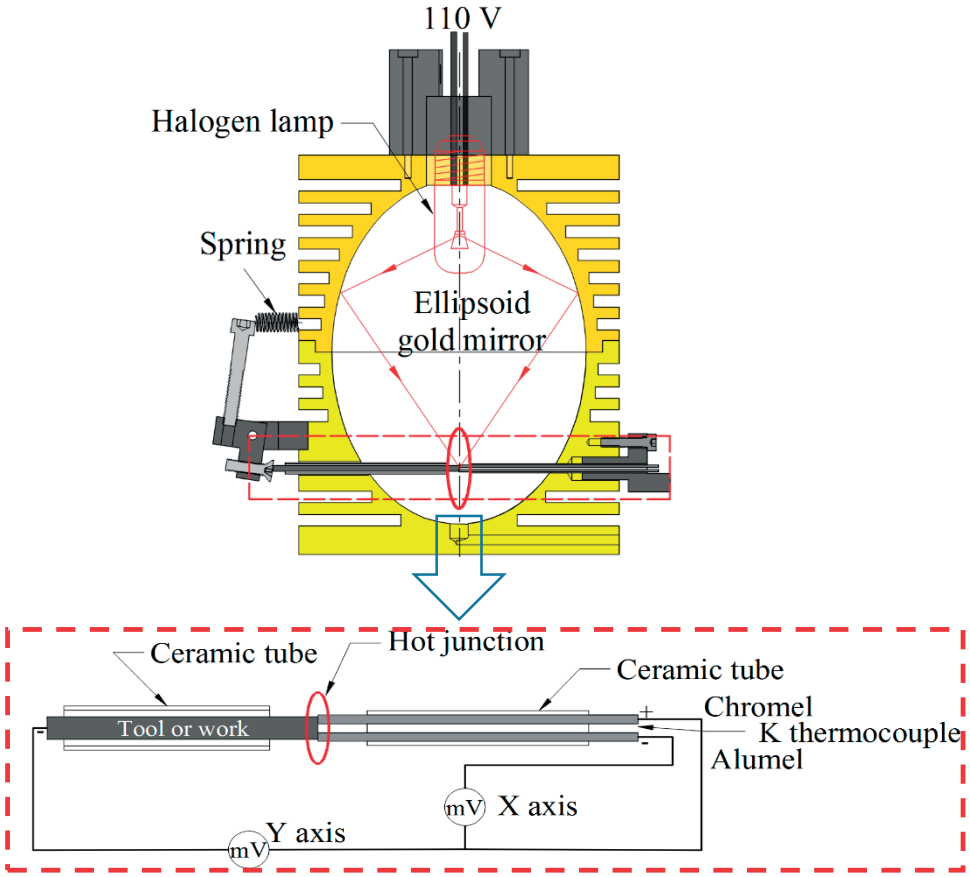

(a) Calibration set-up and circuit.

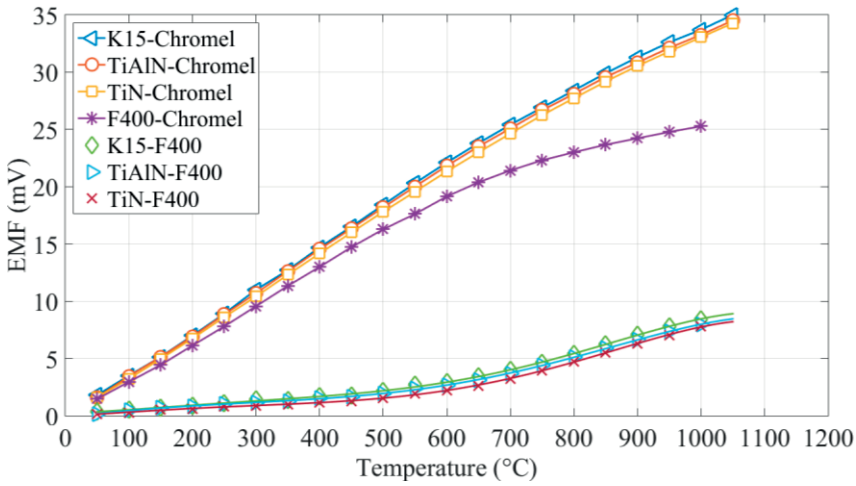

(b) Calibration curves.

Fig. 11. Set-up and circuit used for the calibration curves.

As mentioned above, a K thermocouple was used to find the calibration curves, tables on the relation between electromotive force and temperature are available in literature provided by manufacturers. The rational polynomial function provided by [31], gives an accurate approximation of the temperature according with voltage measured. This equation is as follows:

$$T = T_0 + \frac{(V - V_0)\left(p_1 + (V - V_0)\left(p_2 + (V - V_0)(p_3 + (V - V_0)p_4)\right)\right)}{1 + (V - V_0)\left(q_1 + (V - V_0)(q_2 + (V - V_0)q_3)\right)} \quad (1)$$

Where the coefficients can be evaluated according to the range of emf measured as indicated in the Table 4.

Table 4. Coefficients for rational polynomial function used for thermocouple calibration [31].

Vmin	-6.404	-3.554	4.096	16.397	33.275
Vmax	-3.554	4.096	16.397	33.275	48.838
Tmin	-250	-100	100	400	800
Tmax	-100	100	400	800	1200
To	-121.4716409	-8.793596224	310.18976	605.725621	1018.470523
Vo	-4.179085844	-0.344899142	12.63138642	25.14871778	41.99385085
p1	36.06951328	25.67871906	24.06194895	23.53940069	25.78323885
p2	30.72207573	-0.498879036	4.015862189	0.046547228	-1.836340284
p3	7.791386025	-0.44705222	0.26853917	0.0134444	0.056176662
p4	0.525939908	-0.044869203	-0.009718854	0.000592369	0.000185324
q1	0.939395467	0.000238934	0.169958719	0.000834455	-0.074803355
q2	0.277912853	-0.02039775	0.011413069	0.000461214	0.002384186
q3	0.025163349	-0.001842411	-0.000392752	2.54881E-05	0

Fig. 12 shows the difference between the values from ordinary tables and the value calculated by using the rational polynomial function.

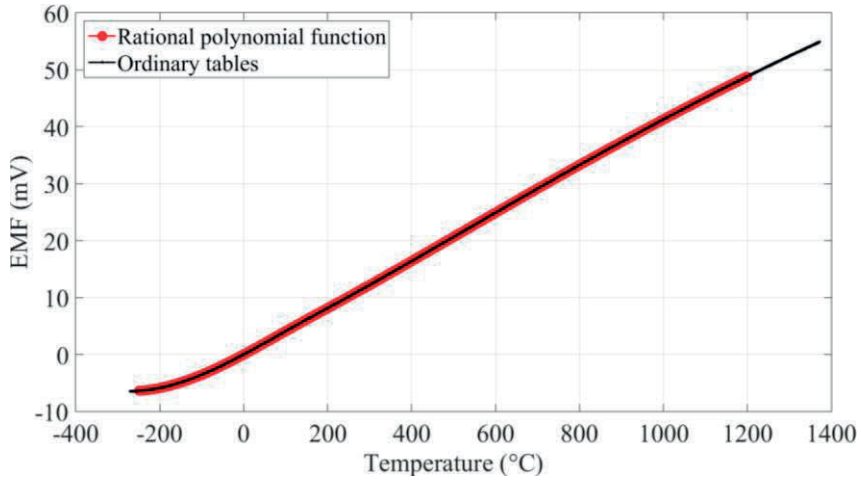

Fig. 12. Use of rational polynomial function for K thermocouple temperature evaluation.

Fig. 11 shows the necessary curves to get the calibration plot for one workpiece, considering that four different workpieces were tested, it is useful to use the equation 1 and all calibration curves in a computer program for a fast and efficient calculation of the cutting temperature. Such program was written in matlab by using GUIDE capabilities. Fig. 13 shows a snapshot of the program used for compute the data points for calibration curve and cutting temperature. This program works following the next steps:

1. The emf data of work-chromel and work-tool is written a excel file (Y axis of the first graph shown in left side of Fig. 13).
2. The emf data for the thermocouple is converted in temperature by using the rational equation above mentioned (X axis of the first graph shown in left side of Fig. 13).
3. With the difference between work-chromel and work-tool, the work-tool calibration curve is calculated.
4. Finally after get the emf data from the cutting test, this data can be input and then the cutting temperature is calculated.

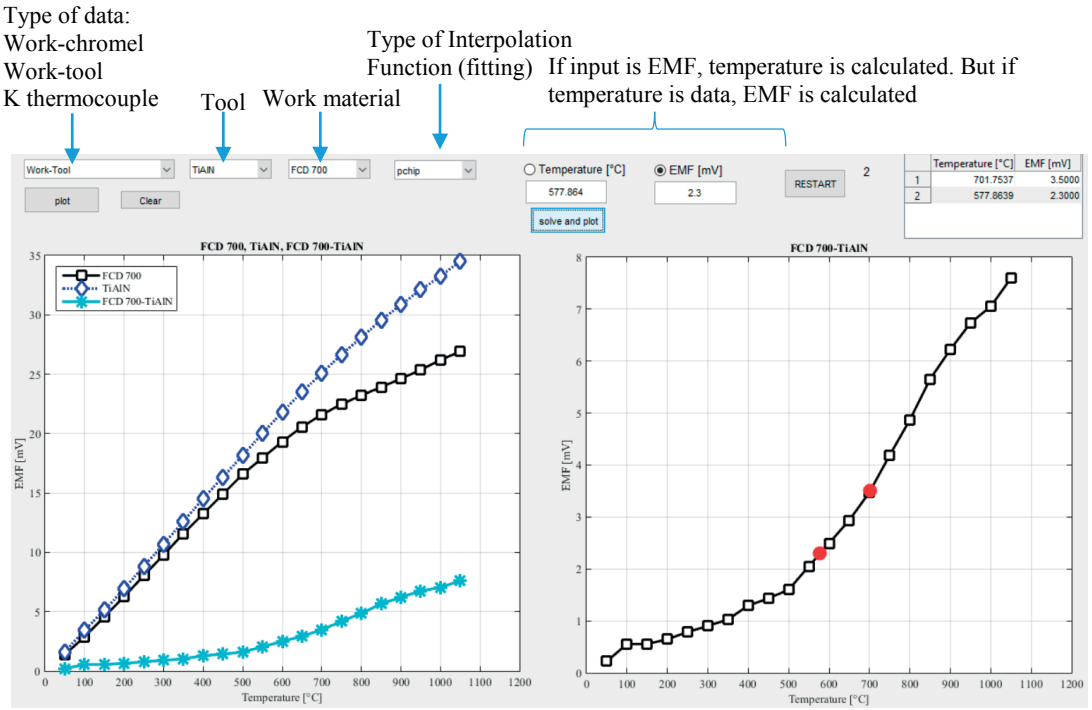

Fig. 13. Snapshot of program for calculating the cutting temperature.

This program is very useful since all data is in form data points and interpolation can be perform straightforward by using any of the built-in functions in matlab.

The set-up for measuring the cutting temperature is shown in Fig. 14. The cutting temperature set-up consist of a slip ring connected to the workpiece. The inner part of the slip ring was connected rigidly to the lathe shaft thus they rotated at the same RPM. The slip ring outer part is fixed. So the outer pars of the slip ring can be connected to an oscilloscope or to an analogic recorder. Finally the accuracy of the calibration method is within 0.4 mV which is approximately equivalent to 2ºC in the final calibration curve [30].

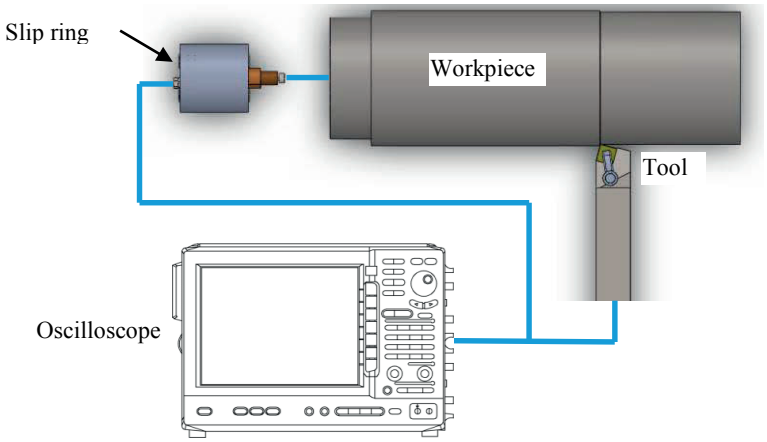

Fig. 14. Cutting temperature calibration set-up.

3.3 Results

3.3.1 Tool wear

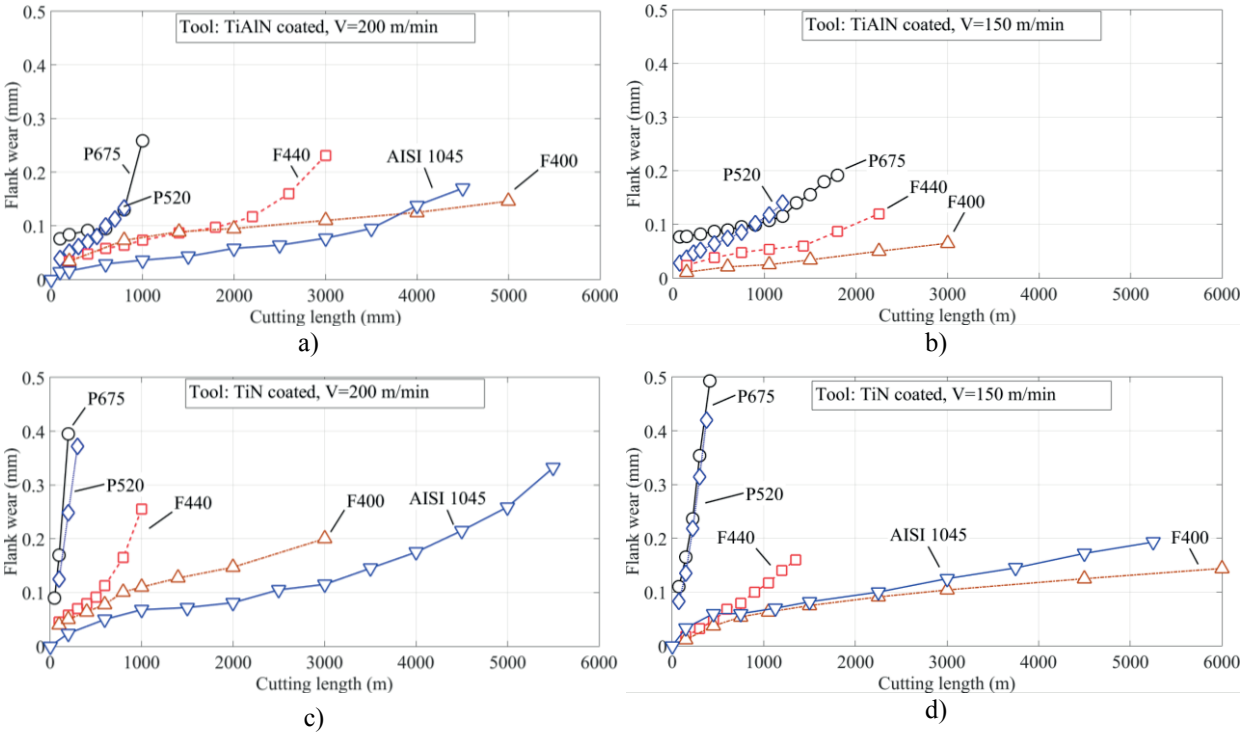

Fig. 15. Flank wear progress on coated tool at 200 m/min and 150 m/min in the turning of ductile cast iron.

Fig. 15 shows the flank wear progress on coated tools when turning different grades of ductile cast iron. For both coated tools at 200 m/min of cutting speed, the flank wear width in the early stage, in turning of F400 and F440 was larger than in the machining of AISI 1045.

However in turning of AISI 1045 with TiAlN coated tool, the wear rate of flank wear changed after 4000 m of cutting length and then became higher than that in F400, meanwhile in the turning of F400 the wear was stable. The tendencies of flank wear in the cutting of AISI 1045 and F400 at 150 m/min were approximately almost the same beyond 1000 m of cutting length, respectively. However, the difference gradually became clear over 1000 m of cutting length, and the flank wear in the cutting of AISI 1045 became larger than that of F400.

It is evident that the flank wear in turning of pearlitic grades (P675 and P520) is severer than in turning of ferritic grades (F440 and F400), independently of the cutting tool. This large difference in flank wear makes difficult to establish a threshold value for comparing both grades. In order to evaluate how high the wear in the machining of pearlitic ductile cast iron was in comparison with ferritic ductile cast iron, the ratio of flank wear and cutting length for the last point measured was calculated and tabulated in Table 5.

From Table 5, the wear ratio of TiAlN at 200 m/min in the machining of P675 was 0.259 mm/km and 0.029 mm/km in the machining of F400. Therefore the wear ratio is 9 times higher in the machining of P675 than in the machining of F400. In the case of TiN, the wear ratio was about 30 times higher in the machining of P675 than in the machining of F400 at 200 m/min. As listed in Table 5, TiAlN coated tool outperform TiN coated tool regarding flank wear, the difference was higher in the pearlitic grades than in the ferritic grades.

Table 5. Ratio between flank wear and cutting length for TiAlN and TiN, (mm/km).

	200 m/min			150 m/min		
	TiN	TiAlN	TiN/TiAlN	TiN	TiAlN	TiN/TiAlN
P675	1.975	0.259	7.625	1.197	0.107	11.218
P520	1.240	0.166	7.459	1.120	0.117	9.600
F440	0.255	0.077	3.312	0.119	0.053	2.222
F400	0.067	0.029	2.283	0.024	0.022	1.108
S45C	0.060	0.038	1.598	0.037		

The large ratio calculated for the pearlitic grades of ductile cast iron in comparison with the ferritic grades of ductile cast iron is due to the better stability at high temperature of the TiAlN coated tool in comparison with the TiN coated tool.

3.3.2 Adhesion

Adhesion on the rake face and flank face was observed on all the tools after turning ductile cast iron at all cutting speed tested. However, the amount of adhesion varied with the cutting speed, work materials and

tool. The left side of Fig. 16 shows the flank face of K15 carbide tool. The right side shows an amplification of the squared area, after remove part of adhered material. The carbide tool grade K15 had significant amount of adhered workpiece as shown in Fig. 16. As can be seen in Fig. 16 after removing part of the adhered material on the carbide tool, a part of the tool material came out causing a visible damage. This means that the adhered workpiece material is not only superficial but is strongly welded in such a way that after removing a kind of crater is revealed.

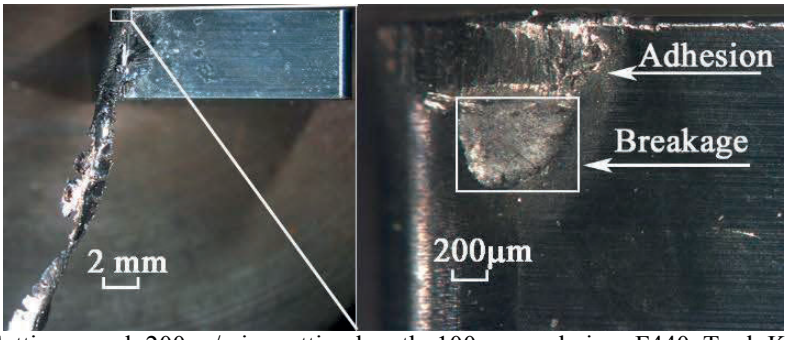

Fig. 16. Cutting speed: 200 m/min, cutting length: 100 m, workpiece F440, Tool: K15 carbide

As the cutting speed and strength of workpiece increase the amount of adhesion decrease. The growing of adhesion was more favored by the use of the carbide tool than by the use of the coated tools. Among the coated tools, lower adhesion was observed on TiAlN coated than on the TiN coated. This fact can be observed clearly in the photographs shown in Fig. 17 and Fig. 18.

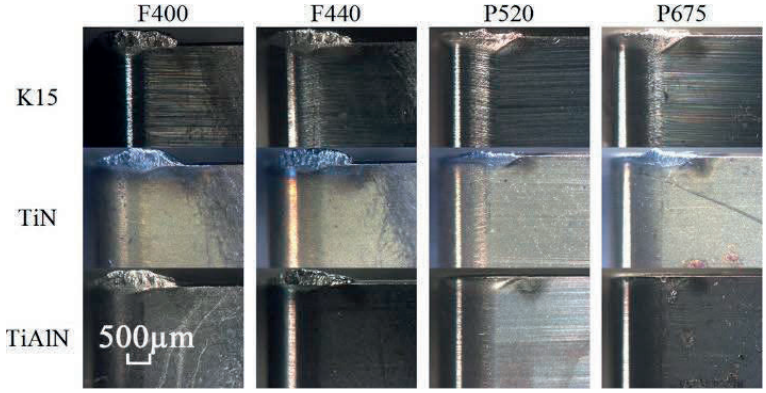

Fig. 17. Cutting speed 50 m/min, cutting length 300 m.

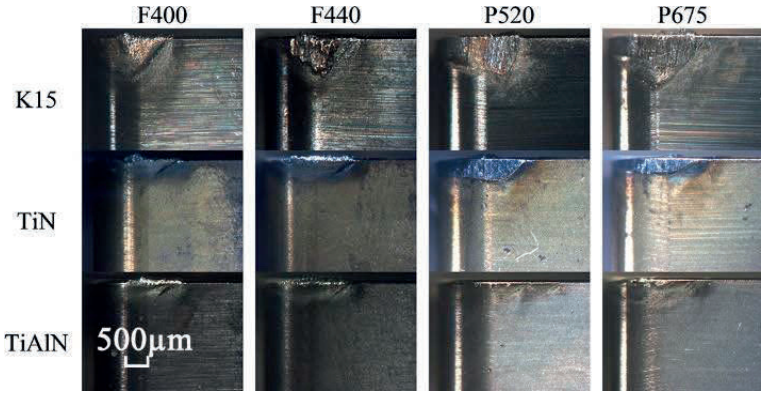

Fig. 18. Cutting speed 150 m/min, cutting length 300 m.

Built-up edge (BUE) can be defined as highly strained workpiece material accumulated on the cutting edge of the tool [4]. Because of its unstable nature, BUE periodically breaks and reforms. Therefore BUE is associated with inaccuracies, poor surface quality, variations in cutting forces and variation in cutting temperatures, which make it an undesirable phenomenon.

In the Fig. 17 it can be observed that BUE is considerably higher at 50 m/min than that at 150 m/min, and with a uniform appearance. The height from the rake face to the top of BUE was measured and shown in Fig. 19. As can be observed in, the height of the BUE was reduced approximately to the half as the workpiece strength increase, even few built-up edge was visible on the TiAlN coated tool in turning of P520 and P675.

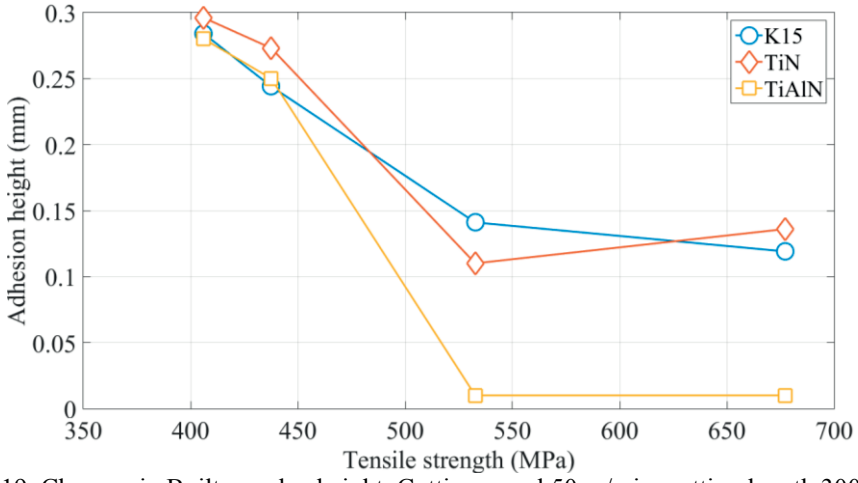

Fig. 19. Changes in Built up edge height. Cutting speed 50 m/min, cutting length 300 min.

The reason behind the high tendency to adhere on the tool of ductile cast iron is related to the amount of ferrite. Ferrite gives to ductile cast iron higher ductility, if it is considered that ductility is a property that has impact in the adhesiveness of workpiece.

3.3.3 Cutting forces

In turning, the cutting forces are measured in the coordinate system X, Y and Z as shown in Fig. 20, it is of common practice call this components as feed, thrust and principal cutting forces. The insert used in the experiments is a rectangular prism with rounded corners and chamfered edges, thus the relative position of the tool with respect of the X, Y and Z axis is defined by the tool holder as shown in Fig. 20.

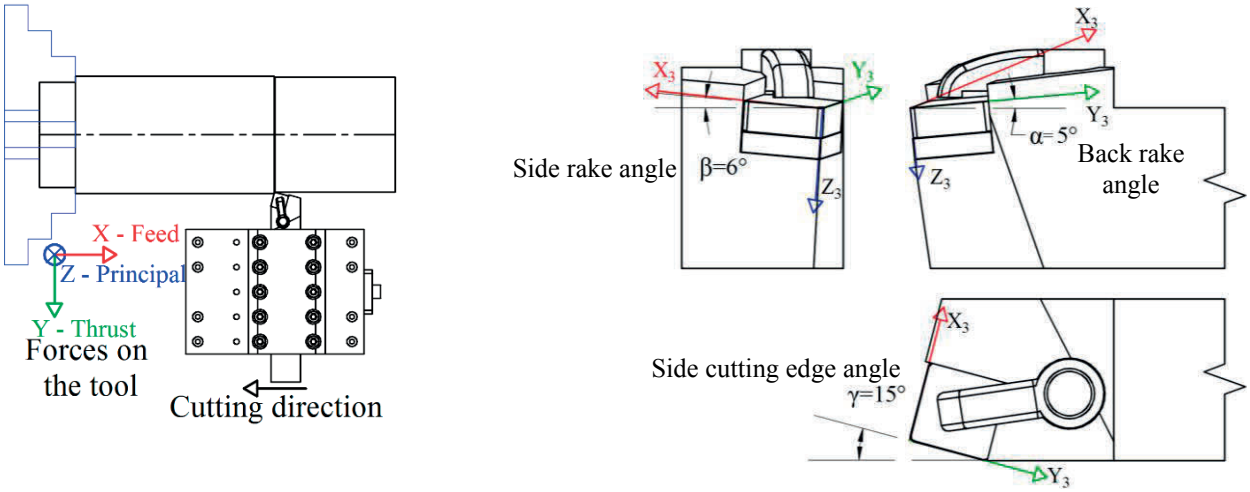

Fig. 20. Cutting force direction in X, Y and Z coordinate system

In the analysis of cutting forces, the cutting forces given in the X, Y and Z (feed, thrust and principal) can be transformed into a different coordinate system. This can be carried out by consecutive turns around a desired axis. For instance, to transform the cutting forces from X, Y and Z system into the X_3, Y_3 and Z_3 coordinate system attached to the tool, three consecutive turns are needed as shown in Fig. 21. All turns are carried out according to right hand rule for vectors.

The first turn around Z axis γ degrees in positive sense gives the next basic transformation matrix:

$$R^{(1)} = \begin{bmatrix} \cos(\gamma) & sin(\gamma) & 0 \\ -sin(\gamma) & cos(\gamma) & 0 \\ 0 & 0 & 1 \end{bmatrix} \quad (2)$$

The second turn around X axis α degrees in positive sense gives the next basic transformation matrix:

$$R^{(2)} = \begin{bmatrix} 1 & 0 & 0 \\ 0 & cos(\alpha) & -sin(\alpha) \\ 0 & sin(\alpha) & cos(\alpha) \end{bmatrix} \quad (3)$$

The third turn around Y axis β degrees in positive sense gives the next basic transformation matrix:

$$R^{(3)} = \begin{bmatrix} cos(\beta) & 0 & -sin(\beta) \\ 0 & 1 & 0 \\ \sin(\beta) & 0 & cos(\beta) \end{bmatrix} \quad (4)$$

Finally the transformation matrix is given as combination of the three basic turns as follows:

$$[T] = R^{(3)}R^{(2)}R^{(1)}$$

$$[T] = \begin{bmatrix} \cos(\gamma)\cos(\beta) + \sin(\gamma)\sin(\alpha)\sin(\beta) & \sin(\gamma)\cos(\beta) - \cos(\gamma)\sin(\alpha)\sin(\beta) & -\cos(\alpha)\sin(\beta) \\ -\sin(\gamma)\cos(\alpha) & \cos(\gamma)\cos(\alpha) & -\sin(\alpha) \\ -\sin(\gamma)\sin(\alpha)\cos(\beta) + \cos(\gamma)\sin(\beta) & \sin(\gamma)\sin(\beta) + \cos(\gamma)\sin(\alpha)\cos(\beta) & \cos(\alpha)\cos(\beta) \end{bmatrix} \quad (5)$$

Since the basic transformation equation consider the positive or negative sense of rotation, it is not necessary to consider the angle as negative in equation (5).

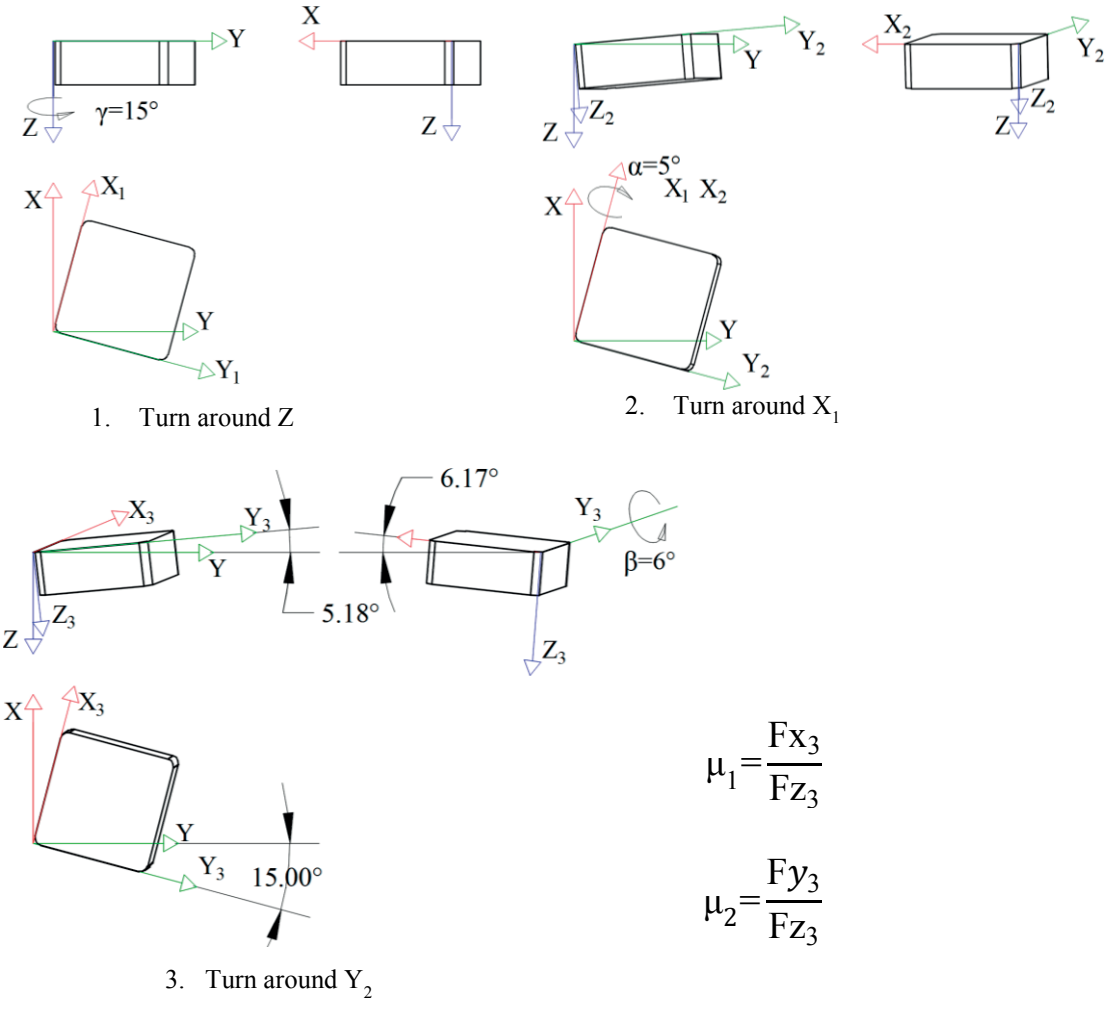

1. Turn around Z

2. Turn around X_1

3. Turn around Y_2

$$\mu_1 = \frac{Fx_3}{Fz_3}$$

$$\mu_2 = \frac{Fy_3}{Fz_3}$$

Fig. 21. Basic turns for transforming the force vector from X, Y and Z of dynamometer to X3, Y3 and Z3 of cutting tool.

The final transformation gives angles quite close to those shown in Fig. 20 provided for the tool holder manufacturer. This result is applied for the calculation of variation in friction coefficient on the rake face, as it was proposed by Tezuka et al. [32] in order to evaluate the adhesiveness to tool-chip interface. This

method is equivalent to calculate the friction coefficient μ_2 in direction of the side edge direction (Y_3) and the friction coefficient μ_1 end edge direction (X_3). In this method is assumed that force components in X_3 and Y_3 are due to the interaction between chip and tool on rake face, thus the ratio between the mean value of μ_2 and the mean value of μ_1 represent the average chip flow angle in the coordinate system fixed on the tool. Therefore, the difference of fluctuation between μ_1 and μ_2 probably is due to the variation of the chip flow direction.

Fluctuation of friction coefficient when machining F400

Fig. 22 shows the fluctuation of friction coefficient when turning F400 with coated and uncoated tools.

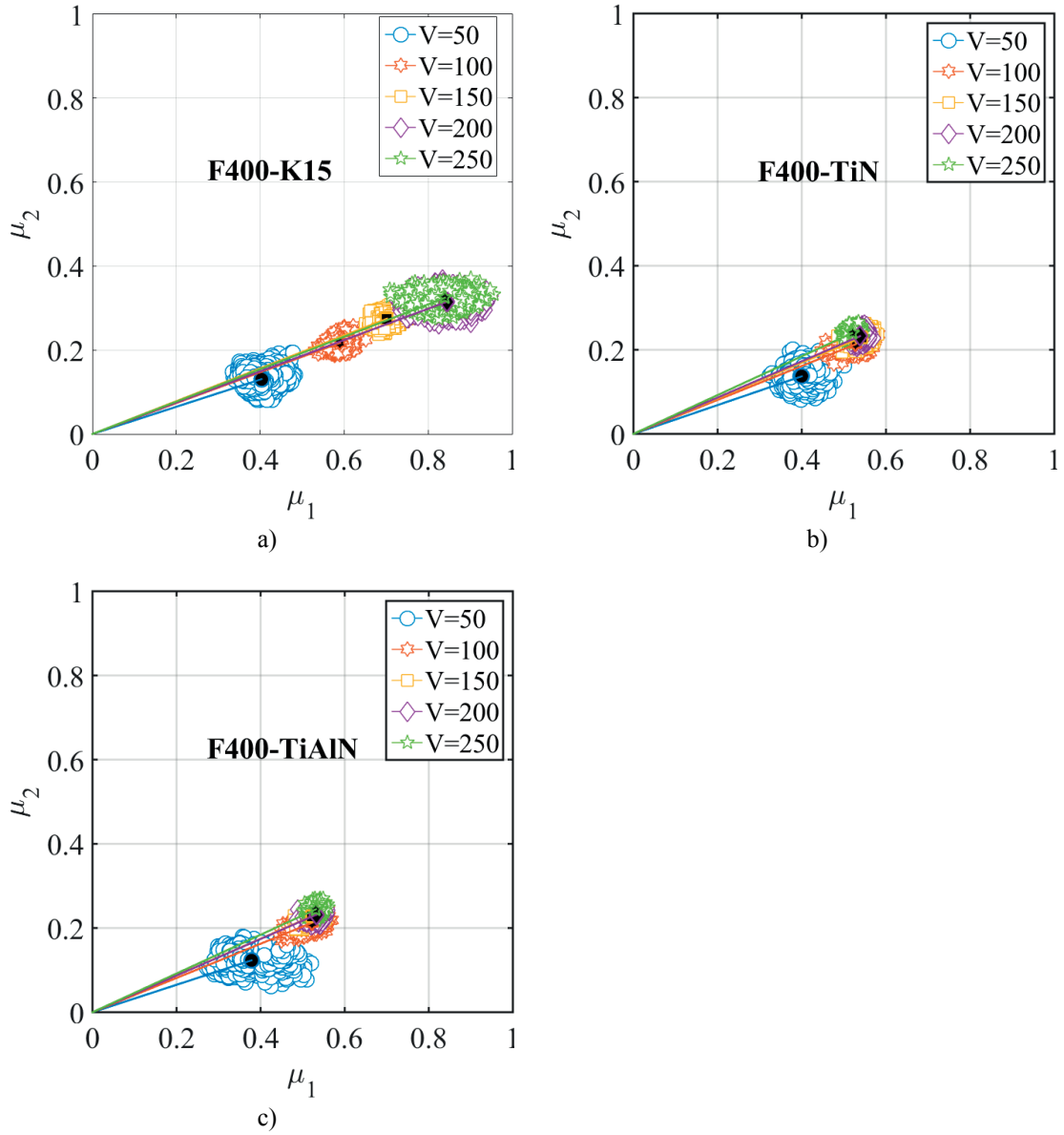

Fig. 22. Fluctuation of friction coefficient when machining F400 with coated and uncoated tools.

When turning F400 with K15, the friction coefficient increases with the cutting speed. At the cutting speed of 200 and 250 m/min the friction coefficient was practically the same. The dispersion of data or variability of friction coefficient can be evaluated in many ways. By visual inspection of Fig. 22, it can be seen that at 50, 200 and 250 m/min, the variability of friction coefficient was the highest. As shown in Fig. 17, when machining ductile cast iron with K15 at 50 m/min high BUE was observed. At cutting speeds exceeding 150 m/min, the adhered workpiece on rake and flank face was quite large. Therefore, the reason of variability of friction coefficient at low cutting speed is thought to be because of BUE and at high cutting speed because of large adhesion (as shown in Fig. 18).

When turning F400 with coated carbide tools, only at 50 m/min the friction coefficient was particularly low. Probably it was caused by BUE on rake angle. As the cutting speed increased the variability of friction coefficient decreased and the mean value became stable. Table 6 shows the standard deviation of friction coefficient. The standard deviation was calculated using the equation 6.

$$S_j = \sqrt{\frac{1}{N-1}\sum_{i=1}^{N}\left|\mu_{j,i} - \bar{\mu_j}\right|} \tag{6}$$

With the standard deviation, the variability of friction coefficient around the mean value can be evaluated. These values confirm what can be visually observed on Fig. 28.

Table 6. Standard deviation of friction coefficient when turning F400 with coated and uncoated carbide tools.

Tool \ $\bar{V}$	50 m/min		100 m/min		150 m/min		200 m/min		250 m/min	
	μ_1	μ_2	μ_1	μ_2	μ_1	μ_2	μ_1	μ_2	μ_1	μ_2
K15	0.022	0.016	0.015	0.010	0.016	0.010	0.038	0.016	0.035	0.014
TiN	0.043	0.017	0.018	0.011	0.012	0.009	0.009	0.008	0.008	0.008
TiAlN	0.022	0.018	0.018	0.011	0.012	0.009	0.009	0.008	0.008	0.007

Fluctuation of friction coefficient when machining F440

Fig. 23 shows the fluctuation of friction coefficient when turning F440 with coated and uncoated tools. When turning F440 with K15 the behavior was similar to that observed when cutting F400. However when turning F440 at cutting speed exceeding 100 m/min, the mean friction coefficient did not change as drastically as that in turning F400. In turning ferritic ductile cast iron at low cutting speed, there was not

evident flank wear but large BUE. However, ferrite in F440 is harder than ferrite in F400, thus ferrite in F440 should be less ductile and less prone to adhere, as consequence BUE could be lower when turning F440 than when turning F400.

On the other hand, when turning F440 with coated tools, the friction coefficient was lower at cutting speeds exceeding 50 m/min. Furthermore the mean friction coefficient converged approximately to the same value at cutting speeds exceeding 50 m/min.

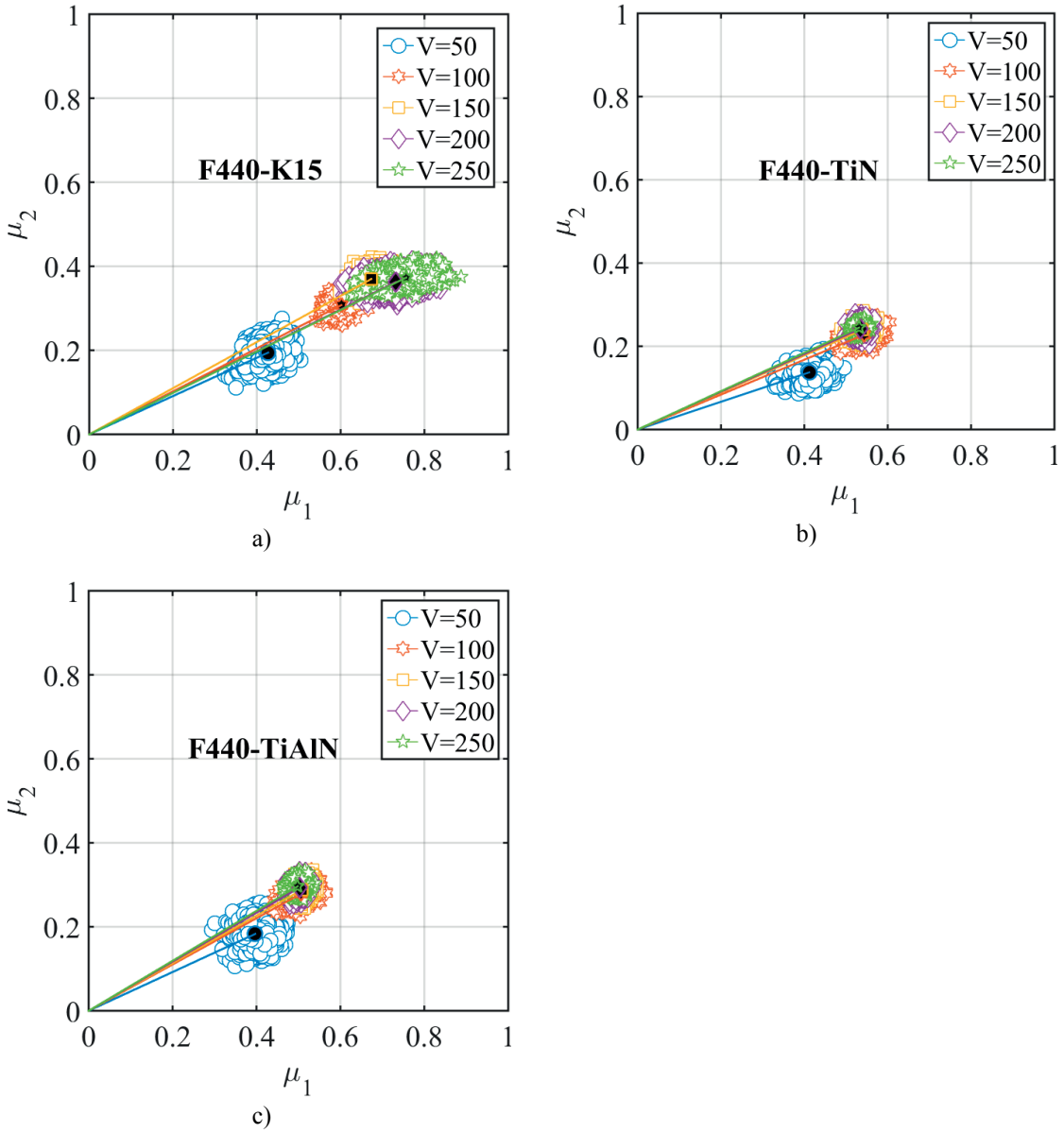

Fig. 23. Fluctuation of friction coefficient when turning F440 with coated and uncoated tools.

Table 7 shows the standard deviation of friction coefficient. If ferritic ductile cast iron is cut at low (~50 m/min) or high (>200 m/min) cutting speed with K15 the variation of friction coefficient is higher than an intermediate cutting speed (100-150 m/min).

Table 7. Standard deviation of friction coefficient when turning F440 with coated and uncoated carbide tools.

Tool \ V	50 m/min		100 m/min		150 m/min		200 m/min		250 m/min	
	μ_1	μ_2	μ_1	μ_2	μ_1	μ_2	μ_1	μ_2	μ_1	μ_2
K15	0.024	0.021	0.017	0.015	0.021	0.015	0.042	0.016	0.041	0.015
TiN	0.025	0.024	0.018	0.015	0.013	0.013	0.010	0.011	0.010	0.011
TiAlN	0.025	0.015	0.018	0.013	0.013	0.012	0.010	0.010	0.008	0.007

Fluctuation of friction coefficient when machining P520

Fig. 24 shows the fluctuation of friction coefficient when turning P520 with coated and uncoated tools.

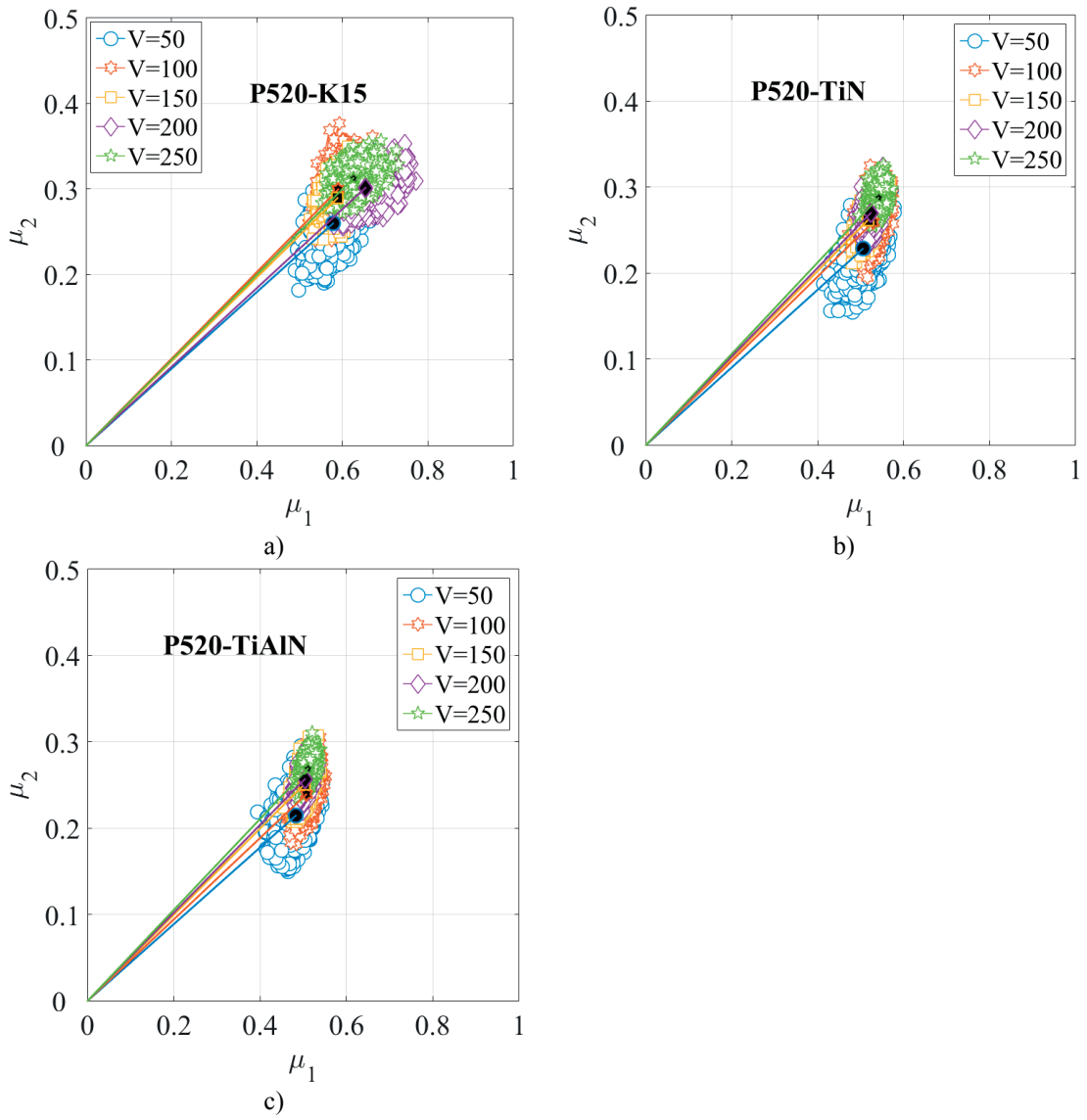

Fig. 24. Fluctuation of friction coefficient when machining P520 with coated and uncoated tools.

In turning of P520 with K15, the mean friction coefficient did not vary with cutting speed as in the case of ferritic ductile cast iron. The standard deviation shown in Table 8, revealed that there was not a specific tendency regarding the variation of friction coefficient. However the standard deviation was higher when cutting with uncoated carbide tool.

As illustrated by Fig. 24 can be observed that both coated tools showed similar behavior regarding mean friction coefficient. Apparently the dispersion of points around the mean value reduce as the cutting speed increase. This can be confirmed with the standard deviations of friction coefficient shown in Table 8.

Table 8. Standard deviation of friction coefficient when turning P52 with coated and uncoated carbide tools.

Tool \ V	50 m/min		100 m/min		150 m/min		200 m/min		250 m/min	
	μ_1	μ_2	μ_1	μ_2	μ_1	μ_2	μ_1	μ_2	μ_1	μ_2
K15	0.027	0.025	0.019	0.019	0.020	0.015	0.031	0.014	0.024	0.012
TiN	0.022	0.022	0.014	0.018	0.011	0.014	0.010	0.012	0.009	0.010
TiAlN	0.024	0.024	0.015	0.018	0.011	0.014	0.011	0.013	0.010	0.011

Fluctuation of friction coefficient when machining P675

The fluctuation of friction coefficient when turning P675 with coated and uncoated tools is shown in Fig. 25. The behavior of friction coefficient fluctuation was similar to that of P675.

Once again, there is not apparent tendency in the variation of friction coefficient when turning P675 with K15 as the cutting speed change. When turning P675 with coated tools, fluctuation of friction coefficient also reduces as the cutting speed increase as confirmed by the standard deviation shown in Table 9.

Table 9. Standard deviation of friction coefficient when turning P675 with coated and uncoated carbide tools.

Tool \ V	50 m/min		100 m/min		150 m/min		200 m/min		250 m/min	
	μ_1	μ_2	μ_1	μ_2	μ_1	μ_2	μ_1	μ_2	μ_1	μ_2
K15	0.0240	0.0192	0.0211	0.0139	0.0273	0.0110	0.0283	0.0098	0.0232	0.0094
TiN	0.0192	0.0182	0.0106	0.0143	0.0084	0.0112	0.0072	0.0098	0.0069	0.0088
TiAlN	0.0162	0.0163	0.0099	0.0134	0.0087	0.0114	0.0082	0.0099	0.0091	0.0086

The standard deviation of friction coefficient confirm what can be observed in the graphs. However it is difficult to check qualitatively and quantitatively the fluctuation of friction coefficient since most of the graphs are overlapped. Therefore, the standard deviation can be used as an indicator of deviation from the mean value.

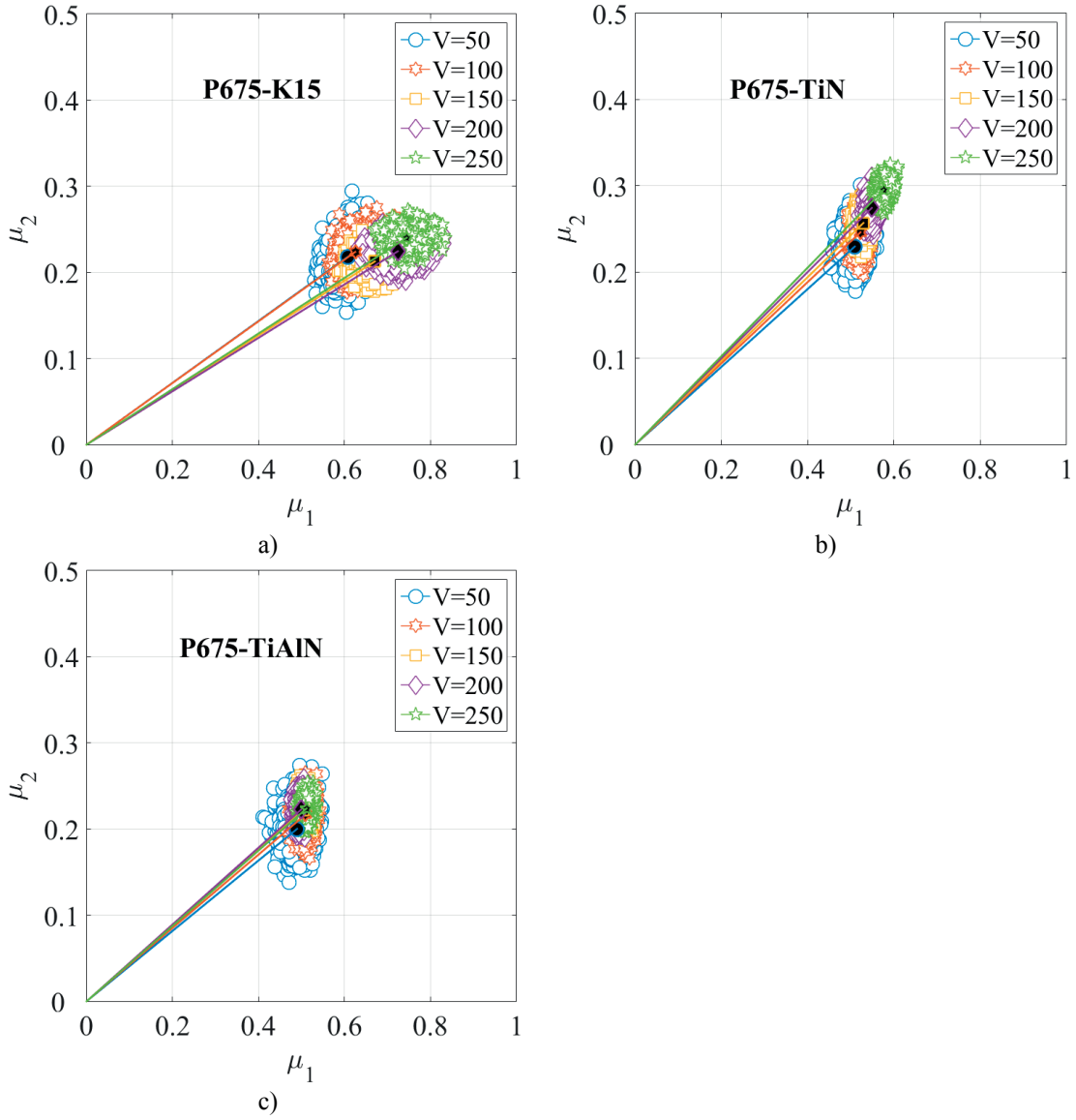

Fig. 25. Fluctuation of friction coefficient when turning P675 with coated and uncoated tools.

Resultant cutting force

The resultant cutting force represents the general behavior of the force components in radial, feed and principal direction, therefore the resultant cutting forces was used to describe the differences in cutting forces during turning a ductile cast iron. The change of mean resultant cutting force with the cutting speed is shown in Fig. 26.

The highest values of resultant cutting force for all the tools was obtained during cutting pearlitic ductile cast iron. While on the contrary the lowest values was obtained by cutting ferritic ductile cast iron, as was expected.

In turning P675 with TiAlN coated tool the maximum cutting force was 734N at 50 m/min. Then, the cutting forces decreased gradually as the cutting speed was increased until reach the minimum of 635 N at 250 m/min. A similar behavior was observed for the P520 but the force decreased from 574 N to 510 N.

In turning of F440 with TiAlN coated tool, the cutting force kept practically a constant value of 440 N in the range from 100 m/min to 250 m/min. However at 50 m/min the cutting force was 382 N. As shown in Fig. 26, the ferritic cast iron has strong tendency to adhere on the tool and form BUE. Thus the low cutting force was attributed to the large BUE. Similar behavior was observed in turning of F400, however the cutting force was approximately 60 N higher than that in F440.

The cutting forces obtained in turning of P675 with TiN coated tool followed approximately the same behavior and the same values as with TiAlN coated tool. The highest difference was observed in the turning of P675 in which the cutting force decreased from 644 N at 50 m/min to 614 N at 250 m/min.

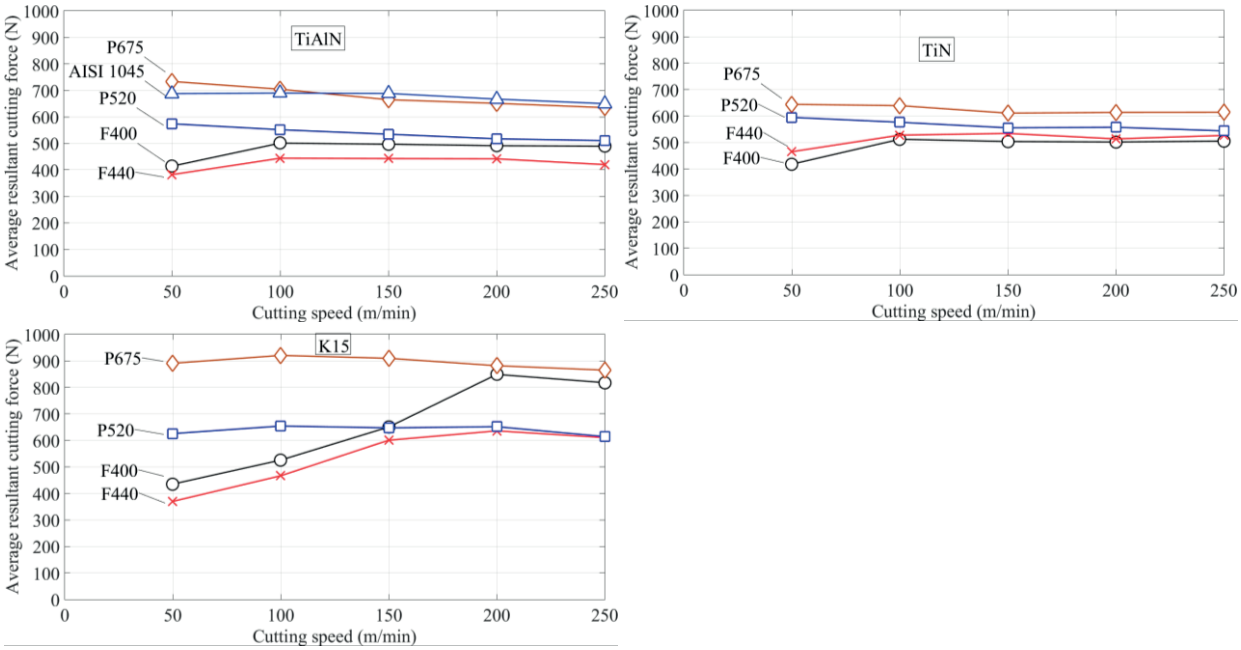

Fig. 26 Cutting forces when turning ductile cast iron with TiN coated, TiAlN coated and K15 carbide tool.

As illustrated by Fig. 26, when the coated tools were used, the cutting forces did not change drastically as the cutting speed increased, but showed a stable behavior. However when the carbide tool was used in turning F400 and F440, the cutting force increased gradually from 50 m/min to 200 m/min and exceeding 200 m/min the cutting force was stable. This behavior was attributed to the BUE observed over the cutting

edge of K15 at 50 m/min which gradually decreased as the cutting speed increased. This can be explained in terms of the high BUE which caused the increase in the rake angle provoking an increase in the shear angle, and therefore a decrement in cutting force [33]. Built-up edge reduces with cutting speed up to the force became stable. After that the cutting forces are no longer influenced by the BUE.

3.3.4 Cutting temperature

The change in cutting temperature caused in cutting of different grades of ductile cast iron at different cutting speed with TiN coated is summarized in Fig. 27.

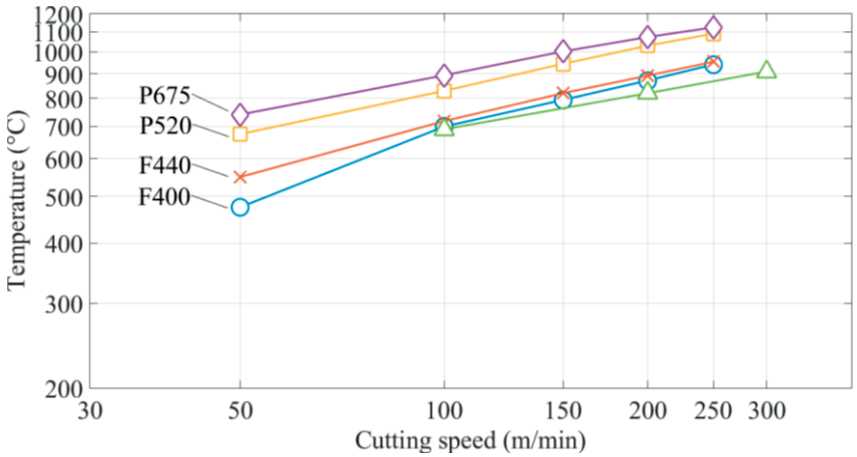

Fig. 27. Cutting temperature on TiN coated tool coated tool in the turning of ductile cast iron.

The difference in cutting temperature between the coated tools was considered negligible. For example, the difference in cutting temperature between TiN and TiAlN coated tools, in turning F400 was only 25°C.

The average cutting temperature increased with both the tensile strength of ductile cast iron and the cutting speed. This behavior was expected from the point of view of the high energy required for cutting materials with high strength at high cutting speed. The highest temperature measured was 1124°C in turning of P675 at 250 m/min, and the lowest temperature measured was 475 °C in turning of F400 at 50 m/min. A linear relationship in logarithmic scale was observed, except of F400 and F440 at 50 m/min. Because the temperature in this point was lower than the recrystallization temperature and BUE was generated.

The cutting temperature was also measured when turning ductile cast iron with the P15 carbide tool (Fig. 28). The behavior of cutting temperature in turning of F400 and F440 was not formed by a single line as in the case of the coated tools, instead two lines divided by the point at 150 m/min of cutting speed were observed. This behavior supports the observation of high BUE on carbide tools.

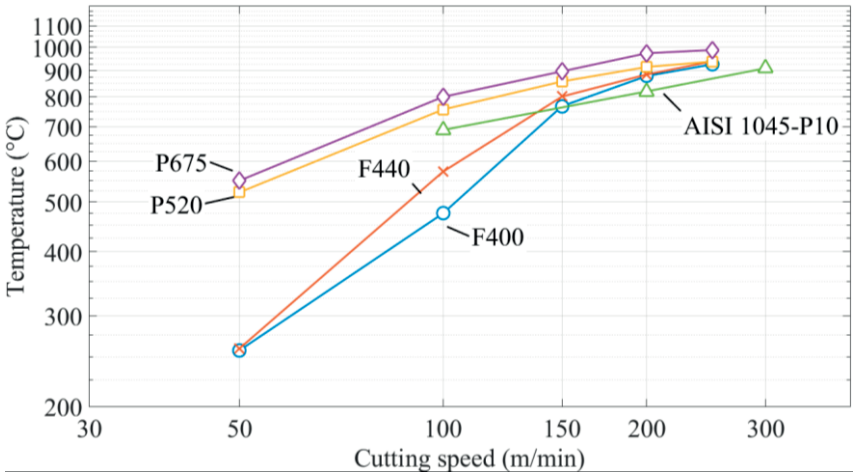

Fig. 28. Cutting temperature in turning of ductile cast iron with the P15 carbide tool.

3.4 Discussion

3.4.1 Characteristic in the machining of ductile cast iron

Ductile cast iron is also known as spheroidal cast iron, because of the spheroidal shape of graphite dispersed randomly on the matrix. In comparison with graphite, the matrix has higher strength and hardness. It is thought that the spheroidal graphite causes a phenomenon similar to interrupted cutting, in which the tool firstly cut through the hard pearlite or ferrite matrix, then passes through the soft graphite and again return to the hard matrix. As this process continues, the adhered material eventually wears out the tool, causing wear by adhesion. In order to evaluate the passes per meter of cutting length, the average spacing between the nodular graphite was calculated by using image processing and programming in Matlab®. The process of nodule identification and spacing calculation can be summarized as follows:

1. Firstly the black graphite nodules were identified (circled and numbered in Fig. 29).
2. The radii and position was acquired.
3. Finally the distance between every spheroid and its nearest neighbor was calculated and averaged.

The accuracy of this method depends on the aspect shape of the nodules, image quality and contrast of color between the black nodules and background (matrix). Other important aspect is that the nodules are randomly dispersed and the direction in which the tool cuts is also random. The intention of this calculation is to have an image of how often the tool (especially cutting edge), passes through soft nodules and return to hard matrix.

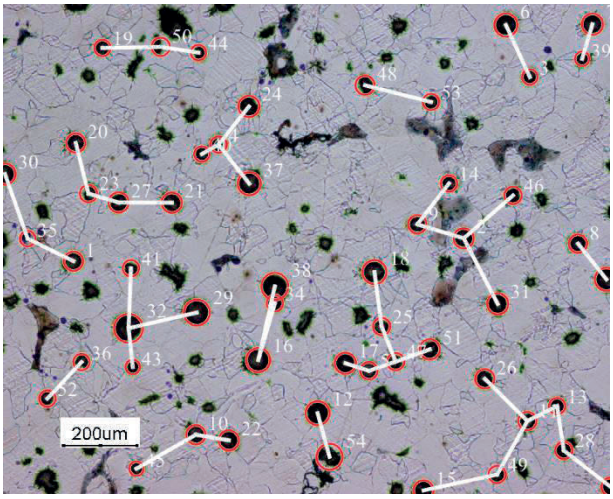

Fig. 29. Nodule identification and distance calculation for F400.

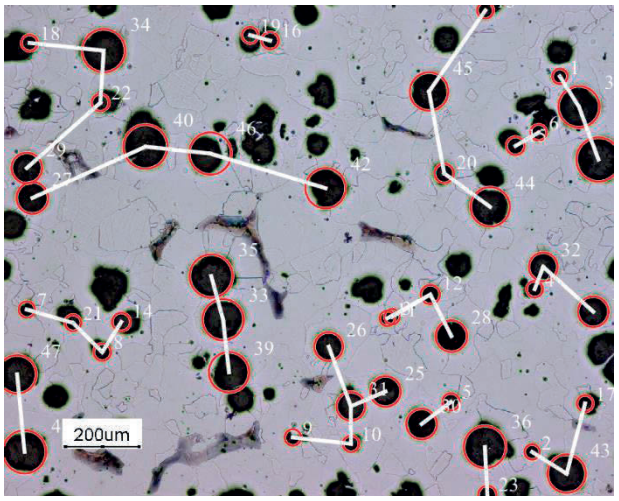

Fig. 30. Nodule identification and distance calculation for F440.

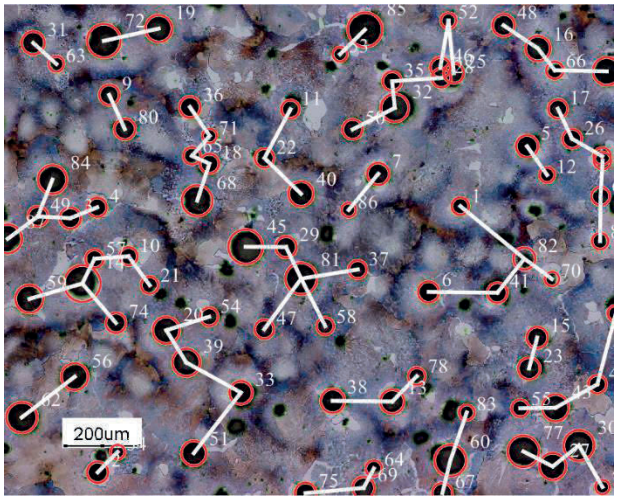

Fig. 31. Nodule identification and distance calculation for F520.

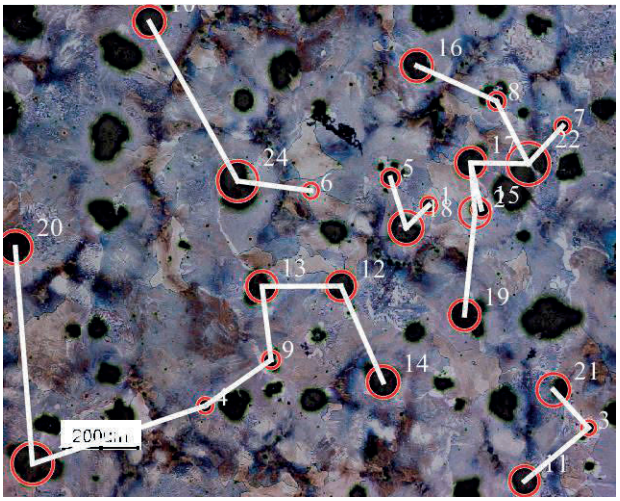

Fig. 32. Nodule identification and distance calculation for F675.

The average minimum spacing was as follows: 76 µm for F400, 65 µm for F440, 46 µm for P520 and 139 µm for P675. Total average diameter of nodules for all workpieces is 53 µm. Total average nodule distance of all workpieces is about 81.5 µm which means that a tool passes from hard matrix to soft graphite a total average of 7440 times per every meter of cutting length.

Fig. 33 shows an illustrative in real proportion of overall graphite diameter approaching to the cutting edge.

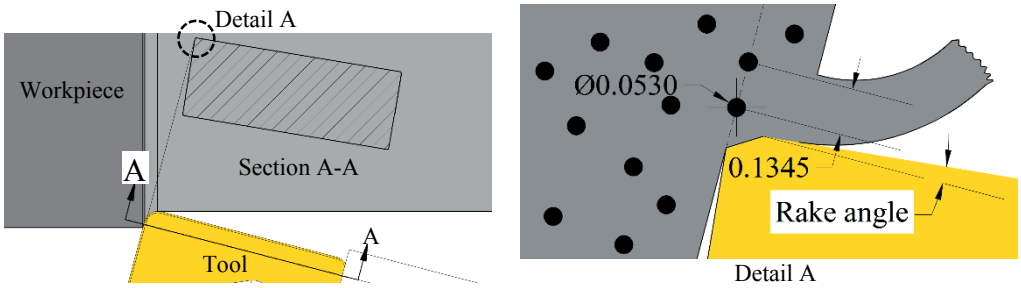

Fig. 33. Illustrative image of graphite in real proportion with respect to the tool and graphite

As shown in Fig. 33, graphite size is enough to cover considerable part of cutting edge. Therefore when a particle of ductile cast iron adheres on the tool, this particle encounter a higher probability to detach in comparison with materials like plain carbon steel, which does not have graphite on its composition and consequently the cutting process is completely continuous.

graphite covers basically all chamfer, therefore when a ductile cast iron particle adheres to the tool, this particle encounter a higher probability to detach in comparison with materials like the AISI 1045, which does not have soft matter in its composition; consequently the machining is completely continuous.

3.4.2 Wear rate differences

It is well known that work materials with high strength and therefore with high hardness produce a detrimental effect on the performance of cutting tools regarding cutting forces and wear. The pearlitic cast iron with its high tensile strength and Vickers hardness caused the highest cutting forces, cutting temperatures and wear rates. As shown in Fig. 34, the difference in wear rate between the pearlitic grades is not as high as between the ferritic grades. This difference is due to the higher micro Vickers hardness of F440 in comparison with F400; also because F440 contains between 4-7% of lamellar pearlite and F400 contains almost not pearlite. If a high hardness workpiece adheres on the tool, the higher damage occurs when adhesion drop off. On the other hand, if the adhered material has low hardness and therefore high ductility, the BUE remains on the tool. As can be observed in the photographs of Fig. 17 and Fig. 18, the high ductile ferritic cast iron adheres easier than the hard pearlitic cast iron. However as shown in Fig. 34, the highest wear rate was found in turning of pearlitic cast iron.

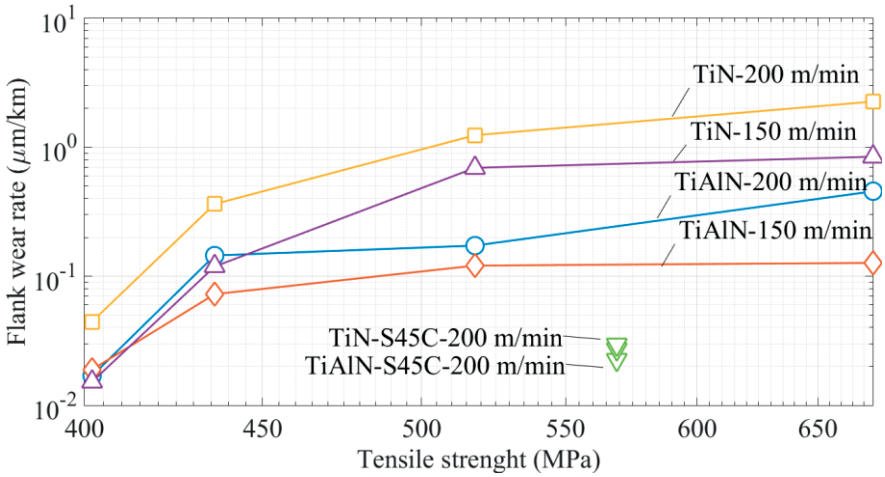

Fig. 34. Wear rate progress on coated tool at 200 and 150 m/min

In spite of the fact that the cutting forces for both coated tools were similar, the flank wear rate was quite different. The wear rate of TiN coated tool was larger than that of TiAlN coated tool, which is likely due to the better chemical and mechanical stability at high temperature of the TiAlN coating. TiN suffer a decrease in its hardness over 400°C of annealing temperature due to recovery and recrystallization. Furthermore TiN coating starts to oxidize around of 550°C, whereas TiAlN coating reacts with hot air at 800°C [34]. On the other hand, the hardness of TiAlN increase in the interval of annealing temperature from 600°C to 950°C [35]. Additionally, TiAlN coating also has the ability for self-adaptation to the thermal load applied during

cutting by age hardening [36]. Measurements of micro Vickers hardness at high temperature indicates that exceeding 750°C, TiAlN has considerably higher hardness than TiN [37].

From Fig. 27, it can be seen that by turning P520 and P675 with TiAlN coated tool at the cutting speed exceeding 150 m/min, the average cutting temperature was higher than 950°C. Therefore high wear rate should be expected due to the reduction in its hardness. For this reason ductile cast iron with similar characteristics of P520 and P675 should be turned at cutting speed below at the cutting speed of 150 m/min. On the other hand, during turning F440 and F400 with TiAlN coated tool, the cutting temperature was lower than 900°C at the cutting speed of 200 m/min and lower than 800°C at the cutting speed of 150 m/min. This indicates that ferritic ductile cast iron can be machined with TiAlN coated tool at the cutting speed of 150 m/min and expect a long tool life regarding flank wear with few adhesion. Also there is tradeoff between high flank wear at high cutting speed (>200 m/min) and high BUE at low cutting speed (<100 m/min) seems to have an equilibrium at the cutting speed of 150 m/min.

A particular characteristic in the behavior of the flank wear progress of coated tools plotted versus the cutting length in logarithmic scale was observed. This characteristic correspond to the change in the slope of the wear curves during the turning of P675, P520 and F440 with TiAlN coated tool at the cutting speed of 200 m/min and 150 m/min. This was also observed when turning F440 at the cutting speed of 200 m/min, P675 and P520 at the cutting speed of 150 m/min with the TiN coated tool. Some of these results are repeated in Fig. 35 but in logarithmic scale. In chamfered tools, the highest concentration of stress and temperature are found on the chamfer zone specifically on the cutting edge. This affirmation is in agreement with the findings obtained from different finite element simulations and experimental results about the stress and temperature distribution on chamfered tools [38], [39] and [40].

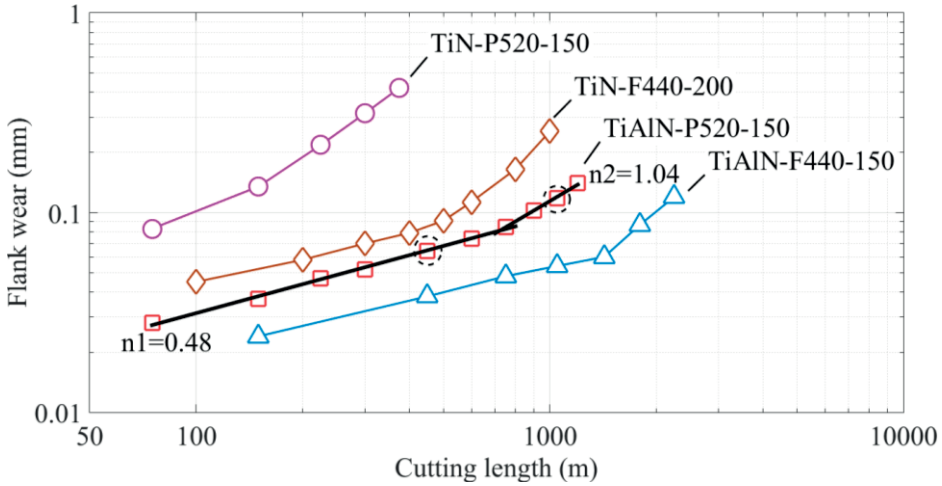

Fig. 35. Flank wear on coated tools vs cutting length in log-log scale.

It is thought that this concentration of stress and temperature contributes to the loss of the coating which cause the change in the wear rate. In order to show the effect of the loss of coating on the wear rate, the flank wear experiment on the TiAlN coated tool at the cutting speed of 150 m/min in the turning of P520 was repeated. In this experiment the points enclosed with dashed circles represent the stage before (in left side) and after (in right side) the wear rate changed. By looking at Fig. 35, the change in wear rate of TiAlN coated tool in turning of P520 at 150 m/min is less noticeable than the other conditions. However the difference in the slope between the first (n1) and the second line (n2) is more than twice.

At the cutting length corresponded to the point marked with a dashed circle, the distribution of Titanium was mapped, over the surface of the cutting tool by using Energy Dispersive Spectroscopy, these photographs are shown in Fig. 36. In Fig. 36 the green color represents the presence of Titanium, the darkest zones were covered mainly by Iron, which means that after the coating layer is worn out, the workpiece adheres easier on the damaged zone. By looking at Fig. 36 the lack of coating layer around the chamfer zone is evident. After the coating layer was worn out, the wear rate depends on the substrate material.

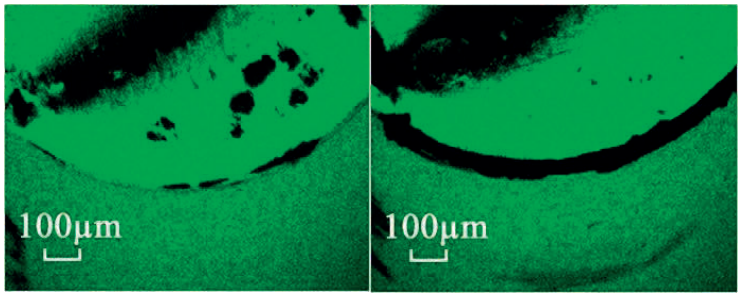

Fig. 36. Titanium distribution on the TiAlN coated before and after the changing in wear rate.

Because the substrate material has poorer properties regarding wear resistance than the coating material, the flank wear became larger at lower cutting lengths than it was when the coating layer prevailed, which means that the wear rate increase.

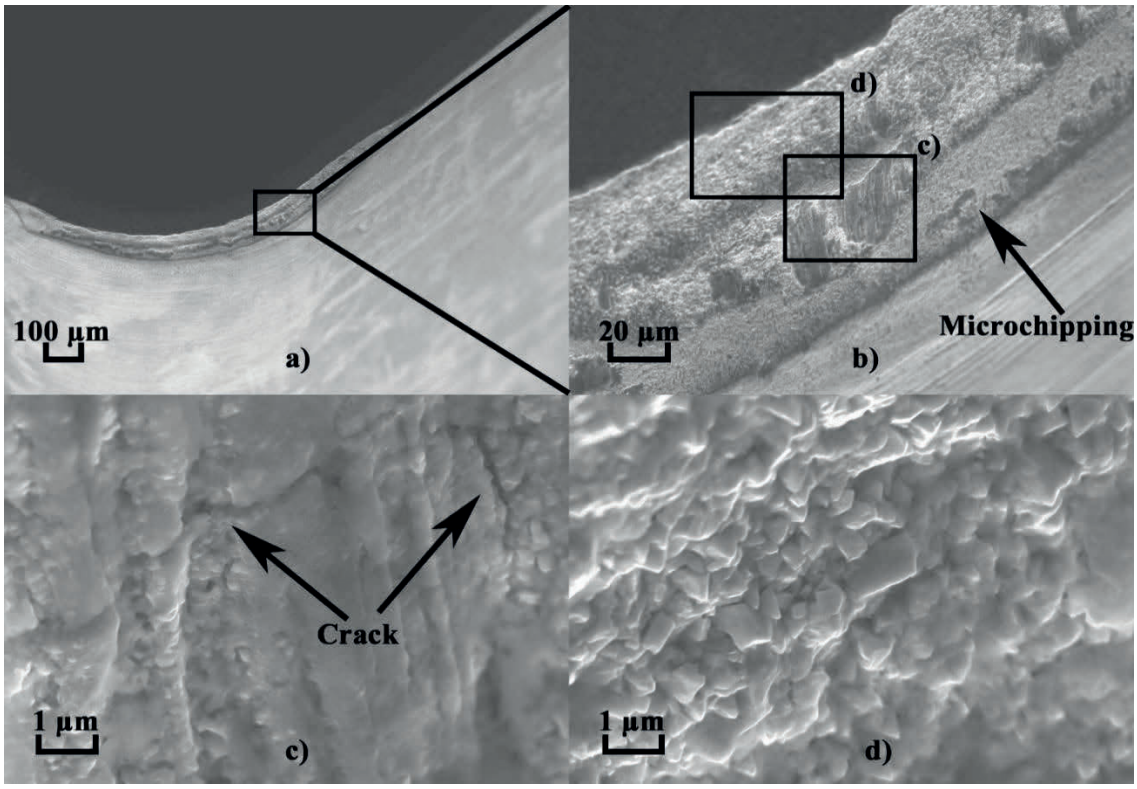

Fig. 37. SEM photographs corresponding to the flank face. Tool: TiAlN coated; workpiece: P520; cutting speed: 150 m/min

Fig. 37a) shows the SEM image of the tool in right hand photograph shown in Fig. 36. Fig. 37b) shows a magnification of the area enclosed by squares in Fig. 37a). In the same way as Fig. 37 b), Fig. 37 c) and Fig. 37 d) shows a magnification of the area enclosed by squares in Fig. 37 b), around the center of the flank wear.

Fig. 37 d) shows clearly exposed WC grains of the substrate material, which confirms the lack of coating. This area corresponds to the nearest zone of the cutting edge. Although most of the adhered workpiece material was removed by the acid bath, some thin layer of iron still remain as shown in Fig. 37 c). It was deducted that in the tool area shown in Fig. 37 c) there is some adhered workpiece because although the WC grains are visible, a kind of layer covering the WC grains made difficult to visualize the WC grains as clear as in Fig. 37 d). Fig. 37 c) shows a crack traveling parallel to the cutting edge and then going down.

If the cutting is continued, probably the zone around the crack break off as a consequence of the crack and the abrasive wear, as a consequence, the WC grains can become exposed as in Fig. 37 d).

Loss of TiAlN coating was reported previously in the turning of the difficult-to-machine material as Inconel 718® [41]. Although this phenomenon is mostly found in the milling hard materials like AISI H13, Inconel 718® and Ti-6442S as reported on [42], [43], [44], [45], because of the nature of interrupted cutting regarding intermittent, thermal and impact loads where a spectroscopy analysis was use in the detecting of coating separation. The complete analysis of the relationship between the loss of coating and the change in wear rate is discussed in the chapter 6. In chapter 6 more evidence about the worn out of coating and its effect on the flank wear progress curves, is given by testing different workpiece materials.

3.5 Conclusion

In this study, four different specimens of ductile cast iron were turned with K15 carbide, TiN coated and TiAlN coated tool in order to investigate the wear characteristics and cutting performance. The wear mechanism was proposed and the tool performance was evaluated in base on the results obtained experimentally; the flank wear width, cutting forces and mean cutting temperature. This results are summarized as follows.

1. Cutting forces and cutting temperatures were similar for both coated tools. However flank wear was considerably higher on TiN coated tool than on TiAlN coated tool. The best stability of TiAlN coated tool at high temperatures such as those found in the turning of pearlitic cast iron and the lowest BUE observed in turning of ferritic cast iron, make it more suitable in turning of ductile cast iron.
2. The tool wear mechanism characteristic in turning ductile cast iron is based on the fact that the tool first cut through the hard matrix, then it passes through the soft graphite and again return to the hard matrix. As this process continues, the adhered material eventually wears out the tool, causing wear by adhesion.
3. The analysis of the wear on coated tools was proposed by means of the wear curves in logarithmic scale instead of the usual linear scale. In this way, the change in the slope of wear was progress easily found; this phenomenon was related with the wear out of the coating layer. The partial loss of the coating layer was confirmed by the SEM photographs and EDS mapping images.

4. Machinability of pearlitic-ferritic ductile cast iron

4.1 Introduction

A special workpiece material (pearlitic-ferritic ductile cast iron) was prepared in order to investigate the gaining in machinability with respect to ferritic and pearlitic ductile cast iron. Pearlitic-ferritic cast iron has intermediate properties regarding tensile strength and ductility with respect to pearlitic and ferritic ductile cast iron; thus, it is expected to find intermediate machinability regarding cutting forces, flank wear and cutting temperature. Surprisingly, flank wear, cutting forces and cutting temperature resulted much closer to those measured when turning ferritic ductile cast iron than those measured when turning pearlitic ductile cast iron. This indicates that pearlitic-ferritic ductile cast iron is more feasible to use, if we consider that the pearlitic-ferritic ductile cast iron has close tensile strength to pearlitic ductile cast iron and keep good ductility at the same time.

4.2 Materials and methods

Materials were basically the same as those described on chapter 3, for completeness the chemical composition and mechanical properties of all workpieces are shown in Table 10 and Table 11, respectively.

Table 10 Chemical composition in mass % of the material tested (Including PF500).

	C	Si	Mn	P	S	Cu	Sn
F400	3.75	2.17	0.22	0.026	0.008	0.063	0.012
F440	3.65	2.59	0.25	0.030	0.005	0.072	0.007
PF500	3.74	2.47	0.23	0.023	0.008	0.026	0.003
P520	3.75	2.53	0.30	0.031	0.010	0.392	0.055
P675	3.75	2.46	0.36	0.019	0.006	0.894	0.050

Table 11. Mechanical properties of workpieces tested (Including PF500).

	UTS1 (MPa)	Rockwell B (HRB)	Elongation (%)	Pearlite amount (%)
F400	402	73.8	23.7	4.2
F440	436	81.4	25.3	4.2
PF500	495	88.8	17.6	44.6
P520	518	97.5	2.7	92.1
P675	674	100.2	4.0	92.6

As shown in Table 11, mechanical properties of PF500 are intermediate among all materials used. It is important to remark that tensile strength of P520 is only about 1.046 times greater than tensile strength of PF500, however, the elongation of PF is 6.5 times greater than that of P520. PF500 has around 45% of

pearlite while F440 and F400 have practically ferritic matrix with low amount of pearlite; on the other hand P520 and P675 matrix is practically all pearlite with low amount of ferrite.

The microstructure of PF500 is shown in Fig. 38. The appearance PF500 microstructure is like bull's eye structure in which the nodules are surrounded by ferrite and ferrite is surrounded by pearlite.

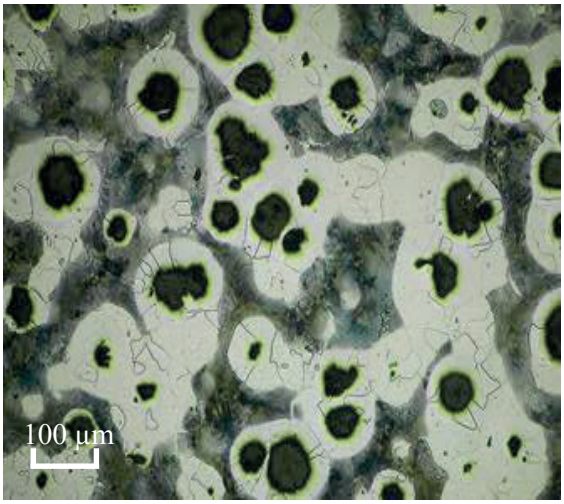

Fig. 38. Microstructure of all ductile cast iron including pearlitic-ferritic ductile cast iron PF500.

Cutting conditions and methods for measuring cutting forces, cutting temperature and flank wear, were the same used in the set of experiments reported in chapter 3. The difference is that only TiN coated tool was used in this set of experiments.

4.3Results

4.3.1 Flank wear

Flank wear progress when turning PF500 is shown in Fig. 39. At the cutting speed of 200 m/min, the flank wear on TiN coated tool when turning PF500 was intermediate between flank wear when turning F440 and F400. However, at the cutting speed of 150 m/min flank wear when turning PF500 was similar to flank wear when turning F440. In any case, the important point is that flank wear when turning PF500 is closer the ferritic grades than when turning pearlitic grades. It is important to mention that the result shown for F440 at 150 m/min was acquired from an experiment repeated by using different workpiece but same type of ductile cast iron that the result shown in Chapter 3. In any case the flank wear of PF500 falls in between of both ferritic grades of ductile cast iron.

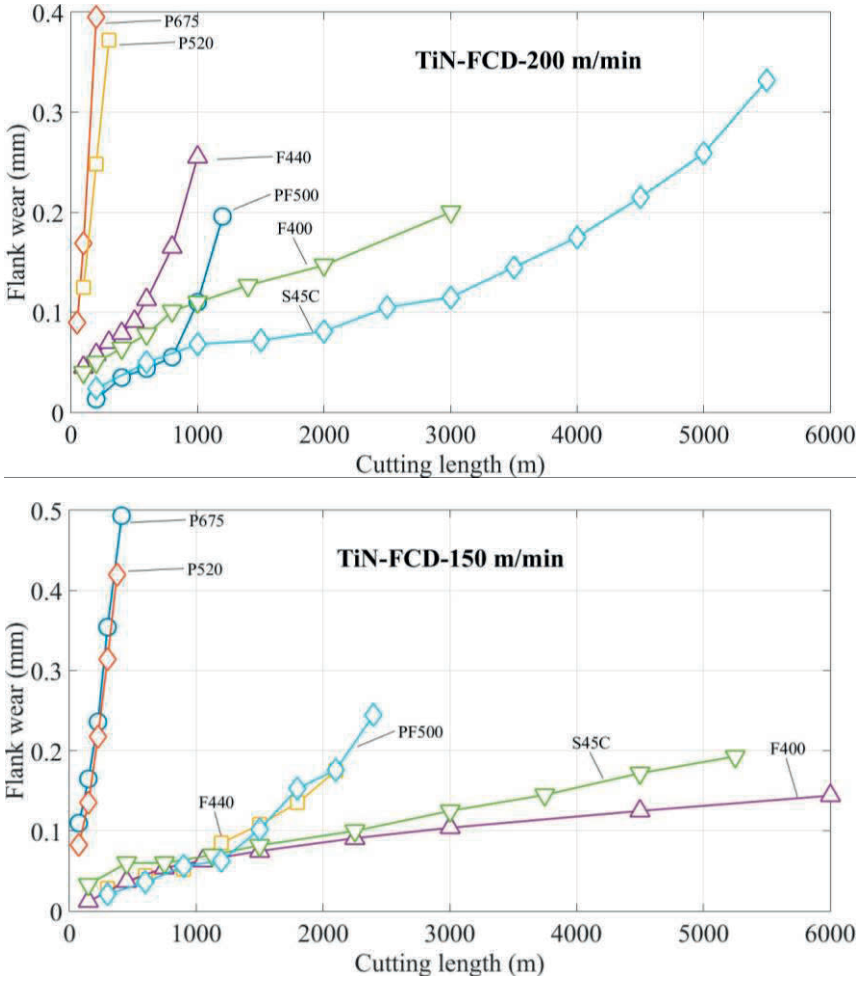

Fig. 39. Flank wear progress when turning pearlitic-ferritic ductile cast iron.

Other important point to be noticed is that the flank wear when turning P520 was much greater than when turning PF500, in spite of the fact that both have not so different tensile strength.

Fig. 40 shows the wear patter on TiN coated tool when turning F400, F440 and PF500. The photographs shown on Fig. 40 of wear pattern confirms numeral results of flank wear progress shown in Fig. 39 about the similarity between tool wear behavior when turning pearlitic-ferritic ductile cast iron and when turning ferritic ductile cast iron.

At 150 and 200 m/min, more adhesion could be observed when cutting F400; even BUE could be observed on the tool. However the machinability of F400 is the best among all workpieces tested regarding flank wear. The wear pattern observed when turning PF500 and F440 at 150 m/min was similar. However at the cutting speed of 200 m/min, flank wear when turning PF500 was lower than that when turning F440.

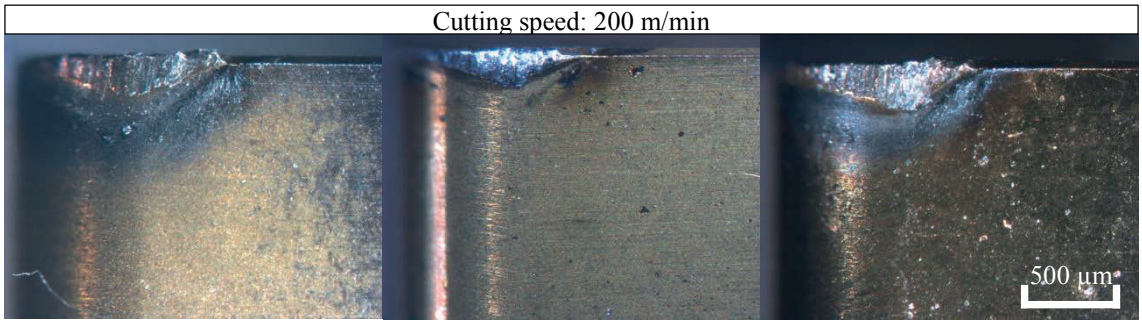

Workpiece: F400	Workpiece: PF500	Workpiece: F440
Cutting time: 15 min	Cutting time: 6 min	Cutting time: 5 min
VB=0.2 mm	VB=0.2 mm	VB=0.255 mm

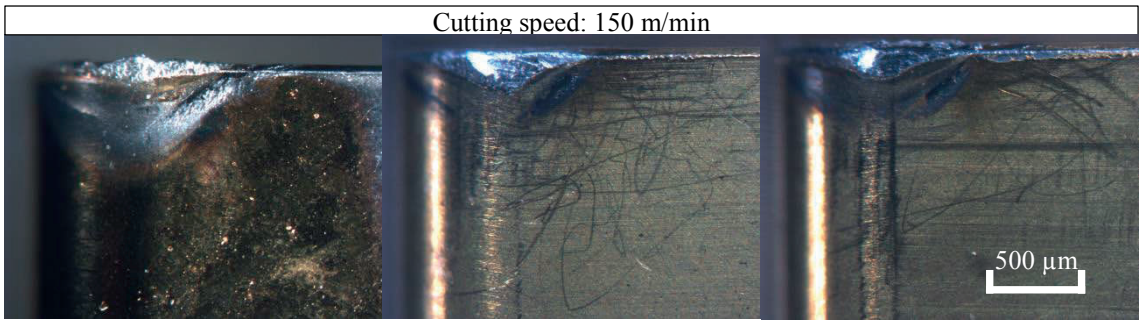

Workpiece: F400	Workpiece: PF500	Workpiece: F440
Cutting time: 40 min	Cutting time: 16 min	Cutting time: 14 min
VB=0.14 mm	VB=0.245 mm	VB=0.175 mm

Fig. 40. Photographs of wear on TiN coated tool when turning F400, PF500 and F440.

4.3.2 Cutting forces

Fig. 41 shows the components of cutting force when turning ductile cast iron. The behavior and magnitude of cutting force when turning PF500 are much closer to that of ferritic ductile cast iron than that of pearlitic ductile cast iron. This means that from the point of view of cutting forces PF500 is easier to cut without significant sacrifice of strength and ductility.

As shown in Fig. 41, the cutting the components in feed and radial direction when turning pearlitic ductile cast iron are stable. However when cutting PF500, F440 and F400 there is a considerable increase in turning force from 50 m/min until 100 m/min. This means that BUE was formed when machining PF500 at the cutting speed less than 100 m/min.

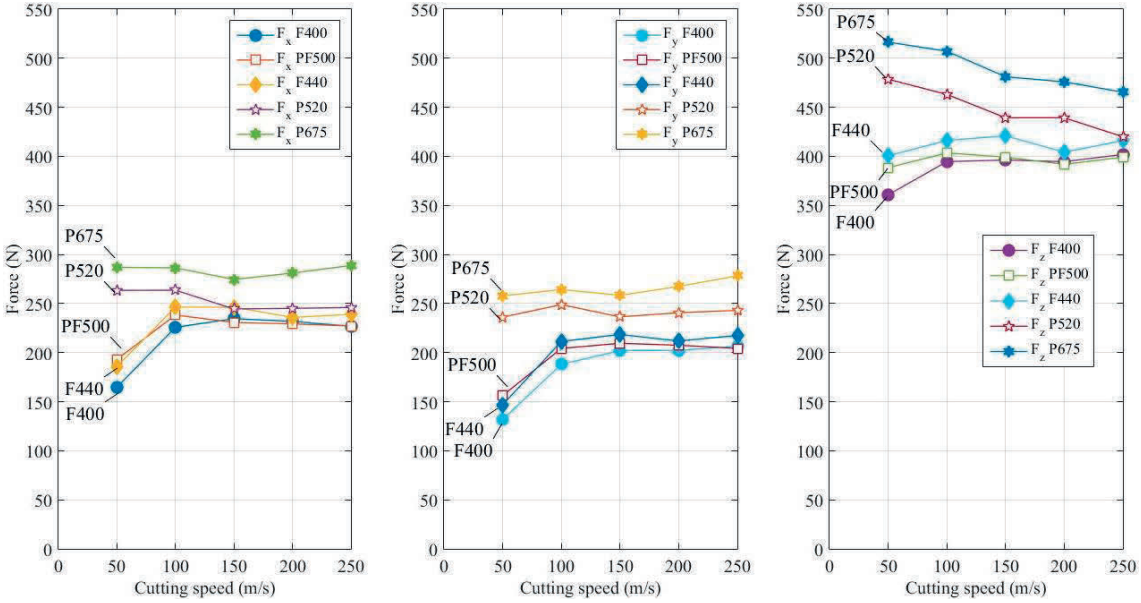

Fig. 41. Components of cutting forces in feed (Fx), radial (Fy) and principal direction (Fz) when turning ductile cast iron.

4.3.3 Cutting temperature

As shown in Fig. 42, the cutting temperature when turning PF500 was closer to the cutting temperature when turning ferritic ductile cast iron than when turning pearlitic ductile cast iron. There is a visible jump in temperature at 500 MPa. This jump is around 100ºC, although the difference in strength is only about 4.6%. Therefor the amount of ferrite has influence on the cutting temperature. This influence can be considered as positive influence since cutting temperature decrease with the amount of ferrite. This can be one of the reasons why the tool wear when turning pearlitic-ferritic ductile cast iron are closer to the tool wear when turning ferritic ductile cast iron.

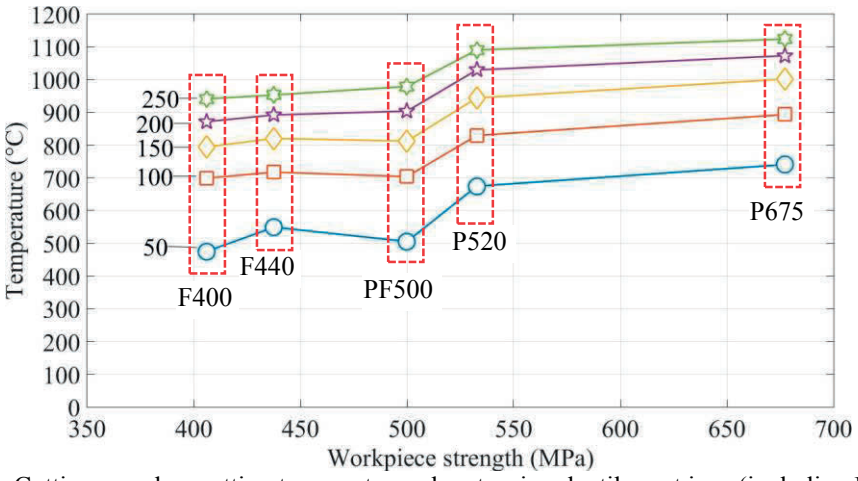

Fig. 42. Cutting speed vs cutting temperature when turning ductile cast iron (including PF500).

4.4 Discussion and conclusion

The results showed an interesting behavior of cutting forces, cutting temperature and flank wear; definitively the amount of ferrite and pearlite have great influence on ductile cast iron properties and its machinability. The radar chart shown in Fig. 43 predicts that pearlitic ductile cast iron causes higher cutting force and cutting temperature than ferritic ductile cast iron.

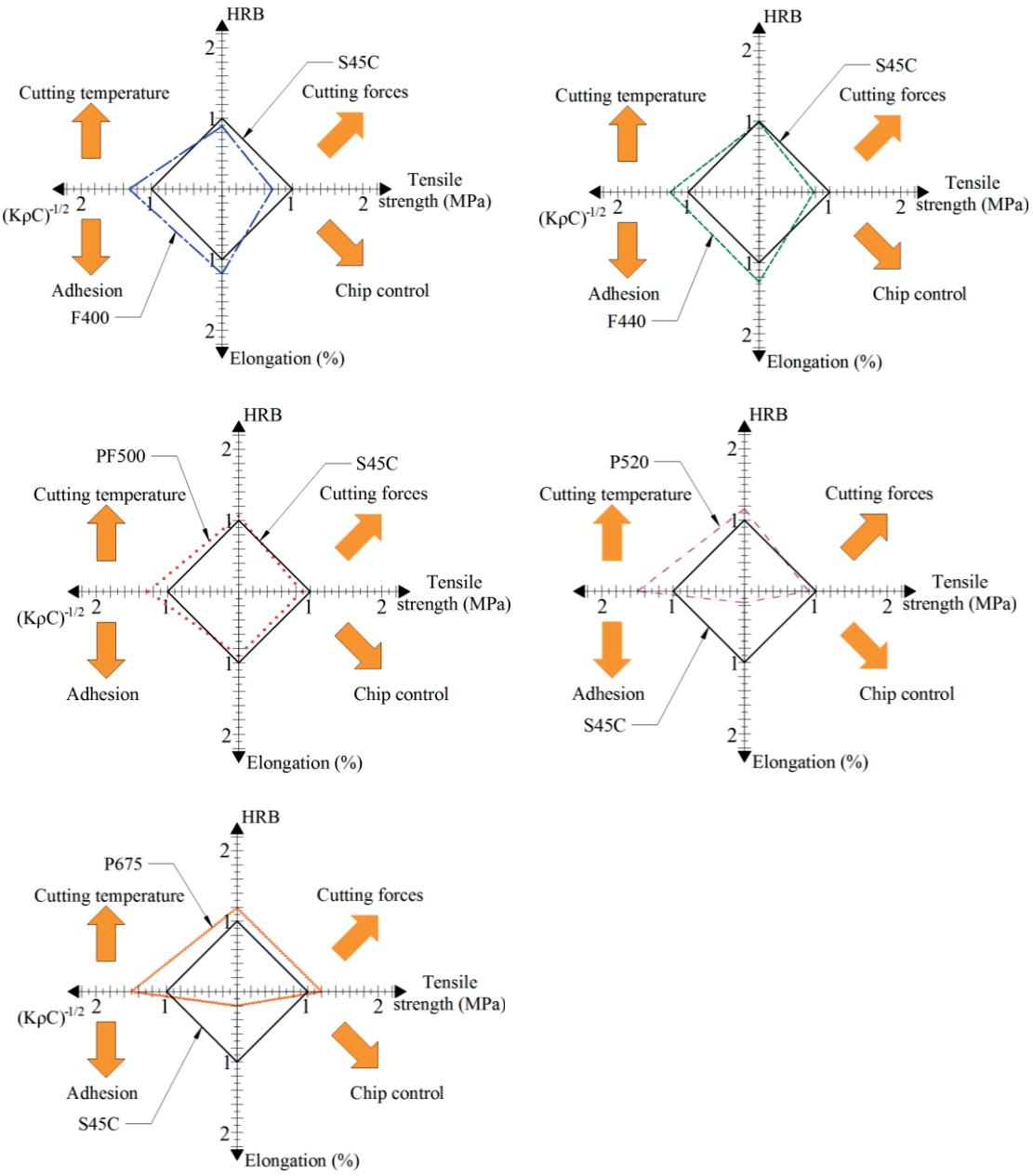

Fig. 43. Radar chart for ductile cast iron.

Table 12 confirms that cutting force and cutting temperature are higher when turning PF500 than when turning F400, but the difference is not as high as the difference between PF500 and P520.

Table 12. Area of every quadrant of radar chart.

Quadrant	1	2	3	4
	Cutting forces	Cutting temperature	Adhesion	Chip control
S45C	1.00	1.00	1.00	1.00
F400	0.62	1.16	1.56	0.85
F440	0.74	1.22	1.60	0.97
PF500	0.92	1.34	1.11	0.77
P520	1.06	1.73	0.20	0.12
P675	1.41	1.77	0.30	0.24

Only abrasive wear can't explain the small difference in flank wear between PF500 and ferritic ductile cast iron at all because it is expected higher abrasive wear from materials with high hardness materials such as ductile cast iron with pearlite in matrix than ferritic ductile cast iron.

Cutting temperature when turning pearlitic cast iron was higher than that when turning ferritic or ferritic-pearlitic ductile cast iron; for instance when turning P675 at the cutting speed of 150 m/min the temperature was 1000ºC. On the other hand, when turning F400, the cutting temperature was 800ºC at the same cutting speed. Jindal et al. reported Vickers hardness of TiN coating at different temperatures; according to their results Vickers hardness at 800ºC was 958 HV and Vickers hardness at 1000ºC was 580 HV [37]. This means that the expected TiN coating hardness when turning F400, F440 or PF500 is about 1.65 times higher than when turning P675 or P520. Reduction in hardness can lead in an increment of tool wear.

On the other hand, the difference in cutting temperature between ferritic and ferritic-pearlitic ductile cast iron was not significant; thus, the effect of thermal wear on TiN coating should be almost the same.

Finally one important conclusion can be drawn from the results on the turning of pearlitic-ferritic ductile cast iron with TiN coated carbide tool. If the amount of ferrite is increased around 55% (PF500), tensile strength can be almost the same as fully pearlitic ductile cast iron (P520); however cutting forces, cutting temperature and tool wear when turning PF520 are closer to those measured when turning ferritic ductile cast iron. Therefore, ductile cast iron with ferrite content of 55% has better machinability (similar to machinability of ferritic ductile cast iron), greater tensile strength and greater ductility than pearlitic ductile cast iron.

5. Wear on coated carbide tools in the face milling of ductile cast iron

5.1 Introduction

In this chapter, the wear characteristics of TiN coated carbide tool and TiCN coated carbide tool in interrupted cutting are discussed. Continuous and interrupted cutting are completely different process. Therefore, it is expected to find different wear characteristics. The experimental results about wear in continuous and interrupted cutting of ductile cast iron using TiN coated carbide tool showed an interesting behavior. In continuous cutting, the tool performance of TiN coated carbide tool was acceptable. However, in the interrupted cutting, TiN coated carbide tool had very poor performance. The difference was due to the appearance of notch wear when face milling ferritic ductile cast iron. On the other hand, when a TiN coated carbide tool was used in the face milling of pearlitic ductile cast iron, the wear behavior was not so different than that in continuous cutting. The following subchapters mainly describe the reasons behind notching wear and possible solutions for the notching wear. The possible causes are chemical wear, surface work-hardening, burr formation and adhesive wear. There is a possibility that the listed causes contribute in certain form to notching wear. However, due to the high tendency of ferrite to adhere on the tool, adhesive wear is pointed as the principal cause of notching wear. Therefore the results presented in this chapter can be of relevance for practical applications, since the results showed that an appropriate choice of the coating material can prevent from notching wear.

5.2 Materials and methods

The work materials used in this set of experiments were the two pearlitic materials previously described (P520 and P675) and one of the ferritic ductile cast iron (F440). Methodology for measuring cutting forces and flank wear does not change from those described for turning. The workpiece was a rectangular prism with 60 mm in width, length and height were variable. The diameter of milling cutter was 100 mm. Cutting conditions are shown in Table 13. This cutting conditions are the same as those used in turning, therefore both process can be compared.

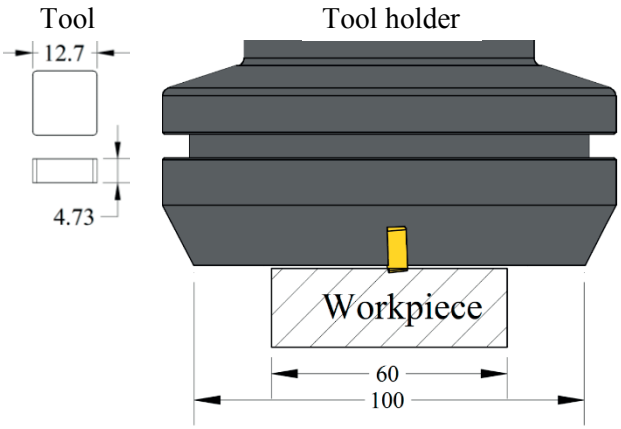

Fig. 44. Tool holder and tool geometry.

Table 13. Cutting conditions for face milling.

Cutting speed:	200 m/min
Depth of cut:	1mm
Feed rate:	0.2 mm/tooth
Coolant:	Dry

The tool angles are defined by the tool holder with ISO designation DNF4100R. Radial angle, axial angle and approach angle are -6º, -5º and 25º respectively.

The experiments were carried out in the CNC vertical machining center Mitsubishi MP4-V45 in dry conditions. Average flank wear (VB) and notching wear (VN) were measured by means of a toolmaker's microscope. Cutting forces were measured with the piezoelectric dynamometer Kistler 9129AA in the X, Y and Z coordinate system shown in Fig. 45, then the cutting forces were transformed into normal and tangential coordinate system using equation 7.

$$\begin{Bmatrix} F_t \\ F_n \\ F_z \end{Bmatrix} = \begin{bmatrix} \sin(\theta) & \cos(\theta) & 0 \\ -\cos(\theta) & \sin(\theta) & 0 \\ 0 & 0 & 1 \end{bmatrix} \begin{Bmatrix} F_x \\ F_y \\ F_z \end{Bmatrix}. \quad (7)$$

Where θ is the angle between two lines that converge in the rotation center of the tool. The first line is parallel to X axis shown in Fig. 45, and the second line goes from the rotation center to the instantaneous position of the tool.

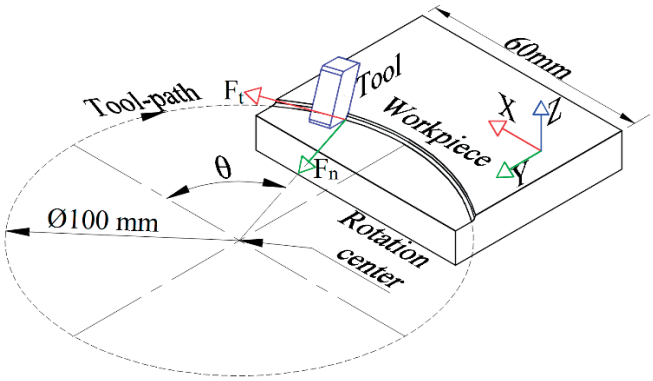

Fig. 45. Cutting force coordinate system.

5.3 Results

5.3.1 Tool wear

The results shown in Fig. 46 revealed that TiCN coated tool outperformed TiN coated tool regarding flank wear VB. Jindal et al. also reported better performance of TiCN coated than TiN coated tool regarding flank wear in the turning of ductile cast iron [37].

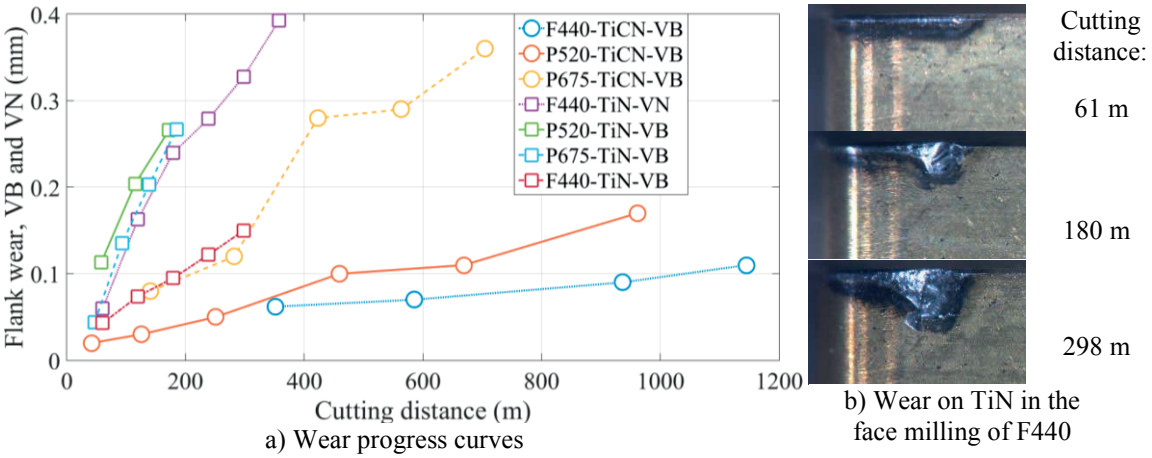

a) Wear progress curves

b) Wear on TiN in the face milling of F440

Fig. 46. Wear progress curves in the face milling of ductile cast iron with TiN coated tool and TiCN coated tool.

In face milling of P675 and P520 with TiN coated, flank wear VB was similar; furthermore, as shown in Fig. 47 b) and c), the appearance of the flank wear was uniform and practically no adhesion was observed. However, when face milling F440 with TiN coated tool the problem lay in notching wear. As illustrated in Fig. 46 b), at the cutting distance 61 m, flank wear had uniform appearance and it was small. From the cutting distance of 180 m, the notching wear VN grew approximately at the same rate as flank wear VB grew when face milling P520 and P675. After the notching starts, the wear rapidly increased because there was not any coating protecting the substrate near the depth-of-cut line. The grooving wear mentioned above can be observed in Fig. 47 a), in the photograph corresponding to the rake face.

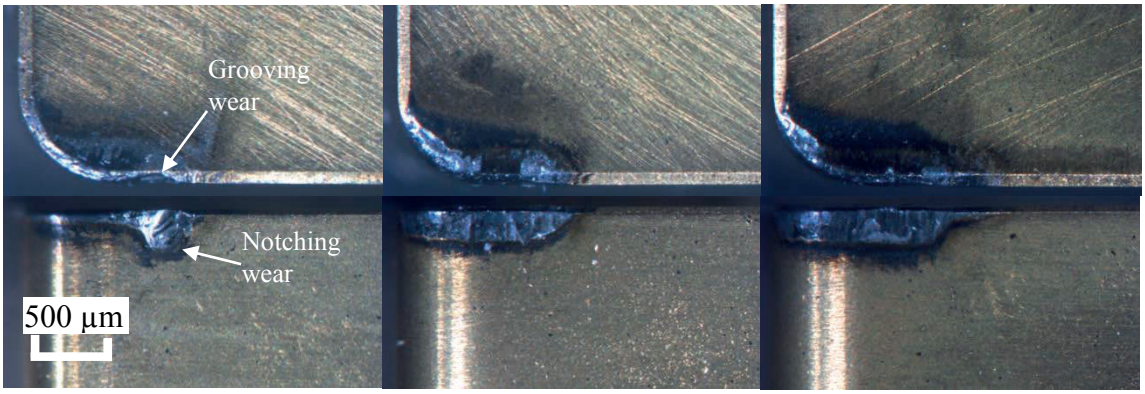

a) Work: F440. Cutting distance: 180 m.
b) Work: P520. Cutting distance: 172 m.
c) Work: P675. Cutting distance: 185 m.

Fig. 47. Wear on flank face (bottom) and rake face (top) of TiN coated tool.

The difference in flank wear between face milling and turning can be observed in Fig. 48. The results shown in Fig. 48 demonstrate that the difference in flank wear between turning and milling of P675 and P520 is not so different. However, the difference between flank wear measured in turning and the notching wear measured in the face milling of F44 is considerably large. If a tool life threshold value is set in 0.2 mm of flank wear VB and notching wear VN, the tool life of TiN coated tool in turning is 6 times longer than that in face milling of ferritic ductile cast iron. Therefore, it can be said that in the face milling of ferritic ductile cast iron the dominant factor of tool life is notching wear.

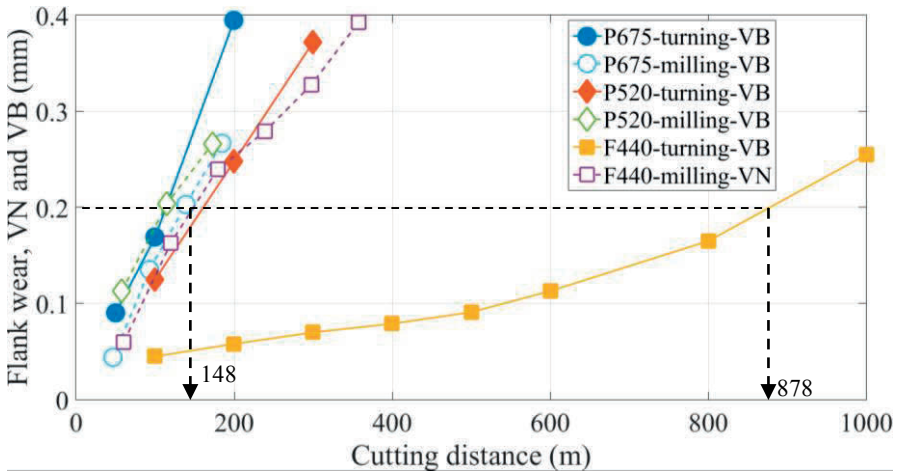

Fig. 48. Wear progress comparison between turning and milling for TiN coated carbide tool.

In the contrary to TiN coated, as can be observed in Fig. 49 a), notching wear was not visible in the face milling of F440 with TiCN coated. However as illustrated in Fig. 49 b) and c), in the face milling of P675 and P520 notching wear was observed on TiCN coated. In face milling of P675 the notching wear appeared after around 0.35 mm of VB, and in the face milling of P520 the notch wear appeared after around 0.17

mm of VB, therefore the flank wear was the main issue in the face milling of pearlitic cast iron with TiCN coated.

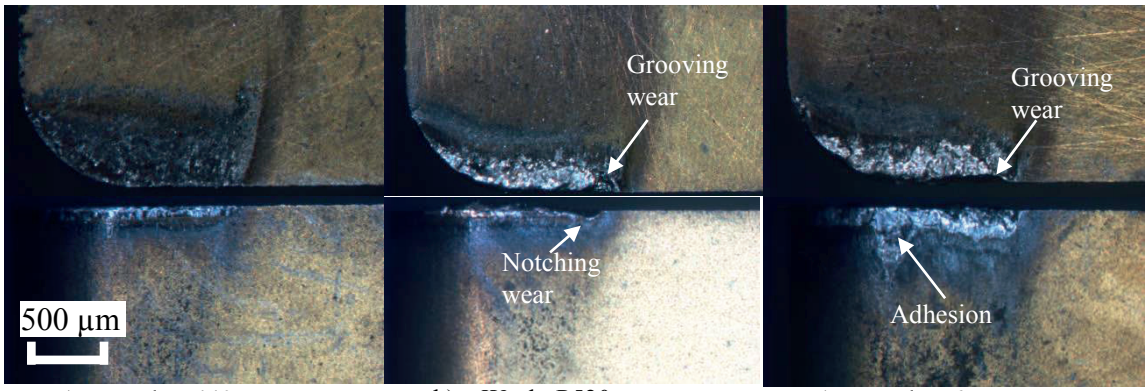

a) Work: F440. Cutting distance: 1145 m.
b) Work: P520. Cutting distance: 961 m.
c) Work: P675. Cutting distance: 704 m.

Fig. 49. Wear on flank face (bottom) and rake face (top) of TiCN coated tool.

5.3.2 Cutting forces

The evaluation of the cutting force is important in machining because it gives information about the amount of energy spend in cutting a workpiece. In face milling the force in tangential direction is the largest. As shown in Fig. 50 a), b) and c) the cutting force in tangential direction was higher in face milling of P675 than in face milling of P53, and F440 causes the lowest cutting forces in tangential direction. Therefore ferritic ductile cast iron is easier to cut than pearlitic ductile cast iron.

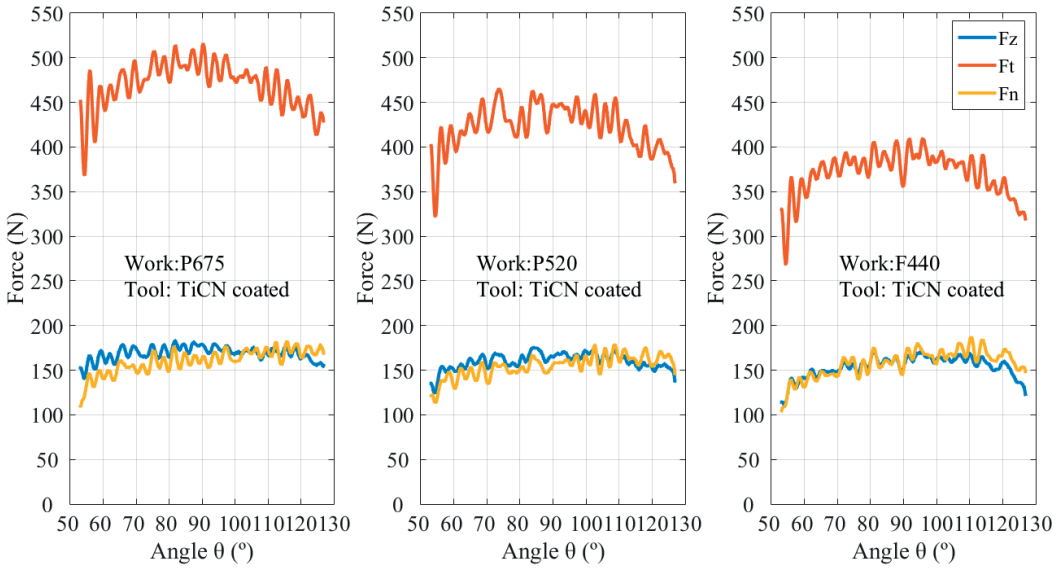

Fig. 50. Cutting forces in the face milling of ductile cast iron.

In face milling, usually the cutting force is expressed as a function of the chip thickness and the specific cutting force. The chip thickness change accordingly to the angle θ and the feed rate (f). If the face milling

cutter diameter and also feed rate are small, the tool's cycloid path can be simplified by circle path and then the uncut chip thickness becomes $fsin(\theta)$ [46]. Therefore the cutting force is function of θ. The angle θ is limited by the workpiece geometry and tool milling cutter diameter, in such a way that θ increase from 53º until 127º. As observed in Fig. 50, in the range of θ, the force in tangential direction approximately follow a sinusoidal behavior. Other interesting characteristic of the cutting force in tangential and normal direction is that both are very similar in quantity and behavior.

5.3.3 Burr formation and surface work hardening

As shown in Fig. 51 forward burr or end burr was observed on F440 workpiece. On the contrary, there was not burr formation on P675 and P520. F440 is more ductile than P675 and P520. Ductility is a property associated with burr formation and also with the ability of work hardening. For this reason, there was burr and some work-hardening as well.

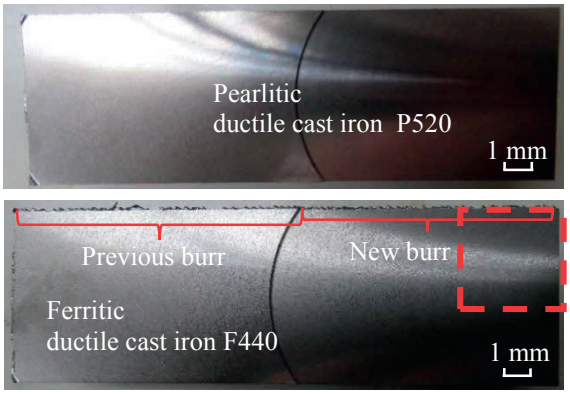

Fig. 51. End burr after face milling

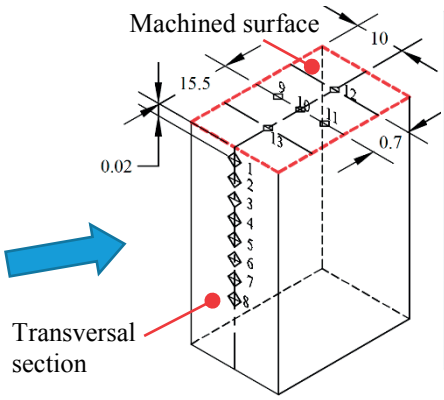

Location	HV
1	288.83
2	293.99
3	249.92
4	266.40
5	283.86
6	302.75
7	301.20
8	269.97
Average	282.12
9	313.27
10	295.84
11	280.29
12	261.72
13	261.83
Average	282.59

Fig. 52. Measurement of Vickers hardness.

According to Chuzhoy et al. [47], ferrite undergoes cyclic hardening while pearlite does not show hardening or softening, in compression-tension experiments. The average Vickers hardness from ten measurements on a virgin surface was 246 HV. The location of the measurements and their numerical values on the machined surface are shown in Fig. 52, the average hardness of machined surface was 282. This means that the hardness increase in about 15% in comparison with the virgin material.

5.4 Discussion

Comparatively the VB on TiN coated tool between turning and milling was not too different in the case of pearlitic cast iron. In turning of ferritic ductile cast iron with TiN coated tool, the progress rate of VB was low. However, notching wear was the primary type of wear in face milling of ferritic ductile cast iron limiting the performance of TiN coating in interrupted cutting. The causes of notching wear are listed as follows:

Oxidation wear. One important difference between continuous cutting and interrupted cutting is that in interrupted cutting, the tool cuts and then it is exposed to the air. On the contrary, in continuous cutting, the tool is engaged continuously with the tool and oxidation is not likely to occur. Trent argued that notching wear was related with oxidation wear caused by the interaction of the tool with the atmospheric oxygen and the workpiece [48]. TiN coated reacts with hot air at about 550ºC, this temperatures can be easily reached in the machining ductile cast iron under the cutting conditions used in the experiments (~ 900ºC in turning [49]). However, in face milling of pearlitic ductile cast iron, there was not observed notching wear and the cutting temperature expected was higher those that in the face milling of ferritic ductile cast iron, therefore oxidation wear can't be the only cause of notching wear.

Work hardening and burr. On the depth-of-cut line, the uncut chip thickness is the largest in the uncut chip area, and the contact with the tool occurs over a larger amount of work-hardened material (~15% of increment in hardness), this may contribute to abrasive type of wear on the depth-of-cut line. The burr is also expected to possess higher hardness than the undeformed workpiece. After the tool exits from the workpiece, it is highly possible that the previously formed burr hits against the tool and cause wear. This process is repeated as many times as the tool get engaged with the workpiece.

Adhesive wear. Adhesive wear is more likely to be the principal cause of notching wear when face milling ferritic ductile cast iron due to the high tendency of ferrite to adhere on the tool. The process of adhesion and detachment is expected to repeat every time the tool hits the workpiece.

This process is repeated about 1600 times per every hundred meter of cutting distance. Probably part of the exit burr also adhere on the depth-of-cut line during the tool passes over the burr.

In order to avoid notching wear, the stability of the coating at high temperature is an important feature since the hardness of coating reduce with the temperature. TiCN coating has better hot-hardness than TiN coating [37], therefore no notching wear was observed on TiCN coated tool. The literature available suggest increase the engage area between the workpiece and tool by means of increasing the approach angle or by using round inserts. In this way, as shown in Fig. 53 the cutting edge is engage with the workpiece in a large portion, thus the cutting forces are distributed on a larger portion of the cutting edge [50].

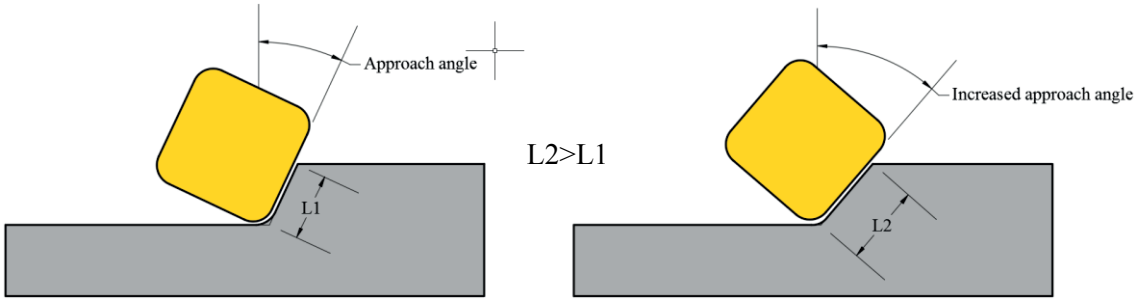

Fig. 53. Illustrative representation of the increase approach angel in order to reduce notching wear.

Other possible option to avoid both burr formation and notching wear is by increasing the amount of pearlite in the workpiece. One important point to remark is that the ferritic ductile cast iron is difficult to be produced because the raw materials used to produce it (pig iron, return iron and scraps) have inclusions that favor the formation of pearlite. If the amount of pearlite increases, the ductility decreases but the tensile strength increases. Ductility is the key property that favors the burr formation, therefore it is expected that burr and notching wear decrease with the amount of pearlite increase. In this way, the reduction in the manufacturing cost of ductile cast iron, burr and notching wear can be achieved at the same time.

5.5 Conclusion

In this study, specimens of pearlitic ductile cast iron and ferritic ductile cast iron were tested in face milling with TiN and TiCN coated carbide tools in order to investigate the tool wear characteristics. From the experimental evidence shown in this study the next conclusions can be drawn:

1. Pearlitic ductile cast iron causes the highest cutting forces and flank wear in both TiN and TiCN coated carbide tools. TiCN coated carbide tool outperform TiN coated carbide tool regarding flank wear, however the photographs reveal that TiCN coated carbide tool caused more adhesion than TiN coated carbide tool.
2. Previous results showed that TiN coated carbide tool had good performance in turning of ferritic ductile cast iron, however large notching wear was observed in face milling. The causes of notching were oxidation wear, work hardening, end burr formation and adhesive wear. It is thought that adhesive wear is the principal cause of the notching wear when face milling ductile cast iron due to the high tendency of ferrite to adhere on the tool.
3. The results demonstrated that TiCN coated carbide tool did not showed notching when face milling ferritic ductile cast iron, therefore an appropriate choice of the coating can prevent for short tool life regarding notching wear.

6 Relationship between coating loss and wear rate in coated tools

6.1 Introduction

In chapter 3, the concept of the relation between the change in wear rate and the loss of coating was introduced. By plotting the flank wear progress curves (cutting distance vs flank wear) in log-log scale, the change in wear behavior of the coated tools was easily detected in turning of ductile cast iron. This may be unique of the ductile cast iron or may be applied to any workpiece. In order to confirm the adequacy of this method, plain carbon steel AISI 1045, low-alloy medium-carbon steel AISI 4135, ductile cast iron and difficult-to-cut material Inconel 718, were turned with TiN and TiAlN coated tools. Linear approximation of the flank wear curve is proposed by the linearization of a power equation ax^n and dividing the wear rate into two parts. Finally the inflection point where the wear rate is expected to change was identified and correlated with the loss of coating.

6.2 Materials and methods

Plain carbon steel AISI 1045 is recognized for having moderate machinability; therefore this material was taken as a baseline for comparing the relative machinability of Inconel 718, AISI 4135 and ductile cast iron. The Fig. 54 shows a radar chart [29] that indicates the ratio of the properties that influences the machinability of Inconel 718, AISI 4135 and ductile cast iron with plain carbon steel AISI 1045. Inconel 718 is considered as difficult-to-cut material, with an increasing use up till the end of the 20th century [51]. The Nickel-base superalloys are an unusual class of metallic materials with an exceptional combination of high-temperature strength, toughness, and resistance to degradation in corrosive or oxidation environments [52]. As shown in Fig. 54, the tensile strength, the Vickers hardness and the inverse thermal effusivity are twice the values of AISI 1045. Therefore, the high cutting forces, cutting temperatures, abrasive wear and adhesive wear are expected to occur. Previous studies confirm that adhesion and abrasion are dominant cause of tool wear when machining Inconel 718 [53]. AISI 4135 is a low-alloy (Cr-Mo), medium-carbon steel commonly used for metalworking applications in manufacturing of auxiliary tooling, such as containers for hot-extrusion dies or holder blocks for molds for processing plastics [54]. This material also

is used for the manufacturing of axles, shafts, connecting rods and other non-high stress demanding components [55].

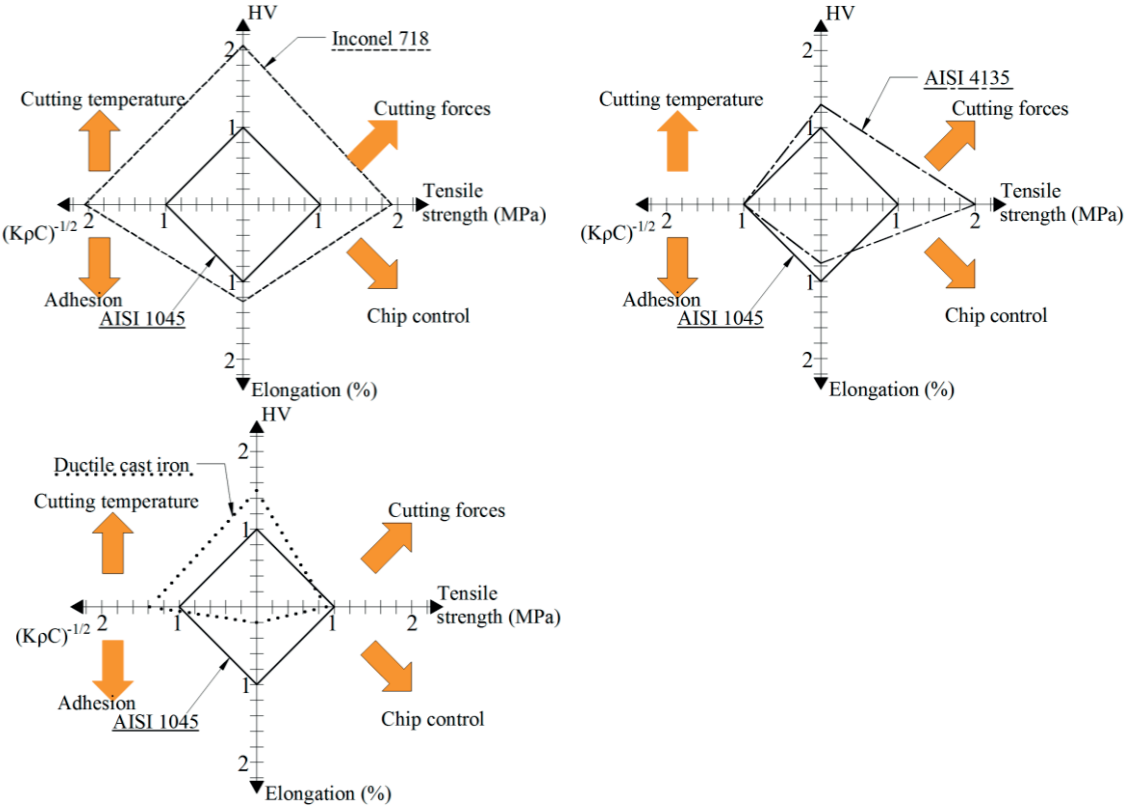

Fig. 54. Radar chart for the workpieces.

Part of the results obtained in turning of pearlitic ductile cast iron (P520) are shown again for the completeness of the present chapter.

The cutting conditions are shown in Table 14. These cutting conditions are similar to the recommended cutting condition for turning of carbon-steel materials. However in the case of Inconel 718, the cutting conditions have to be less aggressive since this material is difficult to cut and cause large wear on the tool.

Table 14. Cutting conditions for the turning of Inconel 718, AISI 4135, AISI 1045 and ductile cast iron.

	Inconel 718	AISI 4135	AISI 1045 and of ductile cast iron.
Coating:	TiN, 4 µm thickness TiAlN, 4.5 µm thickness	TiN, 5 µm thickness TiAlN, 3 µm thickness	TiN, 4 µm thickness TiAlN, 4 µm thickness
Substrate:	K15	K15	K15
Tool ISO designation:	SNGN120408	SNGN120408	SNGN120408
Tool holder ISO designation:	CS-NL2525M-12	CS-NL2525M-12	CS-BNR2525M-12
Cutting speed:	40 and 80 m/min.	150, 200 and 250 m/min.	150 and 200 m/min.
Depth of cut:	1 mm	1.5 mm	1 mm
Feed:	0.1 mm/rev	0.2 mm/rev	0.2 mm/rev
Coolant:	Wet	Wet	Dry

6.3 Results

6.3.1 Flank wear in the turning of AISI 1045

It is well known that the equations of wear rate prediction for abrasive [56], or adhesive wear [57], in general, follow an exponential behavior, which in log-log scale become linear. For this reason, it makes sense to propose a log-log scale in order to make clear the change in the wear rate. The fundamental idea of the proposed wear mechanism on coated tools is based on the fact that before the coating is worn out, the wear is borne by the coating; in this stage, certain wear behavior is expected. After the loss of coating, wear is less effectively borne by the substrate; therefore, wear behavior must change at this point.

Fig. 55 a) shows the relationship between cutting distance and flank wear plotted in linear scale. In Fig. 55 a), the change in wear rate is not evident at all, and this is true for most combinations of work-tool curves of cutting distance versus flank wear in linear scale. On the other hand, if the same data is plotted in log-log scale, the change in wear rate becomes clear. By following the tendency of the points in Fig. 55 b), the curves for TiN and TiAlN can be divided into two parts. Each part independently fits well in a linear behavior in logarithmic scale. Therefore, tentatively, a linearization of exponential function of the kind ax^n can be used for the purpose of linear approximation the two parts of each curve by the least-square technique.

The coefficient a and the exponent n can be evaluated easily as follows:

1. Change $y=ax^n$ into a linear equation by applying log in both sides of the equation as follows: $\log_{10}y=n(\log_{10}x)+\log_{10}a$. Now the equation is linear if the next substitutions are applied: $y'=\log_{10}y$, $x'=\log_{10}x$, $n=\log_{10}a$ and $b=\log_{10}a$.
2. The coefficients of the transformed equation $y'=a'x'+b$ can be calculated by equation (8) and equation (9).

$$n=\frac{N\sum x_i'y_i'-\sum x_i'\sum y_i'}{N\sum x_i'^2-(\sum x_i)^2} \tag{8}$$

Where N is the number of points in x.

$$b=\bar{y}-a'\bar{x}' \tag{9}$$

3. Finally, a is calculated raising b to the tenth power.

Since the change in slope can be easily perceived, at least in the results showed, the values of x can be easily chosen. Other option is iteratively taking point by point until the coefficient of multiple determination R^2 is maximum; R^2 is a measure of the reduction in the variability.

Obviously, the slope of the lines in logarithmic scale is equal to the exponent of the exponential function and this number can be used to compare the difference in flank wear rate.

For instance, in the case of the TiAlN coated carbide tool, the fitting equation for the first line is $0.0375x^{0.542}$, the second is $0.008x^{2.02}$ and the inflection point appears at approximately 2.8 km. In the case of the TiN, the fitting equation for the first line is $0.0606x^{0.532}$, the second is $0.024x^{1.47}$ and the inflection point appears at approximately 2.6 km. For both coated carbide tools, the slope of the second line were about two times greater than those of the first lines. This means that the increase in wear rate at the inflection point is considerable.

Similar analysis was conducted for the turning of ductile cast iron, AISI 4135 and Inconel 718 with TiN and TiAlN coated carbide tools, but typical plots in linear scale were omitted. Since cutting time and cutting distance are analogous amounts, cutting distance versus flank wear plots were used in the following results. Cutting distance provides a simple way to compare flank wear at different cutting speed but with the same cutting distance in order to detect thermal wear at relatively high cutting speeds [58].

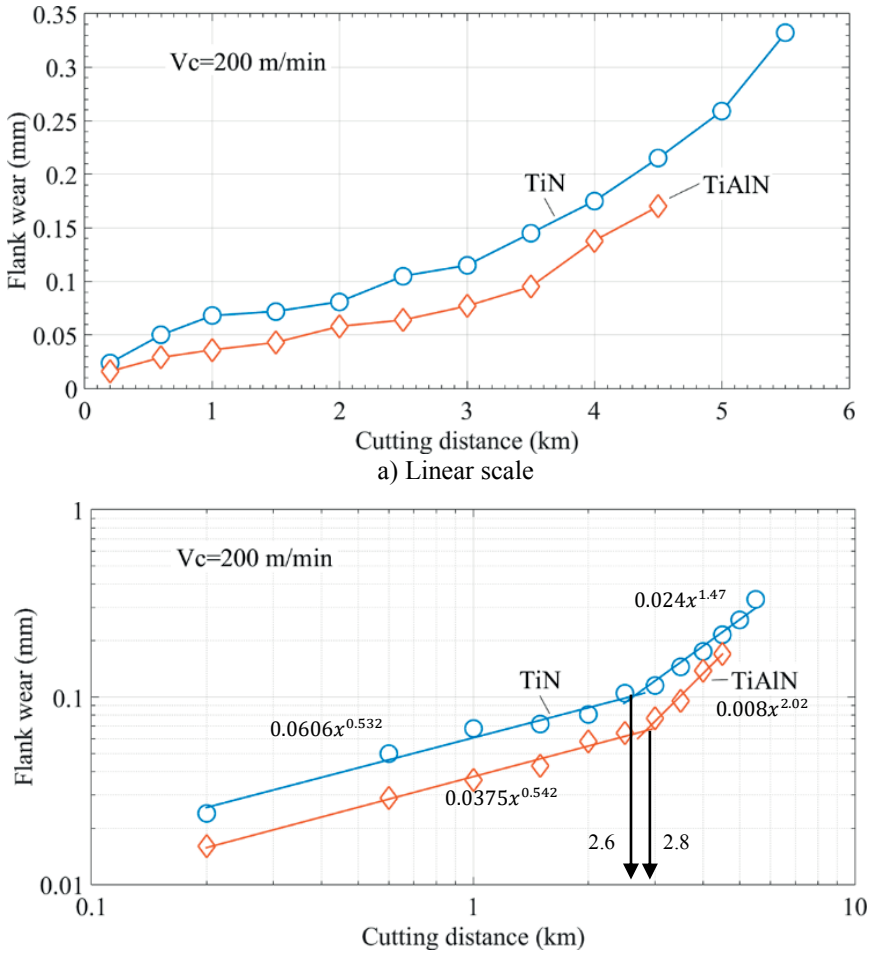

a) Linear scale

b) Log-log scale

Fig. 55. Flank wear vs cutting distance in the turning of AISI 1045 with TiN and TiAlN coated carbide tools at 200 m/min

6.3.2 Flank wear in the turning of ductile cast iron

The appearance of the inflection point was reported previously in the turning of different grades of ductile cast iron [59]. Regarding the pearlitic grade of ductile cast iron, the absence of coating tool after the appearance of the inflection point at the cutting distance of 1 km. The results obtained in turning of pearlitic ductile cast iron are shown in Fig. 56. In the case of the TiN coated carbide tool, at the cutting speed of 200 m/min, flank wear was too severe and the inflection point could not be observed. At the cutting speed of 150 m/min apparently the inflection occurred at the cutting length of 0.15 km, however the flank wear also resulted high and only one point was acquired before the inflection point.

In the case of the TiAlN coated tool, the inflection point was observed at 150 m/min and 200 m/min. TiAlN coating has better wear resistance than TiN coating; as consequence, TiAlN coating was gradually worn and the inflection point could be observed.

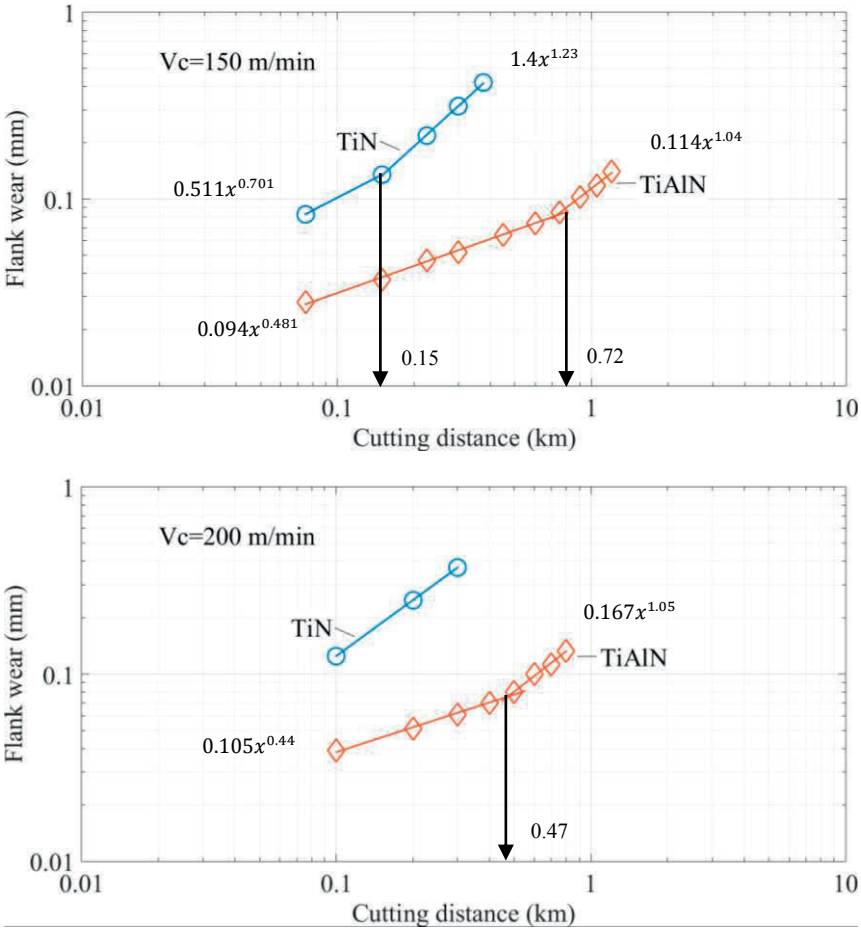

Fig. 56. Flank wear vs cutting distance in the turning of ductile cast iron with TiAlN and TiN coated carbide tools.

6.3.3 Flank wear in the turning of AISI 4135

Fig. 57 shows flank wear progress curve in turning of AISI 4135. At 200 and 250 m/min of cutting speed, the first measured point does not fall on the approximated straight line in log-log scale.

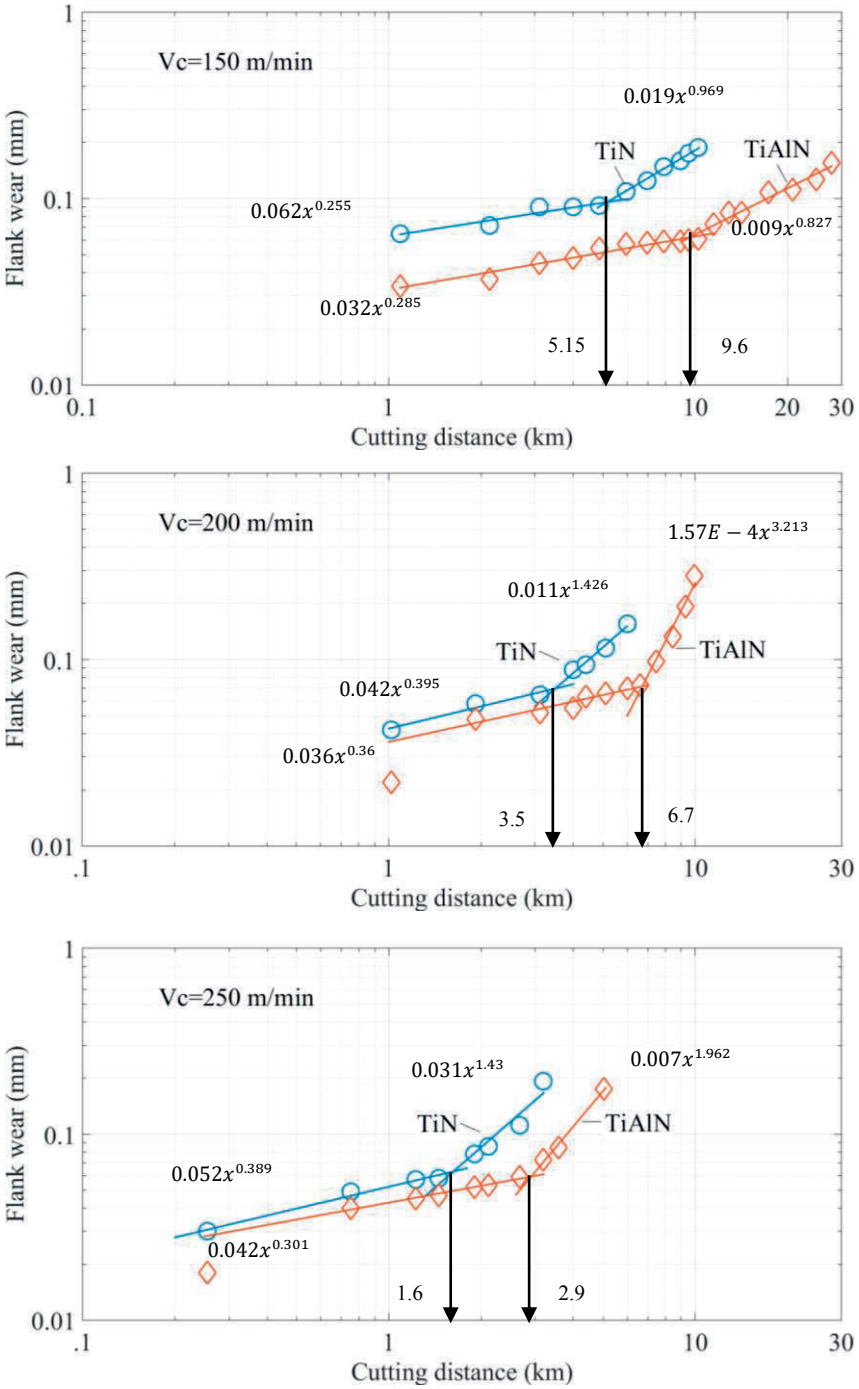

Fig. 57. Flank wear vs cutting distance in the turning of AISI 4135 with TiAlN and TiN coated carbide tools.

This was because the first points were taken in a short cutting distance, and because of the good properties of TiAlN coated tool for bearing wear, the flank wear resulted particularly low. Again, the slope of the second line was considerably greater than the slope of the first line for both coated tools. Furthermore, the inflection point tends to appear in a longer cutting distance as the cutting speed decreased.

In the case of TiN coated carbide tool, in the first stage (first line), the flank wear was higher at the cutting speed of 150 m/min than that at the cutting speed of 200 m/min. However at the cutting speed of 150 m/min, the wear rate changed at longer cutting distance, therefore after the flank wear of 0.1 mm, the flank wear at the cutting speed of 150 m/min became lower than those at the cutting speed of 200 m/min and 250 m/min. There is not difference between the slope of the second line at the cutting speed of 200 and 250 m/min. However the coefficient of the fitting equation at the cutting speed of 250 m/min is larger. In addition, the inflection point occurs at longer cutting distance at the cutting speed of 200 m/min. compared with the inflection point at the cutting speed of 250 m/min.

In the case of TiAlN coated carbide tool, the behavior in the first line is quite similar for all cutting speed. The difference lie in the relative position of the change in wear rate. This means that in log-log scale, the lines of the first stage looks parallel until the wear rate change, after that, the slope became completely different, especially at 200 m/min.

6.3.4 Flank wear in the turning of Inconel 718

Fig. 58 shows the cutting distance versus flank wear plots in the turning of Inconel 718 with TiN and TiAlN coated carbide tools.

As shown in Fig. 58, in the case of TiN coated carbide tool, the cutting distance until the inflection point at the cutting speed of 80 m/min was about 10 times greater than that at the cutting speed of 40 m/min; also the coefficient a and the exponent n were considerably greater at the cutting speed of 80 m/min. This means that flank wear rate rapidly increased with the cutting speed from 40 to 80 m/min.

The effect of cutting speed was completely different on the TiAlN coated carbide tool than that on TiN coated carbide tool. At the cutting speed of 40 m/min, the change in wear rate was not appreciable. On the other hand, at 80 m/min, the wear rate changed at the cutting distance of 0.43 km cutting distance and then the slope of the line became greater. However, flank wear at 40 m/min was higher than that at 80 m/min throughout the course of the test. Usually, flank wear increase with cutting speed at the same cutting distance. The cause of this is the effect of temperature on tool hardness and thermal wear mechanisms. Consequently, wear mechanisms independent of temperature, such as abrasive and adhesive wear, seem to be the cause of the higher flank wear at the cutting speed of 40 m/min. Thangaraj and Weinmann [60] also

reported higher flank wear at low cutting speed, rather than at high cutting speed, in the turning of Inconel 718 with a Silicon carbide whisker-reinforced alumina tool.

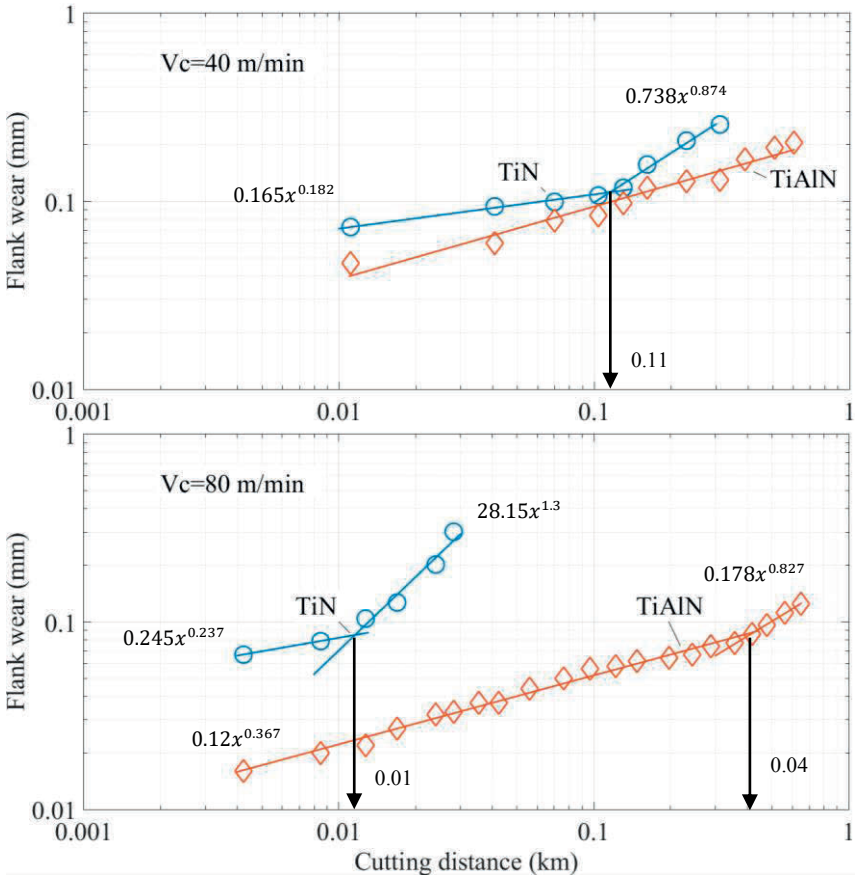

Fig. 58. Cutting distance vs flank wear in the turning of Inconel 718 with TiAlN and TiN coated carbide tools.

In order to analyze the worn out coating on a TiAlN coated carbide tool in detail, the tool was cut through the cross section shown in discontinuous line in a). This cross section passes through the flank wear. Fig. 59 b) is a view in direction normal to the front clearance face. The zone squared in Fig. 59 b) corresponds to the zone analyzed with SEM images and EDS mapping photographs.

Fig. 60a) is a SEM image of the area of interest, which is the same area illustrated schematically in the top of Fig. 60 b). Fig. 60 b) is an expanded SEM image of the area squared in Fig. 60 a). The image of the cutting edge at this magnification reveals the lack of coating on the chamfer. The Fig. 60 c) corresponds to an EDS mapping image of the same area shown in Fig. 60 b). The elements distribution on the tool are

in accordance with the composition of Inconel 718 (Ni), TiAlN coating (Ti) and Tungsten carbide substrate (W).

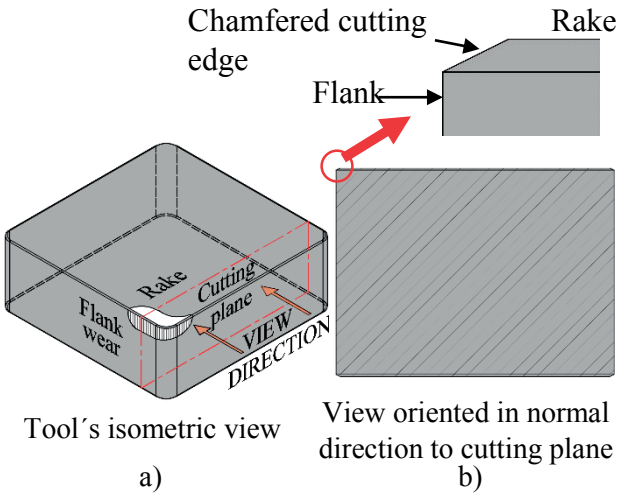

Fig. 59. Illustration of the analyzed area of TiAlN coated tool in the turning of Inconel 718 and ductile cast iron.

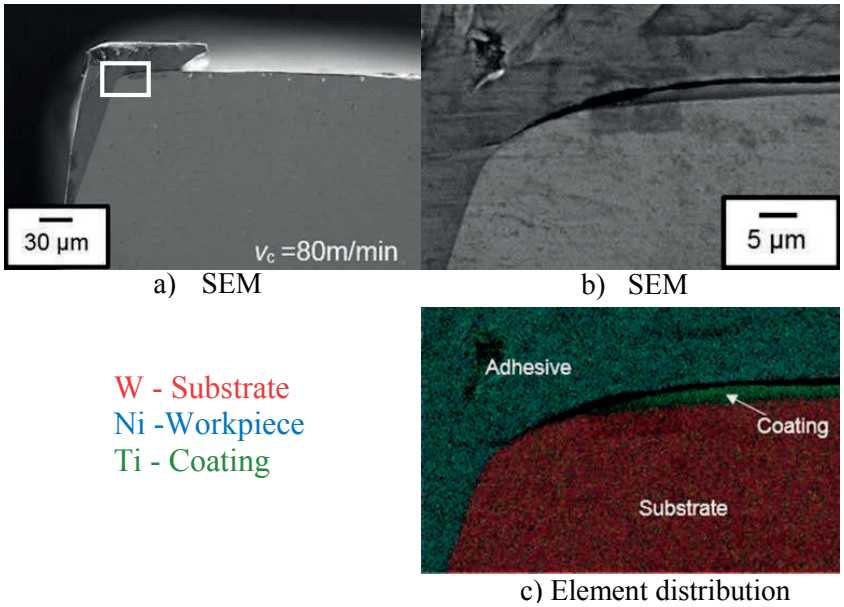

Fig. 60. SEM and EDS in the machining of Inconel 718 at 80 m/min with TiAlN coated carbide tool.

Element distribution confirms that the coating was removed from the cutting edge and flank face; the only remaining coating was localized on the rake face. Additionally, Ni was detected on the cutting edge, which points to adhesive wear. This agrees with previous research about adhesive wear in turning of Inconel 718 [61].

As mentioned previously, adhesive type of wear is pointed as the reason why the flank wear at the cutting speed of 40 m/min was higher than that at the cutting speed of 80 m/min. Furthermore, the change in wear rate was not observed at 40 m/min. Fig. 61 shows SEM and EDS element mapping in the turning of Inconel 718 at the cutting speed of 40 m/min with TiAlN coated carbide tool. As shown in Fig. 61b), the adhesive layer is observed near the cutting edge and extends over the flank. Fig. 61 c), confirms adhesion on the cutting edge and loss of coating as well.

The coating on the cutting edge and flank face was removed probably because of high adhesive wear occurred in the early stage of the experiment; therefore the change in wear rate was not observed at the cutting speed of 40 m/min. Furthermore, crater wear is observed clearly in Fig. 61a).

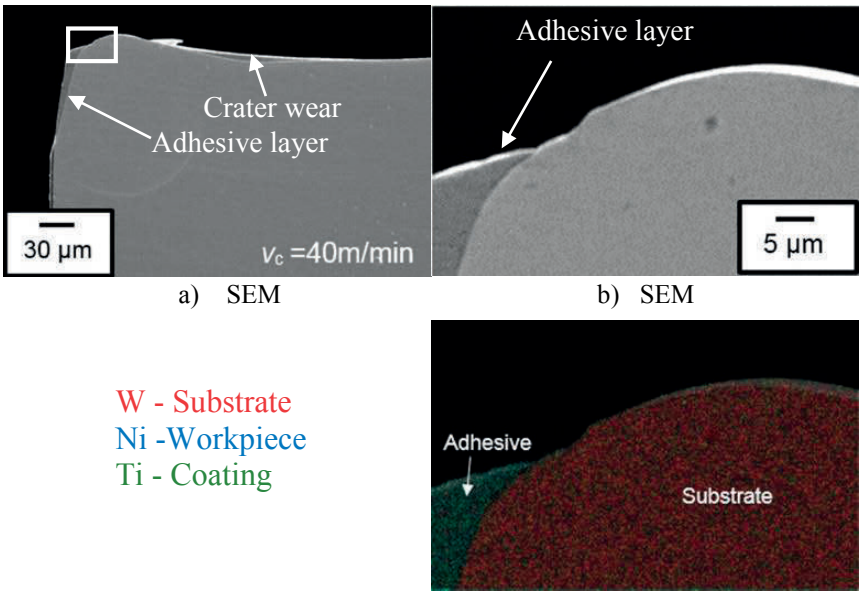

a) SEM b) SEM

c) Element distribution

Fig. 61. SEM and EDS in the machining of Inconel 718 at the cutting speed of 40 m/min with TiAlN coated tool.

6.3.5 Effect of cutting speed on inflection point

Fig. 62 shows the effect of cutting speed on the inflection point for the cases described in results. In general, the inflection point tends to appear in a shorter cutting distance with the cutting speed. As the cutting speed increases, the cutting temperature also increases. This could cause thermal wear that also can lead to the increase in wear rate.

The direct effect of high temperature in TiN and TiAlN coated carbide tools is reduction in hardness. Jindal et al. reported reduction in the hardness of TiN and TiAlN as the temperature increased, being this reduction

higher in TiN coated tool [37]. TiAlN has better stability at high temperatures and higher wear resistance than TiN; thus, in most cases, the cutting distance required to reach the inflection point for TiAlN coated carbide tool was than that for TiN coated carbide tools.

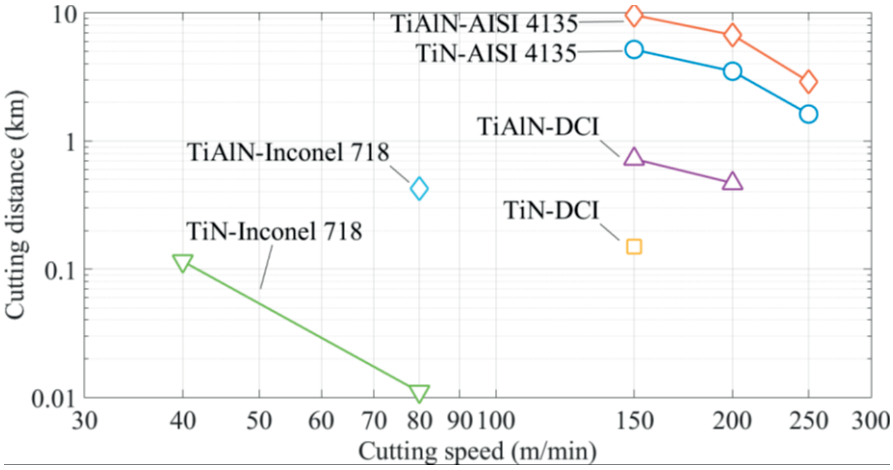

Fig. 62. Cutting speed vs cutting distance in the inflection point.

6.4Discussion

6.4.1 Loss of coating layer on the cutting edge and its relation to wear rate

In general, the coating has higher wear resistance than the substrate. Therefore, tool wear is suppressed as long as the coating remains. However, the coating is eventually worn away as the cutting operation is carried out. It is thought that the change in wear rate observed in the results is influenced by the worn out coating layer. The relationship between cutting distance and flank wear on log-log scale plots is simple but it clearly identifies the changing point of tool wear rate. Detection of changing point of wear rate is quite important for machining engineers because tool wear increases rapidly after the changing point, and high tool wear causes low dimension accuracy and poor surface finish in machined parts. In addition, the changing point of wear rate is important information for tool makers, because the changing point shows the wear characteristics of the coating layer, especially the coating layer on the rake face near the cutting edge.

The cutting edge can be prepared in different geometries, such as sharp edge, rounded edge and chamfered edge. According with Cortés Rodríguez, the chamfered edge is generated by the plane surface that join the tool flank and tool face [62]. This definition implies that the chamfer or land forms the cutting edge.

It is necessary to consider the wear on flank face and rake face separately.

Wear on flank face. It was observed that the coated layer on flank face is worn away and finally is worn out. Wearing out of the coating layer depends mainly on the coating thickness and clearance angle of the flank face; as shown in Fig. 63 a), the following equation relates the flank wear needed to remove the coating on the flank face with the clearance angle β, the coating thickness *t* and the chamfer angle ψ.

$$V_B = t\left(\frac{1}{cos(\psi+\beta)} + \frac{1}{sin(\beta)}\right) \tag{10}$$

However, even if the coating layer on the flank face is worn out, the tool wear is suppressed in some level as long as the layer on the cutting edge exists.

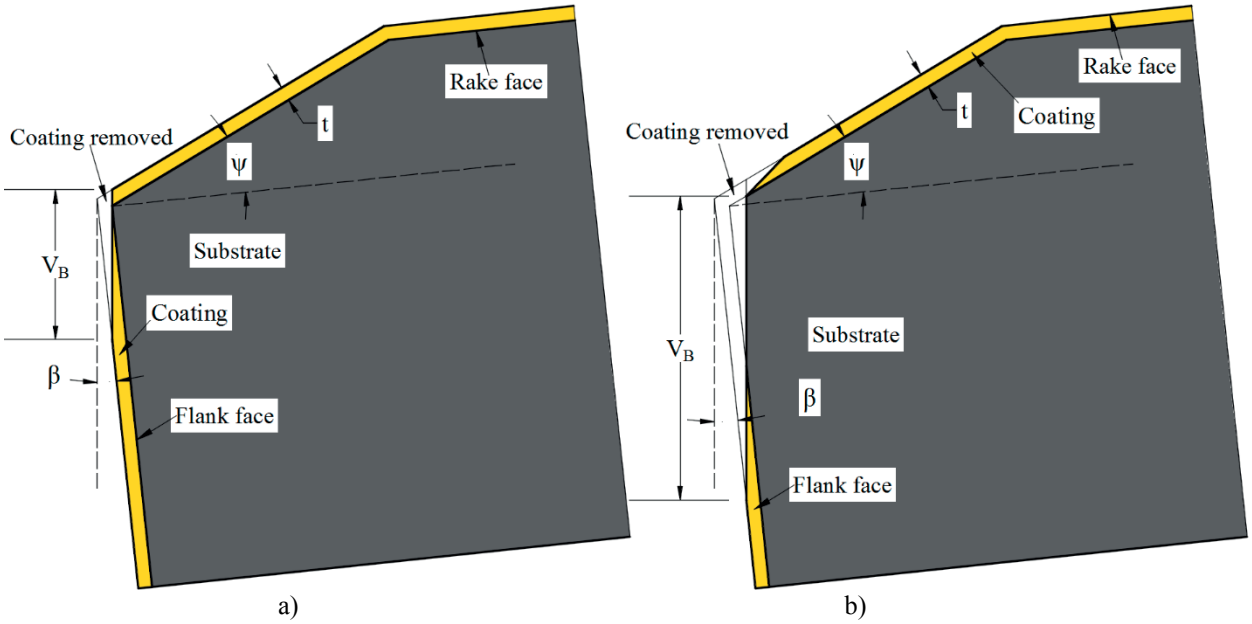

a) b)

Fig. 63. Wear on flank face and rake face (chamfer).

Wear on rake face. After the coating on flank face is worn out, the coating on the rake face is worn away until it is worn out, along with chip sliding on the rake face. When the wear rate of the coating on the cutting edge is low, the coating on the cutting edge remains and the wear rate decreases (Fig. 63 b)). On the other hand, when the wear rate of the coating on the cutting edge is high, the coating on the cutting edge is worn out in short cutting distance. After the coating layer is worn out, the wear resistance of the tool depends on that of the substrate, thus the wear rate increase.

Therefore, the coating layer on the cutting edge is the key of wear. Work material near the cutting edge on the rake face is easy to accumulate compared to that on the flank face. This means that the abrassive effect on the rake face is lower than that on the flank face. However, high pressure and high temperature act on the rake face, therefore thermal stability of the coating layer is required. Thermal stability of the coating

layer properties, such as hardness, thermal diffusivity and oxidation resistivity quickly diminishes as temperature increases. In setting cutting condition, cutting speed, is specially important. If cutting speed is low, tool wear may be low; however, cutting efficiency is reduced. On the other hand, if cutting speed is too high, tool wear increases and tool life decreases. To optimize machining cost, an acceptable cutting speed, from the point of view of tool wear, should be selected.

6.5Conclusion

In this experimental work, TiN and TiAlN coated carbide tools were used in the turning of AISI 1045, AISI 4135, ductile cast iron and Inconel 718 in order to demonstrate the relationship between the loss of coating and the increase in wear rate. From the results, the following conclusions can be drawn:

1. The cutting distance versus flank wear graphs in log-log scale clearly show the change in wear rate. The relation between the change in wear rate and the worn out coating layer was confirmed by means of SEM and EDS images taken before and after the appearance of the change in wear rate. It was observed that the coating was worn gradually until it was worn out; the tool wear was suppressed as long as the coating on the cutting edge prevails. However, after the coating on the cutting edge was worn out, wear was borne by the substrate, thus causing the observed increase in the wear rate.
2. The change in wear rate appears in a shorter cutting distance as the cutting speed increases, thus making flank wear increase. Low cutting speed decreases cutting efficiency, but high cutting speed causes flank wear to increase. Therefore, in order to optimize the machining cost, an acceptable cutting speed must be selected from the point of view of tool wear.

7 General conclusions

In this dissertation, experimental results on the machining ductile cast iron having different tensile strength with coated carbide tools were presented. A new wear mechanism of coated tools when machining ductile cast iron was presented. The relation between loss of coating and the change in wear rate of coated carbide tools was successfully found experimentally. The next conclusions can be drawn:

1. Cutting forces, cutting temperature and flank wear were higher when turning ferritic ductile cast iron than those when turning pearlitic ductile cast iron; therefore, ferritic ductile cast iron possess better machinability than pearlitic ductile cast iron.
2. Tool characteristics desired when turning ductile cast iron are low adhesiveness, stability at high temperature and abrasive wear resistant (high hardness). TiAlN coated carbide tool has higher stability at high temperature, lower adhesiveness and higher wear resistance than TiN coated carbide tool. Therefore TiAlN coated carbide tool is a good candidate to be used when turning ductile cast iron.
3. Ductile cast iron is a kind of metal matrix composite that contains soft spheroidal graphite dispersed in a hard matrix. When cutting ductile cast iron, tool passes through hard matrix and then through soft graphite continuously; since a small size adhesion stuck on tool edge experience continuous small hits, this phenomenon can lead in an increase on adhesive wear. This mechanism can explain the difference in flank wear between plain carbon steel and ductile cast with around the same tensile strength.
4. Pearlitic-ferritic ductile cast iron (~55% of ferrite) has better machinability than pearlitic ductile cast iron with around the same tensile strength. The machinability of pearlitic-ferritic ductile cast iron was close to the that of ferritic ductile cast iron; therefore, the use of pearlitic-ferritic ductile cast iron represent a gain in machinability and strength without sacrifice ductility.
5. The greatest tool wear difference between face milling and turning of ductile cast iron was found when cutting ferritic ductile cast iron. The principal type of wear when turning ductile cast iron was flank wear; on the other hand, when face milling ductile cast iron it was notching wear. The principal cause of notching wear was adhesive wear, however oxidation wear, abrasive wear caused by work-hardened surface layer and adhesion of end-burr have contribution to generate notching wear. An

appropriate choice of coating material can prevent from notching wear, for instance notching wear was not observed on TiCN coated carbide tool.

6. The proposed method of flank wear progress analysis on coated tools by plotting in log-log graph was successfully applied in different types of material workpieces. This plots allow an easy identification of change in wear rate. The change in wear rate was correlated with the loss of coating when turning ductile cast iron and Inconel 718 by means of EDS and SEM images. This method is very simple but effective; thus, hopefully can be applied in the analysis of flank wear progress other researchers, tool makers and production engineers.

8 References

[1] T. Childs, K. Maekawa, T. Obikawa and Y. Yamane, Metal Machining Theory and applications, London: Elsevier, 2000.

[2] ISO Standard, "Tool-life testing with single-point turning tools," ISO, 1993.

[3] T. Childs, K. Maekawa, T. Obikawa and Y. Yamane, Metal machining theory and applications, Burlington: Arnold, 2000.

[4] D. A. Stephenson and J. S. Agapiou, Metal Cutting Theory and Practice Second Edition, Taylor & Francis, 2006.

[5] W. F. Hosford, Physical metallurgy, Boca Raton, FL: Taylor and Francis, 2005.

[6] H. Fredriksoon and U. Akerlind, Materials processing during casting, John Wiley & Sons, 2006.

[7] D. R. Askeland and W. J. Wright, The science and engineering of materials, Cengage learning, 2014.

[8] M. J. McCabe, "How PVD coatings can improve high speed machining," High speed machining conference, IL, 2001.

[9] I. Ham, K. Hitomi and G. L. Thuering, "Machinability of Nodular Cast Irons Part I Tool Forces and Flank Adhesion," *Journal of Manufacturing Science and Engineering ,* vol. 83, pp. 142-153, 1961.

[10] K. Hitomi and G. L. Thuering, "Machinability of Nodular Cast Irons Part II Effect of Cutting Conditions on Flank Adhesion," *Journal of Manufacturing Science and Engineering,* pp. 282-288, 1962.

[11] K. Hitomi and G. L. Thuering, "Machinability of Nodular Cast Irons Part III - Tool Life of Carbide and Ceramic Cutting Tools.," *Journal of Manufacturing Science and Engineering ,* pp. 141-149, 1964.

[12] W. Grzesik, J. Rech, K. Zak and C. Claudin, "Machining performance of perlitic-ferritic nodular cast iron with coated carbide and silicon nitride ceramic tools," *International Journal of Machine Tools & Manufacture,* no. 49, pp. 125-133, 2009.

[13] W. Grzesik and J. Malecka, "Documentation of tool wear progress in the machining of nodular ductile iron with silicon nitride-based ceramic tools," *CIRP Annals-Manufacturing Technology ,* no. 60, pp. 121-124, 2011.

[14] Y. Recep, C. Erdal, F. Fehim and K. Sakip, "Tool life performance of multilayer hard coatings produced by HTCVD for machining of nodular cast iron," *International Journal of Refractory Metals & Hard Materials,* no. 26, pp. 514-524, 2008.

[15] N. Camuscu, "Effect of cutting speed on the performance of Al2O3 base ceramic tools in turning nodular cast iron," *Materials and design,* no. 27, pp. 997-1006, 2006.

[16] M. Cemal Cakir, A. Bayram, K. Kaan Kircali and C. Ensarioglu, "Effects of microstructure on machinability of ductile iron," *Proceedings of the Institution of Mechanical Engineers part B Journal of engineering manufacture,* vol. 224, pp. 1-10, 2010.

[17] H. G. Prengel, P. C. Jindal, K. H. Wendt, A. T. Santhanam, P. L. Hedge and R. M. Penich, "A new class of high performance PVD coatings for carbide cutting tools," *Surface and coatings technology,* vol. 139, no. 1, pp. 25-34, 2001.

[18] A. G. Jaharah, M. Rodzi, A. A. Rahman, M. N. Rahman and C. H. Hassan, "Machinability of FCD 500 ductile cast iron using coated carbide tool in dry machining condition," *International journal of mechanical and materials engineering,* vol. 4, no. 3, pp. 279-284, 2009.

[19] H. G. Prengel, W. R. Pfouts and A. T. Santhanam, "State of the art in hard coating for carbide cutting tools," *Surface and coatings technology,* vol. 102, no. 3, pp. 183-190, 1998.

[20] K. Itakura, M. Kuroda, H. Omokawa, H. Itani, K. Yamamoto and Y. Ariura, "Wear mechanism of coated cemented carbide tool in cutting of super heat resisting alloy inconel 718," *Journal of Japan society for precision engineering ,* vol. 65, no. 7, pp. 976-981, 1999.

[21] A. Bhatt, H. Attia, R. Vargas and V. Thomson, "Wear mechanism of WC coated and uncoated tools in finish turning of Inconel 718," *Tribology International,* vol. 43, no. 5-6, pp. 1113-1121, 2010.

[22] C. Ducros, V. Benevent and F. Sanchette, "Deposition, characterization and machining performance of multilayer PVD coatings on cemented carbide cutting tools," *Surface and Coatings technology,* Vols. 163-164, pp. 681-688, 2003.

[23] M. Y. Noordin, V. C. Venkatesh and S. Sharif, "Dry turning of tempered martensitic stainless tool steel using coated cermet and coated carbide tools," *Journal of Materials Processing Technology ,* vol. 185, no. 1-3, pp. 83-90, 2007.

[24] S. K. Khrais and Y. J. Lin, "Wear mechanisms and tool performance of TiAlN PVD coated inserts during machining of AISI 4140 steel," *Wear,* vol. 262, no. 1-2, pp. 64-69, 2007.

[25] F. Qin, J. Hu, Y. K. Chou and R. G. Thompson, "Delamination wear of nano-diamond coated cutting tools in composite machining," *Wear,* vol. 267, no. 5-8, pp. 991-995, 2009.

[26] J. R. Davis, ASM specialty handbook cast irons, ASM International, 1996.

[27] D. I. Society, "Ductile Iron Data for Design Engineer," 2001. [Online]. Available: http://www.ductile.org/. [Accessed 5 10 2014].

[28] D. C. Montgomery, Design and analysis of experiments, Wiley, 2013.

[29] Y. Yamane and K. Sekiya, "An evaluation of difficulty in machining of difficult-to-cut materials by using difficult-to-cut rating," *Journal of Japan Society for Precision Engineering ,* vol. 70, no. 3, pp. 407-411, 2004.

[30] Y. Yamane, H. Usuki, R. Yin and N. Narutaki, "Calibration system of tool-work-thermocouple with infrared heating," *Bulletin of the Japanese Society of Presicion Engineering ,* vol. 23, no. 1, pp. 5-9, 1989.

[31] Mosaic-industries, "Mosaic documentation web," [Online]. Available: http://www.mosaic-industries.com/embedded-systems/microcontroller-projects/temperature-measurement/thermocouple/type-k-calibration-table. [Accessed 1 11 2014].

[32] R. Tezuka, K. Sekiya, Y. Keiji and Y. Yamane, "The relationship between dynamic components of cutting force and adhesion of tool-chip interface," *Key engineering,* Vols. 407-408, pp. 469-472, 2009.

[33] S. Sukvittayawong and I. Inasaki, "Detection of Built-up edge in turning process," *International Journal of Machine Tool and Manufacturing,* vol. 34, no. 6, pp. 829-840, 1994.

[34] W. D. Münz, "Titanium aluminum nitride films: A new alternative to TiN coatings," *Journal of Vacuum Science and Technology,* no. 4, pp. 2717-2725, 1986.

[35] P. Mayrhofer, F. Kunk, J. Musil and C. Mitterer, "Thin solid films," pp. 415-151, 2002.

[36] P. H. Mayrhofer, A. Hörling , L. Karlsson, J. Sjölén , T. Larsson, C. Mitterer and L. Hultman , "Self-organized nanostructures in the Ti-Al-N system," *Applied Physics Letters,* vol. 83, no. 10, pp. 2049-2051, 2003.

[37] P. C. Jindal, A. T. Santhanam, U. Schleinkofer and A. F. Shuster, "Performance of PVD TiN, TiCN, and TiAlN coated cemented carbide tools in turning," *International Journal of Refractory Metals & Hard Materials ,* no. 17, pp. 163-170, 1999.

[38] A. Kurt and U. Seker, "The effect of chamfer angle of polycrystalline cubic boron nitride cutting tool on the cutting forces and the tool stresses in finishing hard turning of AISI 52100 steel," *Materials and design,* no. 26, pp. 351-356, 2004.

[39] T. Özel, "Computational modelling of 3D turning: influence of edge micro-geometry on forces, stresses, friction and tool wear in PcBN tooling," *Journal of Materials Processing Technology ,* no. 209, pp. 5167-5177, 2009.

[40] Y. Yen, A. Jain and T. Altan , "A finite element analysis of orthogonal machining using different tool edge geometries," *Journal of Materiasl Processing Technology,* no. 146, pp. 72-81, 2004.

[41] A. Bhatt, H. Attia, R. Vargas and V. Thomson, "Wear mechanism of WC coated and uncoated tools in finish turning of Inconel 718," *Tribology International,* no. 43, pp. 1113-1121, 2010.

[42] J. Ghani, I. Choudhury and H. Masjuki, "Wear mechanism of TiN coated carbide and uncoated cermets tools at high cutting speed applications," *Journal of Materials Processing Technology,* no. 153-154, pp. 1067-1073, 2004.

[43] A. Jawaid, S. Koksal and S. Sharif, "Cutting performance and wear characteristics of PVD coated and uncoated carbide tools in face milling Inconel 718 aerospace alloy," *Journal of Materials and Processing Technology,* no. 116, pp. 2-9, 2001.

[44] M. Nouri and A. Ginting, "Wear characteristics and performance of multi-layer CVD coated alloyed carbide tool in dry end milling of titanium alloy," *Surface and Coatings Technology,* no. 200, pp. 5663-5676, 2006.

[45] A. Sharman, R. C. Dewes and D. K. Aspinwall, "Tool life when high speed ball nose milling end milling Inconel 718TM," *Journal of Materials Processing Technology,* no. 118, pp. 29-35, 2001.

[46] M. E. Martellotti, "An analysis of milling process," *Transactions of the ASME,* vol. 63, pp. 677-700, 1941.

[47] L. Chuzhoy, R. E. DeVor, S. G. Kapoor, A. J. Beaudoin and D. J. Bamman, "Machining simulation of ductile iron and its constituents, part 1: Estimation of material model parameters and their validation," *Journal of manufacturing science and engineering,* vol. 125, no. 2, pp. 192-201, 2003.

[48] E. Trent and P. Wright, Metal cutting, Woburn: Butterworth Heinemann, 2000.

[49] I. Martinez, R. Tanaka, Y. Yamane, K. Sekiya, K. Yamada, T. Ishihara and S. Furuya , "Wear characteristics of coated carbide tools in turning of ductile cast iron," *Proceeding of the 8th interantional conference on LEM 21st century ,* 2015.

[50] G. Kuppuswamy, Principles of metal cutting, Universities Press, 1996.

[51] E. O. Ezugwu, J. Bonney and Y. Yamane, "An overview of the machinability of aeroengine alloys," *Journal of materials processing technology,* vol. 134, no. 2, pp. 233-253, 2003.

[52] T. M. Pallock and S. Tin, "Nickel-based superalloys for advanced turbine engines: Chemistry, Microstructure, and properties," *Journal of propulsion and power,* vol. 22, no. 2, pp. 361-374, 2006.

[53] D. Dudzinski, A. Devillez, A. Moufki, D. Larrouquère, V. Zerrouki and J. Vigneau, "A review of developments towards dry and high speed machining of Inconel 718 alloy," *Machine tools and manufacture,* vol. 44, no. 4, pp. 439-456, 2004.

[54] J. R. Davis, ASM specialty handbook, Tool materials, Materials Park, OH: ASM International, 1995.

[55] T. V. Rajan, C. P. Sharman and A. Sharman, Heat treatmen principles and techniques, New Delhi: PHI Learning Private Limited, 2011.

[56] H. Takeyama and R. Murata, "Basic investigation of tool wear," *ASME J. Eng. Ind.,* vol. 85, no. 1, pp. 33-37, 1963.

[57] E. Usui and T. Shirakashi, "Analytical prediction of cutting tool wear," *Wear,* vol. 100, no. 1-3, pp. 129-151, 1984.

[58] R. Tanaka, A. Hosokawa, T. Furumoto and T. Ueda, "Wear characteristics of ceramic tools when turning BN free-machining steel," *Journal of advanced mechanical design, systems, and manufacturing,* vol. 7, no. 3, pp. 474-484, 2013.

[59] I. Martinez, R. Tanaka, Y. Yamane, K. Sekiya, K. Yamada, T. Ishihara and S. Furuya, "Wear mechanism of coated tools in the turning of ductile cast iron having wide range of tensile strength," *Precision engineering,* no. http://dx.doi.org/10.1016/j.precisioneng.2016.07.003, 2016.

[60] A. R. Thangaraj and K. J. Weinmann, "On the wear mechanisms of cutting performance of silicon carbide whisker-reinforced alumina," *Journal of engineering for industry,* vol. 114, no. 3, pp. 301-308, 1992.

[61] A. Devillez, F. Schneider, S. Dominiak, D. Dudzinski and D. Larrouquere, "Cutting forces and wear in dry machining of inconel 718 with coated carbide tools," *Wear,* vol. 262, no. 7-8, pp. 931-942, 2007.

[62] C. J. Cortés Rodríguez, Cutting edge preparation of precision cutting tools by applying micro-abrasive jet machining and brushing, Kassel University press, 2009.

[63] G. Boothroyd and W. A. Knight, Fundamentals of machining and machine tools, Boca Raton: CRC Press, 2005.

[64] E. Posti and I. Nieminen, "Influence of coating thickness on the life of TiN-coated high speed cutting tools," *Wear,* vol. 129, no. 2, pp. 273-283, 1989.

[65] E. O. Ezugwu and S. H. Tang, "Surface abuse when machining cast iron (G17) and nickel-base superalloy (Inconel 718) with ceramic tools," *Journal of materials processing technology ,* vol. 55, no. 2, pp. 63-69, 1995.

[66] ASTM international, "Standard terminology relating to wear and erosion G40," ASTM, West Conshonhocken, 2002.

[67] G. Amontons, "De la resistance caus'ee dans les machines," *Mem. l' Acad. Roy. A,* vol. 12, pp. 252-282, 1699.

[68] J. A. Bailey, "Friction in metal machining -mechanical aspects," *Wear,* vol. 31, no. 2, pp. 243-275, 1975.

[69] S. Kato, K. Yamaguchi and M. Yamada, "Stress distribution at the interface between tool and chip in machining," *ASME J. Eng. Ind. ,* vol. 94, no. 2, pp. 683-689, 1972.

[70] H. Chandrasekaran and D. V. Kapoor, "Photoelastic analysis of tool-chip interface Stresses," *J. Eng. Ind.,* vol. 87, no. 4, pp. 495-502, 1965.

[71] N. N. Zorev, "Inter-relationship between shear process ocurring along tool face and shear plane in metal cutting," *International research in production engineering,* pp. 42-49, 1963.

[72] W. Grzesik, J. Rech and K. Zak, "Determination of friction in metal cutting with tool wear and flank face effects," *Wear,* vol. 317, no. 1-2, pp. 8-16, 2014.

[73] E. G. Thomsen, A. G. McDonald and S. Kobayashi, "Flank friction studies with carbide tools reveal sublayer plastic flow," *J. Eng. Ind. ,* vol. 84, no. 1, pp. 53-62, 1960.

[74] M. Olsson, S. Söderberg, S. Jacobson and S. Hogmark, "Simulation of cutting tool wear by a modified pin-on-disc test," *Int J Mach Tools Manufact,* vol. 29, no. 3, pp. 377-390, 1989.

[75] W. Grzesik, Z. Zalisz and P. Nieslony, "Friction and wear testing of multilayer coatings on carbide substrates for dry machining for dry applications," *Surface and coatings technology,* vol. 155, no. 1, pp. 37-45, 2002.

[76] F. Zemzemi, J. Rech, W. Salem, A. Dogui and P. Kapsa, "Development of a friction model for the tool-chip-workpiece interfaces during dry machining of AISI1042 steel with TiN coated carbide tools," *Int. J. Machining and Machinability of Materials,* vol. 7, no. 3, pp. 361-377, 2007.

[77] F. Zemzemi, W. Bensalem, J. Rech, A. Dogui and P. Kapsa, "New tribometer designed for the characterisation of the friction properties at the tool/chip/workpiece interfaces in machining," *Tribo Test,* vol. 14, pp. 11-25, 2008.

[78] P. Hedenqvist and M. Olsson, "Sliding wear testing of coated cutting tool materials," *Tribology international,* vol. 24, no. 3, pp. 143-150, 1991.

[79] C. Bonnet, F. Valiorgue, J. Rech, C. Claudin , H. Hamdi, J. M. Bergheau and P. Gilles, "Identification of a friction model-Application to the context of dry cutting of AISI 316L austenitic stainless steel with a TiN coated carbide tool," *International Journal of Machine Tools and Manufacture,* vol. 48, pp. 1211-1223, 2008.

[80] J. Brocail, M. Watremez and L. Dubar, "Identification of the friction model for modelling of orthogonal cutting," *International Journal of Machine Tools and Manufacture,* vol. 50, no. 9, pp. 807-814, 2010.

[81] H. Puls, F. Klocke and D. Lung, "A new experimental methodology to analyse the friction behaviour at the tool-chip interface in metal cutting," *Prod. Eng. Res. Devel. ,* vol. 6, pp. 349-354, 2012.

[82] H. Puls, F. Klocke and D. Lung, "Experimental investigation on friction under metal cutting conditions," *Wear,* no. 310, pp. 63-71, 2014.

[83] C. Nobel, U. Hofmann, F. Klocke, D. Veselovac and H. Puls, "Application of a new, severe-condition friction test method to understand the machining characteristics of Cu-Zn alloys using coated cutting tools," *Wear,* no. 344-345, pp. 58-68, 2015.

[84] A. Standard, "Standard test methods of measuring resistance of electrical connections (static contacts)," 2003.

[85] ASTM standard, "Standard Test Methods for Measuring Resistance of Electrical Connections (Static Contacts)," ASTM, 2003.

[86] M. Rosochowska, R. Balendra and K. Chodnikiewicz, "Measurements of thermal contact conductance," *Journal of materials processing technology,* vol. 134, no. 2-3, pp. 204-210, 2003.

[87] T. R. Coelho, E.-G. Ng and M. A. Elbestawi, "Tool wear when turning hardened AISI 4340 with coated PCBN tools using finishing cutting conditions," *International Journal of Machine Tools & Manufactre,* vol. 47, no. 2, pp. 263-272, 2007.

[88] J. R. Davis, ASM specialty handbook cast irons, ASM international, 1996.

[89] F. Cverna, ASM ready reference: Thermal properties of metals, ASM International, 2002.

[90] ASM, ASM Handbook, Volume 1: Properties and Selection: Irons, Steels, and High-Performance Alloys, ASM International, 1990.

[91] W. S. Williams, "The termal conductivity of ceramics," *The Journal of The Minerals, Metals & Materials Society (TMS),* vol. 50, no. 6, pp. 62-66, 1998.

[92] F. Gronvold, S. Stolen, E. F. Westrum, A. K. Labban and B. Uhrenius , "Heat capacity and thermodynamic properties of ditungsten carbide, W2C1−x, from 10 to 1000 K," *Thermochimica Acta,* vol. 129, no. 1, pp. 115-125, 1988.

[93] R. Tezuka, K. Sekiya, K. Yamada and Y. Yamane, "The relationship between dynamic components of cutting force and adhesion of tool-chip interface," *Key engineering materials,* Vols. 407-408, pp. 469-472, 2009.

Acknowledgement

I would like to express my sincere and deep gratitude to my advisors Dr. YAMANE and Dr. TANAKA. Your guidance, support and patient were primordial throughout my studies in Hiroshima University. Thanks for sharing your knowledge with me.

I appreciate all the time that Dr. YAMADA and Dr. YOSHIDA dedicated in reviewing this dissertation.

I would like to thank to the staff of international student support and engineering support office for their kindness and support since I arrive to Hiroshima University until the last period of my stay in Hiroshima University.

I am very thankful with all my labmates for sharing their experiences and for supporting me.

I am grateful to my friend Mr. KOJIMA, for supporting me during the experiments and my life in Japan.

I am grateful with my parents for encourage me to keep going forward.

With all my love to my wife Alicia and my son Israel Jr. Thanks to be the way you are.

I thought I was leaving my family when I came to Japan but I made my family bigger. Thanks to all my friends who I consider as part of family and important part of my life.